In presenting this dissertation in partial fulfillment of the requirements for an advanced degree at Idaho State University, I agree that the Library shall make it freely available for inspection. I further state that permission to download and/or print my dissertation for scholarly purposes may be granted by the Dean of the Graduate School, Dean of my academic division, or by the University Librarian. It is understood that any copying or publication of this dissertation for financial gain shall not be allowed without my written permission.

Signature _____

Date _____

OLDER THAN REFERENCE MAN: THE BIOKINETIC SIGNIFICANCE OF ANATOMICAL AND PHYSIOLOGICAL CHANGES WITH ADVANCING AGE

By

Jason E. Davis

A dissertation

submitted in partial fulfillment

of the requirements for the degree of

Doctor of Philosophy in the Department of Nuclear Engineering and Health Physics

Idaho State University

May 2014

To the Graduate Faculty:

The members of the committee appointed to examine the dissertation of **Jason E. Davis** find it satisfactory and recommend that it be accepted.

_____

Professor Richard R. Brey, Major Advisor

_____

Professor Thomas Gesell, Committee Member

_____

Professor Jason Harris, Committee Member

_____

Professor George Imel, Committee Member

_____

Professor DeWayne Derryberry, Graduate Faculty Representative

Acknowledgements

It is my pleasure to acknowledge and thank all those who made this dissertation possible. The years I have spent in graduate study have been the most challenging but also most interesting and exciting time in my life. I would never have been able to survive all these days and nights of study and research without a great deal of guidance from the many supportive and inspiring people I have met since beginning my graduate work.

First, I would like to thank the Academy! I will always remember the Las Vegas Academy of International Studies, Performing Arts, and Visual Arts as the group of students and teachers that inspired me to press forward, no matter how difficult the road ahead became. Learning early on to balance school work, rehearsals, performances, a part-time job, and some semblance of a social life trained me to prioritize and to continue functioning through sleep deprivation.

With a more reverent tone, I wish to express my deepest gratitude to my major advisor, Dr. Rich Brey for his guidance, patience, instruction, insight, and support. Without his support and encouragement it would have been all too easy to fall between the cracks and lose sight of my eventual career and academic goals.

I would like to especially acknowledge the invaluable contribution and scientific guidance by Dr. Keith Eckerman and Dr. Richard Toohey whose brilliant ideas, vast range of expertise and exceptional skills as mentors enabled me to complete this study. My thanks to both of you for delaying retirement long enough to set me on the road to completion.

Thank you to my committee members Dr. Thomas Gesell, Dr Jason Harris, and Dr. George Imel for valuable comments on my dissertation and for their time and attention.

And, of course, I also wish to thank Dr DeWayne Derryberry for representing the graduate faculty at my defense.

I wish to acknowledge Oak Ridge Associated Universities and, in particular, Dr. Donna Cragle and Karin Jessen for their support, patience, and motivation; as well as for providing me with the opportunity to move to Oak Ridge to work with and learn from some of the best minds in a diverse range of fields.

I thank Dr. Mark Rudin who convinced me I would be bored with a technician-level job and steered me toward the more rigorous study of health physics. To Dr. William Johnson, Dr. Phillip Patton, Dr. Ralf Sudowe, and Dr. Steen Madsen, I thank you for helping me to lay the foundation I need for what I hope will be a long and successful career. I would also like to thank all my fellow students with whom I shared the years of study groups, laboratory reports, PowerPoint poisoning, exam stumbles, and exam triumphs. All of you have been an inspiration to me in one form or another.

A special acknowledgement goes to my parents, brothers and sister, my beautiful children, and especially to my devoted wife. You have all sacrificed as much as I have to enable me to complete this milestone and your love and support are what kept me going when the nights got late and my brain started to turn to mush.

CONTENTS

List of Figures

List of Tables

List of Acronyms/Abbreviations

ADME	Absorption, Distribution, Metabolism, and Excretion
AF	Absorbed Fraction
AI	Alveolar Interstitium
AMAD	Activity Median Aerodynamic Diameter
BAP	Bone-Specific Alkaline Phosphatase
BB	Bronchi
Bb	Bronchioles
BF	Blood Flow
BMD	Bone Mineral Density
BMR	Basal Metabolic Rate
BW	Body Weight
CBFR	Cortical Bone Formation Rate
CBRR	Cortical Bone Resorption Rate
CDC	Centers for Disease Control and Prevention
CO	Cardiac Output
CTX	type I collagen C-telopeptide
DOE	Department of Energy
DXA	Dual-energy X-ray Absorptiometry
EPA	Environmental Protection Agency
ET	Extrathoracic Tissue
FBF	Fractional Bone Formation
FBFR	Fractional Bone Formation Rate

GFR	Glomerular Filtration Rate
GI	Gastrointestinal
HATM	Human Alimentary Tract Model
HRTM	Human Respiratory Tract Model
IAEA	International Atomic Energy Agency
ICRP	International Commission on Radiological Protection
IMBA	Integrated Modules for Bioassay Analysis
LLI	Lower Large Intestine
LNET	Extrathoracic Lymph Nodes
LNTH	Thoracic Lymph Nodes
MIRD	Committee on Medical Internal Radiation Dose
NCRP	National Council on Radiation Protection and Measurements
NHANES	National Health and Nutrition Examination Survey
OC	Ostoecalcin
P1NP	Procollagen type I N-propeptide
PBPK	Physiologically Based Pharmacokinetic Model
PK	Pharmacokinetic
SAF	Specific Absorbed Fraction
SI	Small Intestine
TBFR	Trabecular Bone Formation Rate
TBRR	Trabecular Bone Resorption Rate
TK	Toxicokinetic
ULI	Upper Large Intestine

Dissertation Abstract - Idaho State University - 2014

The dominant contribution to the uncertainty in internal dose assessment can often be attributed to the uncertainty in the biokinetic model structure and parameters. It is generally recognized that all individuals will show some variation from one another in terms of their anatomy and physiology. However, internal dose assessments remain inherently uncertain because existing models are based on standardized data that may not necessarily be directly relevant to the individual under consideration.

Subtle changes to many physiological processes that directly affect the function of individual organs is a natural hallmark of aging. The question that motivated this study is whether or not these physiological changes alter organ function to a statistically significant degree in regards to dosimetric modeling.

To answer this question, a comprehensive review of the literature was performed to determine the extent of human-specific information available to support the use of physiologically-based pharmacokinetic (PBPK) modeling to address the impact of age-specific physiological differences in the assessment of internal dose. Parameter value differences between age-specific data sets were quantified, revealing that there is a statistically significant difference in values between younger and older populations.

A predictive pharmacokinetic framework was developed in Matlab Simulink to characterize the effect of age-based differences on tissue dosimetry. Sensitivity analysis was performed on the model to ascertain which factors are likely to have a statistically significant impact on uptake, retention, distribution, and excretion of radiological materials. Model simulations were run using parameters associated with a reference individual, as well as age-specific parameters for each decade of adult life. Examination of

the physiological data alongside the model sensitivity reveals that there is a possibility for competing influence within the biokinetic model. These findings suggest that there is not a significant change in the predicted organ concentrations or urinary output of a material with age between the third and seventh decades of life. A significant difference from Reference Man predictions was, however, seen in values predicted for the eighth decade of life.

Chapter 1. INTRODUCTION

Due to the difficulties in measuring the absorbed dose to an individual human organ, internal doses must be estimated based on indirect measurements of excreta or environmental concentrations. These measurements may then be used in mathematical models that help to estimate the rate at which a substance translocates among organs or organ compartments and/or the rate at which a substance accumulates in the various tissues in the body. However, internal doses are inherently uncertain because these models are based on standardized data that may not necessarily be directly relevant to the individual under consideration.

The accurate assessment of radiation doses to human beings from radionuclides that are encountered by workers and by members of the population as a whole requires knowledge of some pertinent human characteristics. A practical concept developed more than 50 years ago for application in this field was that of a "standard man" — a formalized description of some specific physical, chemical, physiological, anatomical and biokinetic parameters of relevance in radiological protection (ICRP 1960). This reference individual was later updated and re-named the "Reference Man" in the publication of ICRP Publication 23 (ICRP 1975).

The anatomical and physiological quantities of ICRP Publication 23 (1975) were superseded in parts due to the wealth of biological literature available. ICRP Publication 70 focused on anatomical and physiological aspects of the human skeleton that related to radiological protection (ICRP 1995b). Publication 66 outlines the anatomy and physiology necessary to develop a respiratory tract model (ICRP, 1994), Publication 88 defines how to estimate doses to the embryo and fetus from intakes of radionuclides by the mother (ICRP,

2001), Report 89 updates the parameters of Reference Man (ICRP 2002), and Report 100 describes the human alimentary tract model (ICRP, 2006).

1.1. Motivation and Hypothesis

The bioassay measurements used to assess intakes of radionuclides can include: *in vivo* measurements, excretion measurements, air monitoring measurements, etc. The order of preference of assay type, in terms of ease of measurements and importance of interpretations is body activity analysis, excretion analysis, followed by personal air sampling and, provided the samples can be shown to be representative of the air breathed, general air monitoring (ICRP 1997). Body activity analysis *in vivo* can be used to directly assess the amount of activity in the body, but may only be useful for radionuclides that emit x or γ radiation. Excreta measurements can be used to assess intakes, but there is error due to large differences in the rates at which radionuclides traverse the body and fluctuations in the amount of an individual's daily excretion. The interpretation of air samples may be misleading as the location of the air monitors can affect measurements by a factor of about ten (ICRP 1997). Many bioassay programs rely on the analysis of excretion samples as part of their internal exposure control program due to lower cost and ease of collection. It would be beneficial to be able to use the excretion measurements with simple biokinetic models to assess radionuclide intakes with little error. This would ultimately cut both time and costs of other more accurate, but more arduous intake assessment methods; however, it can often be computationally arduous using more complicated models to assess intakes. Interchanging models or subsystems of models may speed up the assessment process while still providing valid results.

Urinary excretion is removal of material from the body in urine through the bladder. Fecal excretion is the removal of material that either passes unabsorbed through the gastrointestinal tract (GI-tract) or comprises systemic material that is removed through the GI-tract. For some radionuclides, including plutonium, routes of excretion are given explicitly in biokinetic models (ICRP 1993, Luciani and Polig 2000), while other models split excreted activity between urine and feces depending on a constant ratio (ICRP 1989). It can be a difficult task to match the excretion predictions from models that split total excretion to actual bioassay measurements, especially for chronic intakes over long periods of time or cases where radionuclide intake amounts fluctuate over time.

To interpret the measurement of activity in excreta it is important to have knowledge of the behavior of radioactive materials within the human body. The International Commission on Radiological Protection (ICRP) has developed several biokinetic models over the years to describe the translocation of radioactive material throughout the body and through routes of excretion. Some of the models most often used are described in ICRP Publications 23 (ICRP 1975), 30 (ICRP 1979), 56 (ICRP 1989), 66 (ICRP 1994), 67 (ICRP 1993), and 78 (ICRP 1997). These models are usually based on linear, first-order kinetics. Parameters in these models can be modified so that radionuclide flow throughout the body can be represented using the best available information. Biokinetic models have been used for dose calculations, setting dose limits, and for assessing intakes of radioactive material based on bioassay measurements.

Within ICRP Publication 89, is it noted that calculation of radiation doses from internal sources require information about the anatomical and physiological characteristics

of the exposed individual. This need is magnified if one wishes to calculate the dose to a particular body organ or system rather than the body as a whole (ICRP 2002).

The validity of epidemiological studies also depends on reliable estimates of risk and on the uncertainty in the dose estimates. Retrospective dose reconstructions for occupational exposures or accidents, compensation programs such as the Energy Employees Occupational Illness Compensation Program Act (EEOICPA) and the Nuclear Test Personnel Review Program (NTPR) require not only an estimate of dose but also an evaluation of its uncertainty. This estimate of uncertainty is used to evaluate the uncertainty in the probability of causation of a specified disease and, as a result, influences the compensability of an individual's illness based on the likelihood that the illness was caused by radiation exposure (NCRP 2010, U.S. Congress 2000).

The ICRP models use a combination of biological information and nuclide-specific kinetic data in order to predict the disposition of radionuclides for which limited human data exist. It is widely recognized that, in addition to genetic variation, differences in life stage, lifestyle, and health status affect the disposition of substances entering the body. When models are developed for predicting the disposition of substances in the human body, the models frequently represent a standard healthy adult, in part because the human data used to develop such models are often obtained from younger adults.

It is generally recognized that all individuals will show some variation from one another in terms of their anatomy and physiology. However, for the purposes of radiation protection and the establishment of dose limits, it was necessary to develop a standard set of biological characteristics that could be used to standardize calculations and allow for the rapid and efficient estimation of an individual's dose. A practical concept developed

more than 50 years ago for application in this field was that of 'reference man' — a formalized description of some specific physical, chemical, physiological, anatomical and biokinetic parameters of relevance in radiological protection. Earlier work on this topic had led in 1975 to the 'ICRP Reference Man,' found in Publication 23 of the International Commission on Radiological Protection. Despite the updates to this database, international reference models still categorizes all individuals above the age of 15 as a single age group (ICRP 1995), suggesting that once one reaches adulthood, there is little anatomical or physiological variation as an individual ages.

Pharmacokinetic models are developed for predicting the translocation and deposition of radionuclides in humans are based upon data generated from and dominated by healthy adult males. This is largely because this cohort composed the majority of the exposed workforce during the 1950s and 1960s in the United States and Western Europe. Thus children, the elderly and health-impaired individuals represent subpopulations that may benefit from specific consideration during internal dosimetry modeling efforts (Thompson et al. 2009). ICRP has given significant consideration to the physiological parameters of children of various ages, as well as to the significance of gender differences (ICRP 1993; ICRP 1994; ICRP 1995).

Although Reference Man is assumed to be approximately 20 to 30 years of age, ICRP states that the model is useful for individuals up to about 55 years old. Given that United States Census records indicate that the proportion of the United States population over 55 years old has steadily increased over the past several decades as shown in Figure 1, this estimated range leaves a rather significant portion of the population unaccounted for (U.S. Census Bureau 2014). From an occupational radiation protection standpoint, this

omission may leave a large gap in accurate dose assessment for workers when one considers the increase in workers aged 65 and older that continue to participate in the labor force as shown in Figure 1.2 (Labor Statistics 2014).

Peer-reviewed compilations of physiological parameters have been developed for children, laboratory animals, and adult humans (Davies & Morris, 1993; Brown et al., 1997;

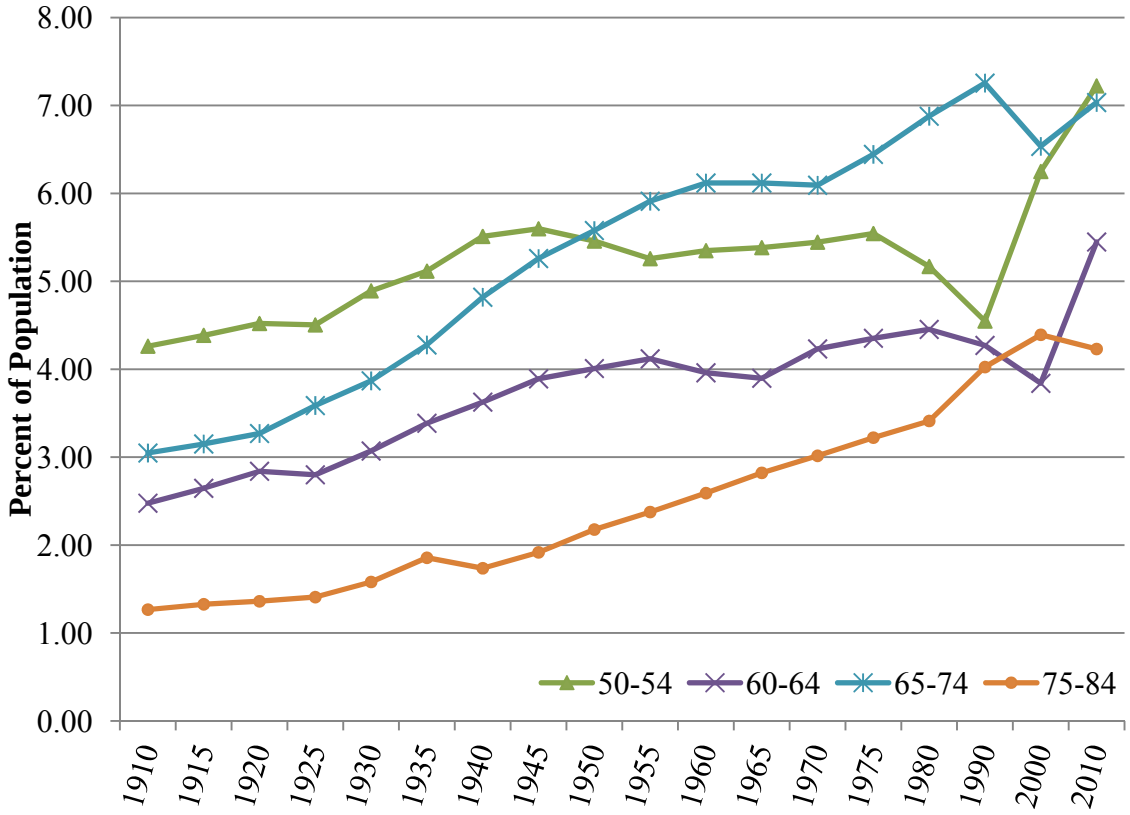

Figure 1.1. Percent of the United States population in four age ranges above 50 years old (Data extracted from: Census Bureau, 2014).

Price et al., 2003a, 2003b; Gentry et al., 2004). A collection of physiological traits in healthy and health-impaired elderly populations has been compiled

(Thompson et al. 2009), but this data has not yet been evaluated for applicability to biokinetic modeling for radionuclide translocation.

Subtle changes to many physiological processes that directly affect the function of individual organs is a natural hallmark of aging. The question at hand is this: considering individuals above the age of Reference Man, do these physiological changes alter organ function to a statistically significant degree in regards to dosimetric modeling? This study is based on the following hypothesis: if the physiology of an individual alters the excretion or metabolism rate of a particular substance, then the deviation of estimated doses derived from reference man values will also be impacted.

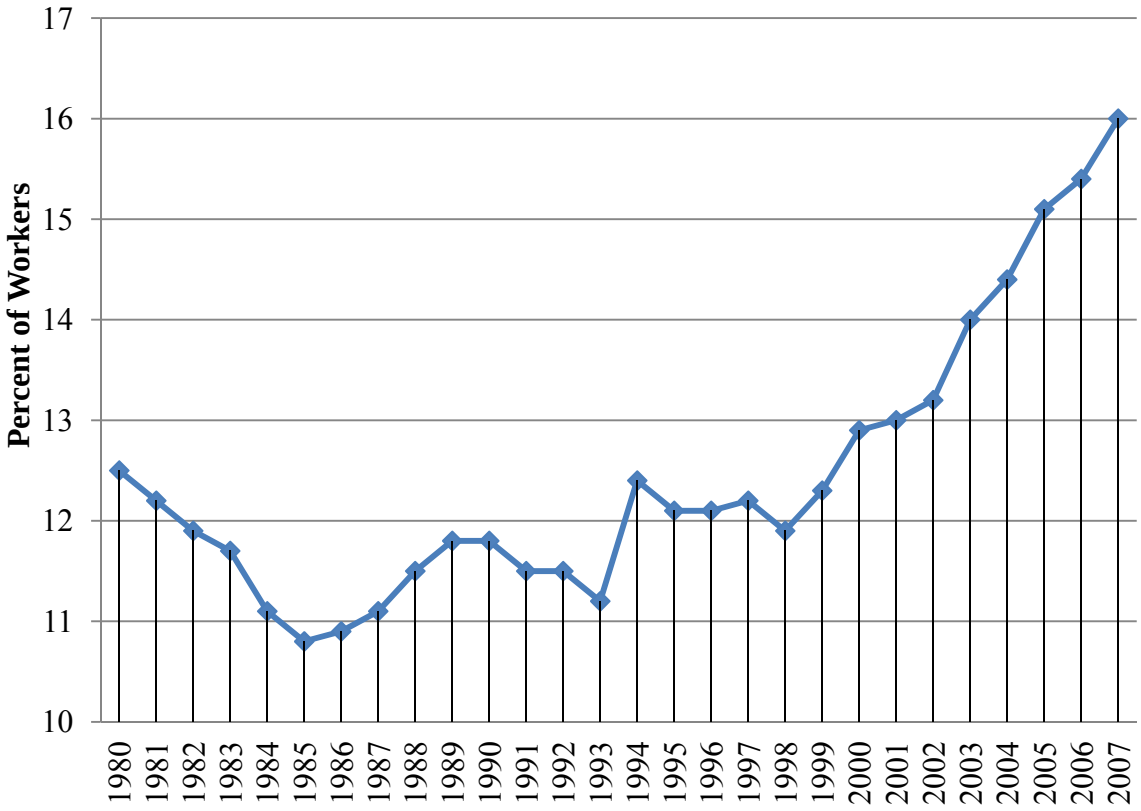

Figure 1.2. Labor force participation rate of workers 65 and over, 1980-2007 (Data extracted from: Labor Statistics, 2014).

1.2. Hypotheses

1.2.1. Hypothesis #1

$H_{(0,1)}$: The Reference Man physiological parameters adequately approximate the physiological parameters of adults above the age of 35.

$H_{(a,1)}$: The Reference Man physiological parameters do not adequately approximate the physiological parameters of adults above the age of 35.

1.2.2. Hypothesis #2

$H_{(0,2)}$: Organ concentrations predicted by biokinetic models built using the Reference Man physiological parameters are not significantly different than those built using age-specific biokinetic parameters.

$H_{(a,2)}$: Organ concentrations predicted by biokinetic models built using the Reference Man physiological parameters are significantly different than those built using age-specific biokinetic parameters.

1.2.3. Hypothesis #3

$H_{(0,3)}$: There are no significant differences between the activity predicted in various organs using Reference Man default parameters and the true measured activity.

$H_{(a,3)}$: There are significant differences between the activity predicted in various organs using the Reference Man default parameters and the true measured activity.

1.2.4. Data analysis

Significance of the difference between reference data and age-specific data can be evaluated using the student's t-test. P-values greater than 0.15 should be considered quite large and p-values less than 0.005 should be considered quite small. Large p-values are

associated with data consistent with the null hypothesis and small p-values are associated with data supportive of the alternative hypothesis. Significance of the difference between data from the reference age range and age-specific data from ages outside the reference age range can be evaluated using the Mann-Whitney U test. A cutoff p-value of 0.05, below which the null hypothesis would be rejected, was chosen for this study. The performance of the model will be tested also by comparing the predicted values of the radionuclide activity in urine to those measured in a sample case.

1.3. Objectives

The purpose of this study is to perform a comprehensive review of the literature to determine the extent of human-specific information available to support the use of physiologically-based pharmacokinetic (PBPK) modeling to address the impact of age-specific physiological differences in the assessment of internal dose. One objective is to organize, from a pharmacokinetic perspective, the key factors that are likely to have a significant impact on the uptake, retention, distribution, and excretion of radioactive materials in the human body. A second objective is to develop a predictive pharmacokinetic framework that can be used to characterize the effect of age differences on tissue dosimetry. The final objective is to use the available data in combination with a PBPK model to develop examples of approaches that could provide data-derived uncertainty factors to be used in place of default values in dose assessment.

The primary process step of this study will be a summary of an age-based literature review of physiological changes in each of seven body systems:

- Skeletal
- Genitourinary
- Nephrological
- Hepatological
- Cardiovascular
- Gastrointestinal
- Pulmonary

Biokinetic parameter value differences between the age-specific data sets will be quantified and assessed for statistical significance.

A comparison of the physiological inputs appropriate for reference man and those for aged individuals will be completed in order to understand the relative uncertainty in physiological input values used for dosimetry calculations. Completion of this comparison will require the development of a computerized modeling framework. The Matlab-Simulink programming environment has previously been reviewed as a tool for PBPK applications (Easterling et al. 2000), and on-line tutorials and examples exist for model development. Models in Simulink can be constructed graphically and linked together within a hierarchical framework. This system of model development reduces the need to learn an independent coding format and produces a model that is readily customizable from the user interface.

Case-study comparisons for radionuclides of interest will be conducted to retrospectively evaluate the variation with age produced in the dosimetric conclusions from previously well-defined cases.

Chapter 2. LITERATURE REVIEW

2.1. Conceptual Introduction to Internal Dosimetry

Internal dosimetry is the field of health physics dedicated to measuring and recording the absorbed doses from radionuclides deposited within the body. It is the scientific methodology used to quantify the radiative energy absorbed in human tissue, causing the ionization and excitation of atoms resulting from the emission of radiation by internally deposited radionuclides (Raabe 1994). Absorbed dose estimates are required for occupational exposures in radiation protection, and in environmental exposure assessments used as inputs to epidemiology (Zanzonico 2000). Internal dosimetry is also essential in assessing the risks involved in medical studies, including diagnostic imaging, therapy, or noninvasive physiological and metabolic studies (Loevinger et al. 1991).

The absorbed dose is the amount of energy absorbed from any type of ionizing radiation per unit mass of any material. Determination of absorbed dose requires knowledge of the biological distribution of the radioactive material within a subject, knowledge of the physical properties of the radionuclide, and the use of a mathematical model representing the subject for whom the dose is calculated. The biological distribution of the radionuclide is the information obtained which describes the duration, location, and amount of activity of the radionuclide within a subject. The physical properties of the radionuclide include the energy released for each type and frequency of energy transition possible. The mathematical model is a representation of the behavior of radioactive materials in the human body, built on a set of parameters defined for a subject that relate to the fraction of energy released by the radionuclide that is absorbed in the tissue of that subject (Smith 1970).

Evaluation of internal doses is a problem complicated with considerable uncertainties. Internal doses cannot be measured directly, but instead must be inferred indirectly from measured quantities such as body or organ activity, excretion rates and environmental monitoring data using the appropriate biokinetic and dosimetric models. Three basic quantities are required in order to calculate the absorbed dose delivered to the whole body or to the particular organ or tissue:

- Intake;
- Number of transformations occurred in a source organ due to the activity deposited in this organ;
- Energy absorbed in a target organ due to the disintegrations in a source organ.

Substances can enter the human body through four pathways: inhalation, ingestion, injection or wound contamination, and absorption through skin. The quantity of activity entering the body is conventionally named the *intake*. After the introduction into the body, a proportion of the activity is absorbed to blood. This absorption of activity is named *uptake*. Activity reaching body fluids (transfer compartments) is referred to as systemic activity. The ultimate distribution of systemic activity in the body can be homogeneous, as for tritium, or localized in specific organs or tissues, such as iodine in the thyroid, alkaline earth metals in bone or plutonium in the bone and liver (Luciani 2002).

Intake is commonly estimated by using in-vivo or in-vitro bioassay data. Urinalysis is the most common method of in vitro bioassay. Typically, 24-hour urine samples are obtained and analyzed via gross counting or spectrometry, with sample preparation depending on the suspected radioactive material. Since intake retention fractions, or the he

fraction of radioactive material that remains in a given organ at a specific time after the intake, for fecal measurements of insoluble compounds are a few orders of magnitude greater than that for urine, fecal data analysis may also be incorporated into an internal dosimetry program (Potter 2004).

Evaluation of the intake based on the monitoring bioassay data requires the knowledge of the time-dependent distribution of material in various organs of the body (Khursheed et al. 1996). Such knowledge is obtained from metabolism studies and biokinetic models. These biokinetic models describe the translocation of radionuclides throughout the body and are based on the physico-chemical and metabolic characteristics of the radioactive material.

2.1.1. Mathematical Properties of Models

Absorbed doses are calculated through the use of anthropomorphic phantoms - mathematical descriptions that approximate in size, shape, and composition the human body. Geometrical structures form the body and internal organs and tissues; minor features are neglected. These structures represent the target and source regions for which absorbed fractions (AFs) are calculated; the regions are fixed in position and mass.

The earliest calculations of AFs for penetrating radiation represented the body as ellipsoids or spheres (Ellett et al. 1964; Ellett et al. 1965; Reddy et al. 1967; Brownell et al. 1968). The first mathematical model, a hermaphrodite adult, was introduced in MIRD Pamphlet No. 5 and approximated a "standard man" (Snyder et al. 1969). The model contained 22 internal organs, homogeneous in composition and densities, which were considered source organs for monoenergetic, uniformly distributed photons. Absorbed

fractions for 25 target organs and 16 source organs were tabulated for 12 monoenergetic photon sources ranging from 10 keV to 4 MeV. These organs were contained within three principal sections of the total body: the head, the trunk, and the legs. The work by Snyder and Fisher improved upon previous calculations of AFs by taking into account the actual size, shape, composition, and density of human organs (Snyder et al 1969).

The Snyder-Fisher phantom, often called the MIRD phantom due to its introduction in a MIRD publication, has been used as the basis for the development of several mathematical models. Cristy and Eckerman (1987) developed mathematical models similar to the Snyder-Fisher phantom for children ages 0, 1, 5, 10, and 15 years and for an adult male. More recently, Stabin and others (1995) produced mathematical models for a nonpregnant woman and a woman at 3, 6, and 9 months gestation.

Several organs and tissues of the body have been modeled specifically for use in internal dose estimates. Examples are the heart wall and chambers (Coffey et al. 1981), the peritoneal cavity (Watson et al. 1989), the urinary bladder (Thomas et al. 1992; Thomas et al. 1999), the prostate gland (Stabin 1994a), and the head and brain (Bouchet et al. 1999a).

The most recent development in anthropomorphic phantoms is the introduction of voxel (volume element) phantoms. These are models based on images produced from CT or MRI scans; the human anatomy is imaged and the data stored in voxel format. The voxels are grouped to form organs and structures within the body and form higher resolution three-dimensional models than previously achieved. The first voxel phantom produced by Zubal and others (1994) yielded a 128 x l28 x 246 matrix with an isotropic cubic voxel resolution of 4 mm. It has been proposed that voxel phantoms will eventually replace the existing sets of anthropomorphic phantoms commonly used today (Stabin et al.

1999). Future advances in computing power and data storage may lead to the ability to use person-specific tomographic data to develop individual anatomical models.

2.1.2. Biological Properties of Radionuclides

Various approaches to the question of internal dosimetry have been developed over the years. Early in the history of radiation protection, standards were developed for individual radionuclides and limits were based on research with those particular materials. The perceived need to develop a standard was generally driven by the potential uses of the radiological material, and so the first individual standards were developed for radium, uranium, and plutonium. These standards established permissible body burdens or airborne concentrations, but did not address the translocation of materials throughout the human body (Potter 2004).

Some of the earliest dose estimates centered on radium and radon implants (capsules, needles, and seeds) which were used to produce exposures that would kill tumor cells while limiting damage to surrounding tissue. The equations used in these early dose estimates considered only the dose from beta emissions because this dose was known to be several times higher than that from gamma emissions. In 1948, Marinelli and others addressed the lack of consideration of other radiation types and proposed a method for calculating the dose from gamma emissions that was similar to that for beta emissions. However, Marinelli noted in 1942 that the main issues encountered in isotope dosimetry involved distribution of the materials within the tissues of interest (Marinelli 1942).

While the theoretical equations for internal dosimetry were being developed, an equally important line of work acquiring biological information was growing in parallel.

The significant events that occurred in this field are revealed in the introduction to the Report of the Task Group on Reference Man (ICRP 1975) and are summarized here.

During the late 1940's it was recognized that a set of biological parameters needed to be defined for use in internal dosimetry calculations. The ICRP advanced much of the developments in this area. Probably one of the most important events in this field was the *Chalk River Conference on Permissible Doses* held in Chalk River, Ontario, Canada in 1949. The objective was to formalize values that could be applied to the average individual, named 'Standard Man'. Data concerning the masses of organs were accepted, as well as data on the chemical composition of the total body and various tissues. However, it was stated in the conference proceedings that much effort needed to be focused on obtaining more accurate data on the chemical compositions of the body and its tissues. Finally, it was decided that the patterns of intake and excretion as well as the duration of occupational exposure should be averages for the normal activity of an individual in the Temperate Zone.

Work on Standard Man was prolific; these values were modified three times between 1950 and 1954, each at different conferences. Two reports by the International Sub-Committee II on Permissible Dose for Internal Radiation then followed, one in 1954 and one in 1959. The first report contained data on 15 naturally occurring elements in the human body; the second contained data on 46 elements. The 1959 report contained a listing of the concentrations of 44 elements in 36 tissues, as well as data concerning elimination and deposition parameters. This report consisted of the most detailed technical description of Standard Man and was widely used as the basis for dose estimation.

Further work began in 1963 when the Task Group was established by Committee 2 of the ICRP to revise and extend the concept of Standard Man. It was suggested by the ICRP that the name be changed from 'Standard Man' to 'Reference Man'. The Task Group was assigned the duty of reviewing and adapting the specifications defined for Standard Man to account for the current needs of health physicists. The product, *Report of the Task Group on Reference Man* (ICRP 1975), is the defining document of biological data for dosimetry calculations.

The guidelines of the Task Group are quoted here, as they should be recognized in understanding the extent and importance of this report (lCRP 1975):

a) It was agreed that the Task Group would limit its attention to those characteristics of man which are known to be important or which are likely to be significant for estimation of dose from sources of radiation within or outside the body...

b) The Task Group agreed that it is neither feasible nor necessary to specify Reference Man as representative of a well-defined population group... Reference Man is defined as being between 20 to 30 years of age, weighing 70 kg, is 170 cm in height, and lives in a climate with an average temperature of from 10° to 20°C. He is a Caucasian and is a Western European or North American in habitat and custom.

c) The Task Group agreed that it was not feasible to define Reference Man as an "average" or a "median" individual of a specified population group and that it was not necessary that he be defined in any such precise statistical sense. ... Only a very few individuals of any population will have characteristics which approximate closely those of Reference Man, however he is defined. The importance of the

Reference Man concept is that his characteristics are defined rather precisely, and thus if adjustments for individual difference are made, there is a known basis for the dose estimation procedure and for the estimation of the adjustment factor needed for a specified type of individual. ...

d) Ideally, each characteristic which is specified should have some indication of the range of this parameter in the population... Except for a few characteristics - such as weight, height, etc. - which are obtained rather easily, it is likely that the health physicist will have to be content with data which embody all these imperfections for some time to come.

e) The Task Group agreed to distinguish carefully the values specified for Reference Man from others quoted to indicate the extent and variety of the data available on each characteristic.

The Task Group recognized its own limitations in providing this compendium, but laid the foundation for the gathering of biological data by the health physics community. The authors advised that "it remains for the various organizations with control of radiation exposure at the national or regional levels to determine what modification of Reference Man, if any, may be appropriate for the population at risk." As well, they hoped that this publication would be useful despite its imperfections, and that it would be improved upon and extended in the future.

In the 1960s, there was a shift from the use of radionuclides for therapeutic purposes to diagnostic purposes; radiopharmaceuticals emitting gammas that could escape the body and provide information about the location of decay were emphasized over

therapeutic beta-emitting radionuclides. This prompted several members of the Society of Nuclear Medicine (SNM) to improve the methods of estimating radiation absorbed dose. Deficiencies identified at the time included incomplete descriptions of radionuclide emissions, inconsistent methods of estimating dose, inadequate models of the human body, and inaccurate and limited biokinetic information. The Society's ad hoc committee on dose calculations was organized to address these concerns and held its first meeting in 1964. During the second meeting of this committee, the name Medical Internal Radiation Dose (MIRD) Committee was chosen (Smith 1968).

2.2. The MIRD Approach

The MIRD Committee sought a formalism for internal dosimetry that could be applied to all radionuclides and models, regardless of the classification of emissions. The Committee developed a simplified approach for estimating absorbed doses to normal organs and to the whole body from administered radiopharmaceuticals. This approach is largely based on the unified theory for calculating radiation absorbed dose published in 1968 (Loevinger and Berman 1968a).

The mean absorbed dose to an organ from an internally deposited radionuclide is dependent on the physical and chemical characteristics of the radionuclide in terms of the type of radiation emitted and the spatial and temporal distribution of the radionuclide in the body. The material in which the energy is deposited is commonly referred to as the target, while the material from which the ionizing radiation originates is referred to as the source. Hence, the average absorbed dose to a target region irradiated by a source region is given as (Howell 1994):

$$\bar{D}_{(target \leftarrow source)} = \left(\frac{\tilde{A}_{source}}{m_{target}}\right) \times \sum_i \Delta_i \varphi_{i(target \leftarrow source)} \quad (1)$$

where

- $\bar{D}$ = the mean radiation absorbed dose (mGy);
- $\tilde{A}$ = cumulated activity (MBq h);
- m = mass (kg);
- i = type of radiation emitted;
- Δ = mean energy emitted per nuclear transition (originally termed the equilibrium dose constant) (mGy kg MBq^{-1} h^{-1}); and
- φ = absorbed fraction, or AF.

It should be noted that a target region may also be a source region. In this case, the dose to the target region from itself is termed the self-dose; it is almost always the largest contributor to an organ's total absorbed dose. The total body could be considered a source region when the radionuclide is uniformly distributed throughout the body.

The cumulated activity is the time integral from zero to infinity of the activity within the source region:

$$\tilde{A}_{source} = \int_0^\infty A_{source}(t)dt \quad (2)$$

where

- A = activity (MBq); and
- t = time (h).

The mean energy emitted per nuclear transition and the AF are calculated respectively as:

$$\Delta_i = K \times n_i E_i \quad (3)$$

where

- K = constant (0.5757 when E is expressed in MeV);
- n = the mean number of particles or photons emitted per disintegration; and
- E = the mean energy per particle or photon (MeV).

The mean radiation absorbed dose equation is a general dose equation; other dose equations derived from these may be considered special cases. The size or uniformity of the source or target regions, the source activity, and the absorbing material do not limit these equations (Loevinger and Berman 1968b).

The concept of the absorbed fraction was introduced by Ellett et al. (1964; 1965) to facilitate the calculation of absorbed dose from gamma rays. Later extended by Loevinger and Berman (1968a) to the concept of the specific absorbed fraction (SAF), these parameters represent the fraction of photon energy absorbed in a target region that is emitted from a source region. The calculations of absorbed and SAFs are complicated functions that depend on several factors. These factors include the shape, mass, and composition of the source and target regions, the distance between the regions, the composition of the medium through which the photon is traveling, and the probabilities of photon interactions for a given photon energy (Schlesinger 1978).

Calculation of the AFs for photons is complicated by the fact that the majority of the emitted energy is absorbed outside the source volume. Determinations of the AF and

the SAF can be made using Monte Carlo techniques, or the point isotropic function reported by Berger (1968) may be used to calculate values for the absorbed fraction and specific absorbed fraction directly:

$$\Phi_{\text{point}}(x) = \left[\frac{\mu_{en}}{\rho} \times \frac{e^{-\mu x}}{4\pi x^2}\right] \times B_{en}(\mu x) \quad (4)$$

where

- Φ_{point} = point isotropic specific absorbed fraction (kg^{-1})
- x = the distance between pairs of points in the source and target (cm)
- μ_{en} = linear energy absorption coefficient for photons (cm^{-1})
- ρ = mass density (kg cm^{-3})
- μ = linear energy attenuation coefficient (cm-1)
- B_{en} = point isotropic energy absorption buildup factor.

This equation describes the absorbed fraction of an isotropic point source within and infinite uniform absorber. The equation assumes that the energy absorbed around the point source is a function only of the distance from that source (Loevenger et al 1968b). It follows then that the SAF for any target and source regions is the mean of the point isotropic SAF for all pairs of points within the target and source regions (Loevenger et al. 1991):

$$\Phi_{\text{ip(target}\leftarrow\text{source)}} = \frac{1}{v_{\text{target}} \times v_{\text{source}}} \int_{\text{target}} \int_{\text{source}} \Phi_{\text{ip}}(x) dv_{\text{source}} dv_{\text{target}} \quad (5)$$

where

- Φ_{ip} = the isotropic specific absorbed fraction for a given point and a given radiation
- v_{target} = the target volume
- v_{source} = the source volume

Calculation of the AF for non-penetrating radiation is somewhat simpler because the range of these emissions in soft tissue is on the order of millimeters (Cloutier and Watson 1987). Hence, non-penetrating radiation distributed within a source is defined as depositing all its energy within that source and none outside. Then the equations for the absorbed fraction are (Cloutier and Watson 1987):

$$\varphi_{np(target \leftarrow target)} = 1 \tag{6}$$

$$\varphi_{np(target \leftarrow source)} = 0 \tag{7}$$

and the equations for the specific absorbed fraction are:

$$\Phi_{np(target \leftarrow target)} = \frac{1}{m_{target}} \tag{8}$$

$$\Phi_{np(target \leftarrow source)} = 0 \tag{9}$$

Tabulated AFs were recalculated in 1974 using the methods developed in MIRD Pamphlet No.5, but with a more realistic phantom and better statistical results (Snyder et al. 1974). The primary method of calculating AFs for photons was the Monte Carlo technique, which has the advantage of being able to take into account the approximate size, shape, position, density, and composition of the organs and the surrounding materials. When the coefficient of variation of these results exceeded 50%, the point isotropic specific absorbed fraction was used. Unlike MIRD Pamphlet No.5 values were reported for each case (Snyder et al. 1974).

In addition to recalculating the SAFs, the tabulated quantity S was introduced by Snyder and others (1974; 1975) as the absorbed dose per unit cumulated activity:

$$S_{(target \leftarrow source)} = \sum_i \Delta_i \Phi_{i(target \leftarrow source)} \quad (10)$$

where the S-value has units of mGy MBq^{-1} h^{-1} and all other variables have been previously described. This quantity simplified calculations by tabulating the mean energy emitted per nuclear transition and the SAF for selected radionuclides given specific source and target pairs. The dose equation then becomes:

$$\overline{D}_{(target \leftrightarrow source)} = \widetilde{A}_{source} \times S_{(target \leftrightarrow source)} \quad (11)$$

2.2.1. Biodistribution

To ascertain the absorbed dose to a subject from an internally deposited radionuclide, it is necessary to quantify the biodistribution of the substance throughout the tissues of the body. The distribution of the radionuclide will depend on its chemical form, the method of intake, the age and sex of the subject, as well as the metabolic function of the subject's organs and tissues in their healthy or diseased states.

Direct measurements of biological uptake, retention, and excretion of the radionuclide may be achieved by obtaining bioassay samples and through serial images of organ activity. Biological distribution data are most frequently acquired through animal experiments, where the animal is sacrificed at predetermined intervals after administration of known compounds of radioactive materials and the organs harvested for counting (Stabin 1994b). Animal data are then extrapolated to humans, usually according to the percent of activity found in the organ compared to the total body.

The data acquired must be processed to determine the total activity accumulated in those regions identified as sources, including the total body. Numerical and analytical methods, or a combination thereof, may be employed to determine the cumulated activity within each source. Alternatively, a compartmental model can be fit to the data when it is difficult to obtain an adequate representation of the time-course of the drug within multiple organs of the body. The activities determined from these methods are used to estimate the absorbed dose to the subject from the radionuclide of interest.

2.2.2. Residence times

It is often convenient to describe the biological distribution in a source region according to its fractional distribution within the body. This parameter, referred to as the residence time, may be described as the mean time that the radionuclide spends in a region (Berman 1977). It represents the biokinetic properties of the radionuclide within the body and is calculated as:

$$\tau_{source} = \frac{\int_0^\infty A_{source}(t)dt}{\int_0^\infty U(t)dt} \tag{12}$$

$$= \frac{\tilde{A}_{source}}{A_0} \tag{13}$$

where τ = residence time (h)
U = rate of intake (MBq h^{-1}); and
A_0 = intake activity (MBq).

The absorbed dose equation is now:

$$\overline{D}_{(target \leftarrow source)} = A_0 \tau_{source} \times S_{(target \leftarrow source)} \tag{14}$$

but can be rearranged to yield the mean dose to a target from a source per unit activity:

$$\frac{\overline{D}_{(target \leftarrow source)}}{A_0} = \tau_{source} \times S_{(target \leftarrow source)} \quad (15)$$

2.2.3. Limitations of the MIRD approach

There are limitations that affect the accuracy of radiation absorbed dose estimates. Some of these limitations are the consequence of producing this practical schema. These limitations include: 1) the assumption of uniform activity distribution within a target, 2) the assumption of uniform activity distribution within the remainder of the body, 3) the assumption that each region is homogeneous in composition and density, 4) the assumption that non-penetrating radiation emissions are completely absorbed within the source, and 5) the use of generalized S-values for subjects who vary in age, size, and metabolic function (Loevinger 1990; Kassis 1992; Howell et al. 1999).

The physical properties of radionuclides are well characterized and much effort is placed on continuously improving the mathematical properties of models, both at the macroscopic and microscopic scales. However, these are only two of the three requirements for calculating radiation absorbed doses; a void still exists in the knowledge of biological properties of most radiopharmaceuticals, and the uncertainty in this component is far greater (Loevinger 1969; Stabin 1999; Wilder et al. 1999).

2.3. The ICRP Approach

ICRP has developed models to represent the behavior of radionuclides that have entered the human body via inhalation and ingestion, and also systemic models for the metabolism of radionuclides after the uptake into the blood. Beginning in the 1950s,

methods were developed for modeling the metabolism of radionuclides. The resultant models were used to infer the dose in an individual using default parameters for size and weight of individuals and their organs. ICRP Publication 2 presented recommendations for the dosimetry of internally deposited radionuclides. These recommendations focused on controlling the dose to one or more critical organs and described retention patterns in these organs using single-component exponential functions. Within these early models, no consideration was given to recycling of material back into systemic circulation after being excreted from an organ (Boecker 1998).

The recommendations, models, and physiological parameters given in ICRP Publication 2 were revised in the 1970s in a series of publications, beginning with the introduction of Reference Man within Publication 23 in 1975 (ICRP 1975). Publication 26 was issued in 1977 and included new dose limits and secondary limits for use in radiation protection. ICRP Publication 26 introduced and defined two dose limits for internal exposure. The first limit of 0.5 sievert (Sv) committed dose equivalent was to control non-stochastic effects to any organ or tissue, where committed dose refers to dose accumulated over 50 years following an exposure. The second dose limit of 0.05 Sv committed effective dose equivalent was to control stochastic effects to the body (ICRP 1977).

Publication 30 (ICRP 1979) and its Supplements (ICRP 1980, 1981, 1988b) incorporated large amounts of data beyond that contained in Publication 2 while referencing the recommendations issued in Publication 26 (ICRP, 1977) and the anatomical and physiological data in Reference Man (ICRP, 1975). The respiratory tract model provided in ICRP Publication 30 contained 10 compartments (including pulmonary

lymph nodes), and described translocation from one compartment to another within the respiratory tract, translocation to the gastrointestinal tract, and absorption into the bloodstream. Pathways including absorption from the GI tract of material previously cleared from the lung and swallowed were considered (Potter 2004) and organ retention patterns were described using sums of exponential functions (Boecker 1998).

2.3.1. Description of the ICRP Method

ICRP Publication 30 (ICRP 1979) presents a dosimetric formulation that is similar, in structure, to that of the MIRD method. Publication 56 (ICRP 1989) extends the formulation to address age-specific dosimetry. These publications present the dosimetric framework, provide biokinetics data for selected nuclides, and include tabulations of the dose per unit intake (dose coefficient) for inhalation and ingestion intakes as applicable to a reference individual.

The ICRP dosimetric formulations focus attention on two parameters that represent: (1) the activity within the source regions and (2) the dose in the target tissues per unit activity in the source regions.

2.3.2. Metabolic Models

The metabolic models recommended in ICRP Publication 30 (1979) are generally considered to be the best supported comprehensive set of models describing the biokinetics of radioelements. These models were designed and intended for interpreting occupational exposures of a typical adult; however, for lack of commonly accepted approaches applicable to special subgroups of the population, they are frequently viewed as the proper

point of departure for evaluation of internal exposures to the general population.

Each of the metabolic models of ICRP 30 is a mathematical summary of observations and assumptions concerning the net retention of a radioelement in organs or the whole body of adult humans. These models are based on direct observations of the early distribution and the net retention of radioelements in organs or whole bodies of experimental animals and humans, the equilibrium distribution of elements in Reference Man as described in ICRP Publication 23 (1975), analogies among chemical families of elements, and broad assumptions where information is lacking (Leggett et al. 2008).

Publication 30 applies the term transfer compartment to the various body fluids that allow for the distribution of a radionuclide to the systemic organs following an intake (ICRP 1979). The activity in any body compartment is described in terms of a system of linear ordinary differential equations:

$$\frac{d}{dt}A_i = \sum_{\substack{j=1 \\ j\neq i}}^{n} \lambda_{ij} A_j - A_i \sum_{\substack{j=1 \\ j\neq i}}^{n} \lambda_{ji} \qquad (16)$$

where

- λ_{ij} = the fractional transfer of material from compartment j to compartment i
- λ_{ji} = the fractional transfer of material from compartment i to compartment j

The system of equations is solved as an initial value problem; that is at time zero, nonzero activities are assigned to the intake compartments with all other compartments assigned a zero value. In ICRP Publication 56, the transfer coefficients between compartments i and j are dependent on age of the individual which, of course, changes during the period the radionuclide resides within the body.

Inhalation

The ICRP 30 lung model is applied to radionuclide-bearing aerosols introduced into the breathing passages by inhalation. The model identifies four major respiratory regions: nasopharynx (NP), tracheo-bronchial tree (TB), pulmonary region (P), and lymphatic tissue (L). Inhaled materials are assumed to belong to one of three discrete clearance classes, according to how rapidly they are removed from the pulmonary region. These solubility classes are designated as D (removal accomplished in days), W (weeks), and Y (years). Fractional depositions of inhaled particles in the first three of these regions are given by the fraction D_{NP}, $D_{TB,}$ $D_{P,}$ respectively. The sum of these fractions is less than one, with the remainder being material that is exhaled. The deposition fractions are functions of the activity median aerodynamic diameter (AMAD) of the inspired aerosol (Eckerman 1994).

Each major region is subdivided into compartments, and labeled with the letters *a, b,..., j*. Material deposited in the NP region in compartment *a* is available for absorption into body fluids, while that deposited in compartment *b* is eventually swallowed and enters the GI tract. Similarly, material deposited in compartment *c* of the TB region is absorbed into body fluids, while Compartment *d* represents material that is being moved upward by ciliary action, out of the lungs and into the GI tract. Material from compartments *f* and *g* of the pulmonary region also enters compartment *d* and is moved upward and into the GI tract, with material from *f* being cleared rapidly from the lungs while that from *g* progresses very slowly. Compartment *e* in the pulmonary regions represents absorption into body fluids, and material is removed from compartment *h* by lymphatic drainage (Eckerman 1994).

Under this system, lymphatic tissue is divided into two compartments (*i* and *j*), with material that leaves compartment *i* entering body fluids. Compartment *j* represents material that is strongly retained in lymph and is applied only in the case of Class Y material to 10% of the lymphatic burden (Eckerman 1994).

A task group was created to review the respiratory model presented in ICRP-30 and make revisions based on research since the 1960's. This was done in part because many studies involving animals resulted in radioactive material being cleared from the respiratory tract at different rates than those given by the ICRP-30 model. The D, W, and Y classifications were revised. The research used to derive the model entailed greater knowledge of the anatomy and physiology of the respiratory tract, the deposition and clearance of particles, and the biological effects of radioactive particles. The ICRP-30 respiratory model is used to calculate dose by averaging over the entire mass of the lung while the ICRP-66 respiratory model takes into account differences in radiation sensitivity among the different tissues of the lung and allows the calculation of dose to these specific tissues. This respiratory model is much more complex than that of the ICRP-30 respiratory model as more detail is taken into consideration including: age, race, sex, breathing characteristics and habits, health detriment of the lungs, and target tissues with different sensitivities to radiation (ICRP 1994). The model of the ICRP-66 respiratory tract considers the morphometry of the respiratory tract, the respiratory physiology, the radiation biology, deposition, clearance, and dosimetry.

The ICRP 66 Human Respiratory Tract Model (HRTM) distinguishes five regions: Extrathoracic airways, divided in anterior nasal passage (ET_1) and posterior nasal-oral passage (ET_2), including also pharynx and larynx. Thoracic airways are divided into

bronchial (BB), bronchiolar (bb) and alveolar-interstitial (AI) regions (ICRP 1994). The alveolar region is arbitrarily divided into three compartments to describe different phases of clearance from this region. Thus, compartments within the AI region are defined on a kinetic basis rather than an anatomical or physiological basis (Leggett et al 2008).

Lymphatic tissues (LN_{ET} and LN_{TH}) are associated with extrathoracic and thoracic airways, respectively. Deposition in each region of the respiratory tract is determined by the aerosol particle size and breathing parameters. Clearance from the respiratory tract is treated as two competing processes: (1) particle transport by mucociliary clearance and translocation to lymph nodes and (2) absorption to blood. Particle transport is a function of the deposition site in the respiratory tract and of particle size.

Since mechanical transport is time dependent, most regions are subdivided into several compartments with different clearance rates. Material deposited in ET_1 is removed mechanically either by nose blowing or mucosal removal. Absorption to the blood is treated as a function of the deposition site in the respiratory tract and of the physicochemical form of the radionuclide. Specific dissolution rates are normally recommended. If no specific information is available, default absorption parameters are given for three dissolution types (Doerfel et al 2008);

- Type F: 100% absorbed with a half-time of 10 minutes. Almost all of the material deposited in BB, bb, and AI is rapidly absorbed. 50% of the material in ET_2 is rapidly absorbed, with the remaining 50% being cleared to the GI tract by particle transport.
- Type M: 10% of material is absorbed with a half-time of 10 minutes. The remaining 90% is absorbed with a half-time of 140 days. 70% of the material

deposited in the AI region makes it to body fluids, and there is rapid absorption of about 10% of the material that deposits in the BB and bb regions, as well as 5% of the material deposited in the ET_2 region.

- Type S: 0.1% of the material is absorbed with a half-time of 10 minutes and 99.9% is absorbed with a half-time of 7,000 days. 10% of material deposited in the AI region eventually reaches body fluids, but there is little absorption from the ET, BB, or bb regions.

The respiratory tract deposition is material specific in the case of the inhalation of vapors. The HRTM assumes that total and regional deposition in the respiratory tract is determined only by the size distribution of the aerosol particles (Doerfel et al 2008). Values are given for three default classes, namely SR-0, SR-1 and SR-2, which characterize different solubility and reactivity features of inhaled compounds (ICRP 1994).

Ingestion

The ICRP model describing the behavior of ingested radionuclides was originally described in Publication 30. This model is composed of four compartments describing the kinetics in the stomach (St), small intestine (SI), upper large intestine (ULI) and lower large intestine (LLI). Mathematically, each segment is viewed as a compartment whose contents clear into its successor by first-order kinetics, without feedback. The uptake into blood takes place from the small intestine at a rate $\lambda_{ab}\, q_{SI}$, where λ_{ab} is the transfer coefficient (d^{-1}) and q_{SI} is the activity within the content of the small intestine (Eckerman 1994). The equations describing the four primary compartments of the model are:

$$\frac{d}{dt}q_{St} = -(\lambda_{St} + \lambda_R)q_{St}, \qquad q_{St}(0) = 1 \tag{17}$$

$$\frac{d}{dt}q_{SI} = -(\lambda_{SI} + \lambda_R + \lambda_{ab})q_{SI} + \lambda_{St}q_{St}, \qquad q_{SI}(0) = 0 \tag{18}$$

$$\frac{d}{dt}q_{ULI} = -(\lambda_{ULI} + \lambda_R)q_{ULI} + \lambda_{SI}q_{ULI}, \qquad q_{ULI}(0) = 0 \tag{19}$$

$$\frac{d}{dt}q_{LLI} = -(\lambda_{LLI} + \lambda_R)q_{LLI} + \lambda_{ULI}q_{ULI}, \qquad q_{LLI}(0) = 0 \tag{20}$$

The transfer coefficients λ_{St}, λ_{SI} , λ_{ULI} , and λ_{LLI}, govern clearance from the segment indicated by the subscript into the successor, or in case of the lower large intestine, out of the tract. The coefficients are the reciprocals of the mean residence times tabulated in the Publication (ICRP 1979).

Absorption from the GI tract is characterized by a transfer factor (f_1) that specifies the fraction of activity in the small intestine transferred to blood. Its value is related to the chemical properties of the ingested compounds (ICRP 1979). This factor ignores the loss of material due to radioactive decay and, therefore, the f_1 value is given by:

$$f_1 = \frac{\lambda_{ab}q_{SI}}{(\lambda_{SI} + \lambda_{ab})q_{SI}} \tag{21}$$

ICRP Publication 100 (2006) greatly expanded the Publication 30 model with the Human Alimentary Tract Model (HATM). The HATM gives consideration to all alimentary tract regions, including the oral cavity, esophagus, stomach, small intestine, right colon, left colon, and rectosigmoid colon. Gender- and age-dependent parameter values are given for organ dimensions and content transit times through regions of the tract. Publication 100 maintains the Publication 30 default assumption that absorption to blood occurs exclusively in the small intestine. However, the HATM allows absorption to be

specified for other regions when such absorption is supported by new information (Doerfal et al. 2008).

Other Routes of Intake

When considering other routes of intake, such as absorption through the intact skin or wound, less information is available. Internal exposure resulting from wounds almost always arises because of accidents in the workplace, rather than as a result of routine operations that are subject to the normal environmental controls. Uptake from wounds can vary greatly depending on the circumstances of a particular incident and in practice the assessment of internal contamination is treated on a case-by-case basis. As a result, the ICRP has generally not given advice on assessing doses from intakes of radionuclides transferred from wound sites to blood and other organs and tissues (ICRP 2012). Information on the transfer of radionuclides from wound sites has, however, been reviewed by a Scientific Committee of NCRP and these data have been used to develop a model to describe the transfer of material from wounds after intakes in different physico-chemical forms (NCRP, 2007).

There is no general model for the entry of radionuclides through the skin. This is largely due to the many factors that must be taken in to account, such as: the chemical form of the radioactive material, the location of the contaminated area, and the physiological state of the skin. Generally, intact skin is an effective barrier against the entry of substances into the human body. However, a few elements, such as tritiated water or iodine, may be readily transferred across the skin barrier into tissue and body fluids (ICRP 1979, ICRP 1995a).

Systemic models are also proposed by ICRP for modeling the metabolism of radionuclides after the uptake into blood. These models are used in connection with the above intake models in case of a contamination via inhalation or ingestion, but they are applied also directly in case of a systemic contamination (e.g. by injection or skin contamination from tritiated water). Specific models are given for each radionuclide or for groups of chemically similar radionuclides. Publication 30 models were intended to be applied to workers, and Publications, 56, 67, 69, and 71 analyzed 31 elements and provided biokinetic models that may be applied to infants, children, and adult members of the public (ICRP 1979; ICRP 1989; ICRP 1993; ICRP 1997a; ICRP 1995c).

As the availability of data has allowed, the ICRP models have been made to be physiologically realistic with regard to the dynamics of organ retention and excretion so that they are applicable to the interpretation of bioassay data as well as the calculation of dose coefficients. The trend is increasingly toward the tendency to develop more realistic biokinetic models based on physiological information that result in both more realistic dose and bioassay coefficients. Such kinds of models already were developed, for example, for alkaline earths and actinides in ICRP Publication 67 (1993). Because most activity is not excreted directly from the source organs or tissues, but is transferred to blood again from where it distributes to source organs or tissues again or is excreted, these types of models are often called “recycling models (Nosske et al. 2011).”

2.3.3. Limitations of the ICRP Models

The format for the type of metabolic models eventually used in ICRP Publication 30 evolved at a time when computations were done largely by hand and simplicity of

model structure was an overriding concern. The requirement of a simple mathematical format and the lack of a firm physiological foundation lead to a rather inflexible retention model with some major disadvantages. As an example, the underlying curve-fitting approach precludes the incorporation of a great deal of valuable physiological information and physiologically reasonable assumptions that could be used in characterizing the sometimes complex behavior of radioelements in humans (Leggett et al. 2008).

The format of the ICRP models often does not permit extension to non-standard man (person with anatomical or metabolic characteristics different from Reference Man, such as a child or older individual), because there is usually insufficient data with which to develop new parameter values for special subgroups by the fitting techniques that characterize most of the reference man models. This issue was recognized by the IAEA and prompted the creation of a Reference Asian Man that better approximated the anatomical and physiological characteristics of that subpopulation (IAEA 2008), and by the ICRP, leading to the creation of its set of age-specific dosimetric models (ICRP 1989; ICRP 1993; ICRP 1997a; ICRP 1995c).

Age limitations have specifically been recognized by the ICRP. The ICRP has recognized that many anatomical and physiological parameters reach a plateau in the 30s and then decline after about age 45. Adults over the age of 70 years old are generally excluded from modeling data sets because of the substantial changes in the body after that age (Cristy 1994). ICRP-89 was published in 2003 for the purpose of revising and extending "the information in Publication 23 as appropriate, and to provide additional information on individual variation among grossly normal individuals resulting from differences in age, gender, race, or other factors." Publication 89 presents reference

values for further anatomical and physiological data for adult males, females, and children (ICRP 2002). Nevertheless, adults beyond the age of 15 years old are lumped into two sex-segregated classes, irrespective of the physiological changes that occur later in life.

It has been postulated that these problems can be overcome to a large extent by building biokinetic models upon a strong physiological foundation. If such an approach were used, the complexity of the structure needed could be varied from one situation to another. As an example, to estimate doses accurately for a very short-lived radionuclide, one could use a highly detailed and realistic representation of the movement of that material during the time shortly after entry into the body. If considering longer-lived radionuclides, one may be able to simplify and/or combine many tissues and fluids that are important only for descriptions of very short-term kinetics (Leggett et al. 2008). The chief limitation of the ICRP models for the purposes of this study is that the physiological component of transfer coefficients from one compartment to the other are often not described in the publications well enough to allow a researcher to determine the impact of physiological changes on the kinetics of the material being studied.

2.4. Pharmacokinetic Models

Pharmacokinetics (PK) is defined as the study of the time course of drugs and their metabolites in the human body; as they move through the different bodily fluids and organ systems and get eliminated in urine and excreta. The definition also includes the mathematical relationships that form the building blocks required to develop models so as to be able to understand and interpret data obtained from such studies (Gibaldi and Perrier 1975). When this approach is used in an environmental context, xenobiotics such as a

specific radionuclide are studied in place of a drug and the field is referred to as "toxicokinetics" (TK).

2.4.1. Basic Principles of Pharmacokinetic Modeling

One of the simplest forms of PK/TK modeling involves performing a mathematical analysis of the time course data for a population. A model is developed and the data are fitted so as to be able to predict the rate constants involved in the modeled processes such as the rates of metabolite formation. A model is then laid out and the data are fitted to estimate the rate constants k_1, k_2, k_{12} and k_{21} (Andersen 2003).

A second form of modeling is compartmental modeling, where the body is divided into different units called "compartments". The simplest of this form of modeling is the "single-compartment" model, where the entire body is considered to be one homogenous unit. This does not mean that the chemical concentration is the same in the entire body. It means that the change of chemical concentrations in the plasma will influence similar chemical changes in the organ systems of the body. The single compartment models also assume a linear or first-order rate of elimination of a chemical from the body.

2.4.2. Physiologically-Based Pharmacokinetic Models

Physiologically based toxicokinetic and pharmacokinetic (PBPK) models are the mathematical descriptions of absorption, distribution, metabolism, and excretion (ADME) of xenobiotics in humans or animals. These models are used to estimate the levels of chemicals in the body tissues and fluids such as blood, hair, and urine. Fundamentally, the models consist of mass balances on different compartments in a human or animal body.

These compartments may represent specific organs, or multiple tissues lumped together. Physiologically-based pharmacokinetics/toxicokinetics aims to incorporate physically realistic restrictions and biological knowledge on the systems of equations. PBTK models can include many different organs and describe mass balances as differential equations. In these models, the chemical dose levels in the human tissues are calculated by integrating equations that use data on chemical properties and metabolic pathways from literature to estimate some of the parameters used in the model. The blood leaving all compartments recycles through a central compartment, typically the lung or a compartment representing the blood.

The most important facet of designing such PBPK/TK models is determining the number of compartments that the model will have. When determining how to group organ systems into compartments, both the anatomy and physiology of the body are considered. However, grouping determination may be complicated when sufficient information on the chemical kinetics and interactions in the human body are unavailable. Thus, the preliminary choice is often made based on the pool of information available in experimental literature.

Following the determination of compartments, mass balance equations are written for the various compartments accounting for the initial, free (and thus mobile) and bound portions of the chemical. When the membrane permeability (PA) for a particular chemical is much greater than the blood flow rate into the compartment (Q_j), then the compartment is said to be flow limited or perfusion limited. This means that the rate of chemical uptake into a compartment is influenced more strongly by the blood flow rate into that compartment rather than the rate at which the chemical partitions into the compartment,

which depends on the cell membrane permeability.

Since this is a flow limited compartment, the concentration leaving the compartment is equal to the free product or the mobile portion of the chemical that had entered the compartment and did not bind to the tissue. The concentration subsequently leaving the compartment is simply the chemical concentration in the compartment divided by a unitless tissue-blood partition coefficient for the radionuclide.

There already exist databases of values for partition coefficients for humans and animals for a wide variety of chemicals (Poulin and Krishnan 2005a; 2005b; 2006a; 2006b). PBPK models are often intended to estimate target tissue dose in species and under exposure conditions for which little or no data exist. Thus, if a complete pharmacokinetic data set were available, then there would be no need to develop a PBPK model (NCEA 2006).

Chapter 3. MATERIALS AND METHODS

3.1. Statistical Comparison of parameter values

A one-sample t test was conducted on the parameter values to evaluate whether their means were significantly different from the accepted ICRP parameter values for Reference Man. Data were analyzed using Microsoft Excel for Windows, and a p-value of less than 0.05 was determined to be statistically significant.

A Mann-Whitney U test was selected to compare the data from the reference man age group to the data from age ranges above the maximum expected age for reference man because the data was considered to be continuous and nonparametric. As with the one-sample t test, data were analyzed using Microsoft Excel for Windows, and a p-value of less than 0.05 was determined to be statistically significant.

3.2. Model development

The chief limitation of the ICRP dosimetry models for the purposes of this study is that the physiological component of transfer coefficients from one compartment to the other are often not described in the publications well enough to allow a researcher to determine the impact of physiological changes on the kinetics of the material being studied. Due to that limitation, a model in which the physiological processes are explicitly presented is needed.

PBPK models offer the ability to estimate chemical concentrations in specific organs or tissue by mechanistically considering whole tissue systems linked together dynamically by blood flow (Shelley et al., 2008). The body organs are treated as parallel compartments that represent organs or tissues, with each compartment characterized by

appropriate physiological, physico-chemical, and biochemical parameters. Compartments can represent single organs or can represent a family of tissues or organs. Tissues are consolidated into a single compartment whenever feasible, unless the physiological, physicochemical or biochemical parameters have noticeably different effects on the chemical uptake and disposition (Krishnan et al. 2001).

Most PBPK/PBTK models developed to date focus on the pharmacokinetics of large drug molecules rather than elements or simple molecules. Because of this, existing PBPK models may not sufficiently reflect the kinetics of simple molecules in the human body. Metals and metalloids in particular present unique modeling challenges. The half-lives of key toxic metals in humans span days (e.g. arsenic and chromium), months (e.g. methylmercury), and decades (e.g. lead and cadmium). Existing model formulations for metals differ greatly to account for the varying toxic endpoints and distribution mechanisms in the body (El-Masri and Kenyon 2008; Nordberg and Kjellstrom 1979; O'Flaherty 2000; Shipp et al. 2000), making comparison to other models difficult.

3.2.1. Overview

Model building is a complex process that requires an accurate understanding of the physical processes being modeled as well as reliable sources of data that can be used in the models. Physical processes are often explained by virtue of the rates at which they occur. As an example, in calculus based mathematical modeling the inter-relationships between the processes are equations and the rates are derivatives. These derivatives are differential equations, which form the building blocks of the mathematical modeling of physical processes.

The overall structure of a whole-body PBPK model is a series of tissue and organ blocks linked together by blood circulation, mimicking the anatomical structure of mammalian body. Although there are no rules available regarding which tissues should be included or excluded, a typical whole-body PBPK model consists of core, special, and reservoir tissues (Nestorov 2003). The core tissues comprise blood, heart-lung segment, liver (for metabolized materials), kidneys (for urinary excreted drugs), and adipose tissue (for lipophilic materials). The special tissues include sites of material administration, sites of material action or deposition, tissues with atypical (e.g., nonlinear) kinetics, and tissues for which experimental data is available. Tissues that constitute a considerable mass of the mammalian body such as muscles, skin, adipose, and bone may be included as reservoir tissues.

PBPK models compartmentalize various tissue groups into a system on the basis of physical and biochemical parameters. Mass-balance differential equations are used to represent the behavior of a substance within the system (Brown 1994). The first widely recognized PBPK model was completed by Ramsey and Andersen in 1983. They simulated the behavior of inhaled styrene in rats and humans (Ramsey and Andersen 1984). Their model organized tissue into the following four groups:

- highly perfused tissues
- moderately perfused tissues
- slowly perfused tissues
- tissues that metabolize a large amount of styrene (liver).

The model was first simulated to represent rats and then scaled up to represent human exposures. The rat model was found to be very accurate when compared to actual

rat exposure data used in experiments. This provided a rational basis for the use of PBPK modeling in the extrapolation of animal data to chemical hazards in humans (Ramsey and Andersen 1984).

The Ramsey and Andersen model has become the foundation of PBPK research (Brown 1994). The alveolar space and lung blood compartments in this model represent the initial intake of a lipophilic chemical through inhalation. The fat tissue compartment is very important due to a chemical's affinity for fat. The muscle tissue compartment falls under the slowly perfused compartment, and represents lean tissues. The richly perfused tissue group would include those organs where blood flow is rapid, such as the heart, kidney, and brain. And finally, the liver compartment represents significant metabolic activity. Each of these compartments is linked through arterial and venous blood flow (Q variables) and specific chemical concentrations (C_v and C_{art} variables) to each compartment.

Using numerical integration of a system of differential mass balance equations, the rate of input, output, and metabolic activity through each compartment in the model can be simulated (Brown 1994). This basic model can be changed to include more tissue compartments to address a specific exposure, as well as account for the parameter differences between subpopulations.

Though a PBPK model is designed to simulate the “real body,” determining which tissues to be included as compartments is based primarily on the intended use of the model. Tissue compartments generally included are a) essential elimination organs, such as liver and kidney; b) important depots, such as adipose for lipophilic drugs (Fiserovabergerova 1992); c) plasma/blood compartment for compounds with significant binding to plasma

protein or accumulation in red blood cells (Tanaka et al., 1999); d) tissues related to specific exposure routes, such as lung for inhalation exposure and skin for dermal exposure (Sarangapani et al. 2002; Reddy et al. 2005); e) target tissues (Blakey et al. 1997). At the same time, model development should follow the principle of parsimony in order to avoid unnecessary over-parameterization.

Based on the available physicochemical and biochemical information of the material of concern, such as molecular size, lipophilicity, tissue membrane permeability, tissue protein binding, and tissue metabolism, the tissue blocks are categorized into flow (perfusion) rate-limited or permeability rate-limited. Flow rate-limited models represent the simplest and the most widely used case. They are based on the assumption of a well-mixed model, where drug partitioning across tissue membranes is instantaneous and homogenous (Nestorov 2003; Gibaldi and Perrier 1975). Thus, the rate limiting step is blood flow and sub-compartments can be combined into a single compartment. Flow models are normally assumed when the material being modeled has a small molecular weight or when the tissue has a relatively small volume (Nestorov 2003; Blakely et al. 1997; Igari et al. 1982; Ritschel and Banerjee 1986).

Models for different chemicals have alternative lumping arrangements or compartment perfusion assumptions. However, they can be considered subsets of the same generalized model outlined in Figure 3.1. Blood flow rates and volumes of compartments which are common to different models are equal, regardless of chemical. Parameters of lumped compartments (e.g. slowly perfused and rapidly perfused) vary by chemical, but are constrained to be consistent with the sum of remaining whole body parameters. As stated earlier, software has been developed to estimate physiological values for a majority

of the tissue groups outlined in Figure 3.1 (e.g. PK-SIM (Edgington et al. 2006; Willmann et al. 2003; Willmann et al. 2007), P3M (Price et al. 2003)).

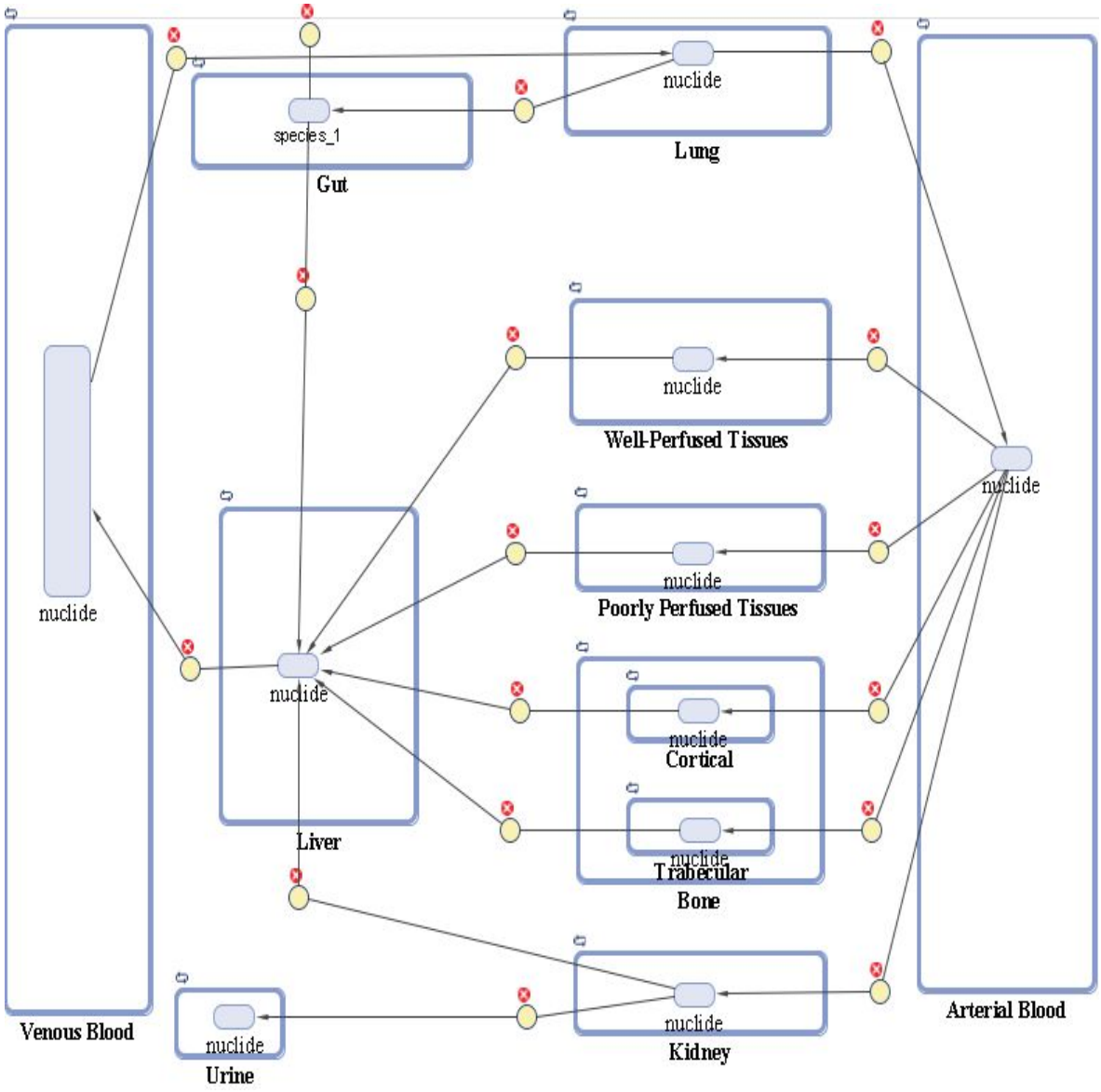

Figure 3.1. Generalized PBPK model with lumped compartments.

Because this study is intended to apply to multiple radionuclides and multiple routes of intake, lumping arrangements may not be appropriate and a model must be described in which the majority of organs are considered independently.

When constructing such mathematical models certain steps are followed. These include the following:

1. The independent and dependent variables are determined and letters are assigned to represent the variables.
2. The appropriate unit of measurement for each variable is selected.
3. The basic principle describing the process is written. The principle is then expressed mathematically in terms of the earlier defined variables. This may involve the introduction of physical constants or parameters and determination of appropriate values for them, or it may involve the use of auxiliary or intermediate variables that must then be related to the primary variables.
4. The solution of these functional interrelationships provides the model outcome.

In probabilistic applications, distributions describing organ physiology are defined for the generalized model. The relationships between the generalized model and chemical-specific PBTK sub-models are deterministic. This property is useful when applying sensitivity analysis methods to integrated exposure/PBPK models for multiple contaminants, and when simulating mixtures consistently from source-to-dose in “virtual" individuals of a population. PBTK models in the literature often include components specific to a transport process, absorption route, or physiological condition. Some examples include distributed-parameter models for diffusion into skin (Roy et al. 1996) and bone (O’Flaherty 2000), maternal/fetal models for pregnancy (Corley et al. 2003), and kidney sub-compartments for renal transport processes (Corley et al. 2005). Despite discretization of compartments, total tissue volumes and blood flow rates remain

consistent with the whole-body model.

3.3. Model equations

The equations for this model are developed based on the model for styrene inhalation in rats previously developed by Ramsey and Andersen (1987) and the more recent PBPK model developed by Cole (2001). The format of the equations from these sources is adopted and they are then modified and extended based on the modeling needs of this study. Each tissue compartment is typically described with a mass balance ordinary differential equation (ODE) in time which describes the change in the amount of the chemical over time, typically in units of mass per time or number of particles per time. The general form of an ordinary differential equation describing a compartment shows that the accumulation (or change in amount per unit time) in any compartment is the sum of all input rates minus the sum of all output rates. Hence:

$$V\frac{dC}{dt} = \sum Q_{in}C_{in} - \sum Q_{out}C_{out} \qquad (22)$$

where the concentration C (mass/volume) is represented as a function of inlet arterial concentration C_{in}, compartment blood flow rate Q (volume/time), and the compartment volume V. Usually, the differential equations are expressed in terms of mass rather than concentration since compartment volumes may change with time. Mass balance equations for compartments become more complex with the addition of metabolic or transport terms, and with the discretization of the compartment space.

Mass balance must be maintained throughout the model, e.g., total blood flow (cardiac output) should equal the sum of blood flows to the various compartments. The

mass balance differential equations, which serve as a mathematical representation of the body, can be numerically integrated to calculate the amount of contaminant in a tissue or organ (i.e., compartment).

3.3.1. Compartment mass balances

Compartments that are perfusion-limited assume that rapid diffusion occurs for a chemical between the blood and tissue, causing blood flow rate to be the limiting transport step. Diffusion-limited compartments assume diffusion to be the rate-limiting step. Since diffusion is a function of both the chemical and tissue properties, the incorporation of perfusion- or diffusion-limited compartments vary by the PBTK model. As mentioned previously, perfusion-limited models represent the simplest and the most widely used case. The majority of the tissues considered are assumed to be well-stirred compartments, i.e. that the unbound tissue concentration is at equilibrium with the unbound concentration in venous blood emerging from the tissue.

Once the structure of the whole-body PBPK model and the rate-limiting features of the tissue blocks have been defined, the model is mathematically represented by a series of mass balance differential equations. If a non-eliminating tissue with flow limited mass transport was encountered, the mass balance equation would be:

$$V\frac{dC}{dt} = Q\left(C_{art} - \frac{C}{K_P}\right) \tag{23}$$

where Q, V, and C are the blood flow, anatomic volume, and concentration of the drug in the tissue, respectively. C_{ART} is the material concentration in the arterial blood, K_P is the tissue-to-blood partition coefficient. Examples of tissues that fall into this category are the adipose tissue, skeletal muscle, cardiac tissue, brain, skin, and tissues of the pancreas.

Modeling eliminating tissues, or those whose uptakes are not governed by flow-limited mass transport, is more difficult.

Because bone is a much more dynamic organ than was once thought (O'Flaherty 2000), determination of the amount of material deposited on and incorporated into bone depends on several different parameters and processes. First, bone may be considered to be two distinct organs; cortical or compact bone, and trabecular or spongy bone. During our analysis, bone marrow was considered separate from the mineralized portions of bone and was, instead, lumped in with adipose tissue.

3.3.2. Bone Surface and Matrix

Total bone volume before the age of 30 years old can be estimated as a fraction of total body mass (O'Flaherty 1993; O'Flaherty 2000):

$$V_{Bone} = 0.0168 \times BW^{1.188} \quad (24)$$

Cortical and trabecular bone volumes can then be determined as follows (O'Flaherty 1993; O'Flaherty 2000):

$$V_{Bone} = V_{B-C} + V_{B-T} \quad (25)$$

where cortical bone volume is estimated to remain a constant fraction of total bone given by $V_{B-C} = 0.8 \times +V_{Bone}$ and trabecular bone volume is assumed to be a constant fraction of total bone given by $V_{B-T} = 0.2 \times +V_{Bone}$. At the age of 30 in both males and females, trabecular bone growth ceases and the tissue is assumed to have reached its maximum mass. Cortical bone is assumed to do so the same before the age of 35. At this point, bone volume can no longer be estimated solely based on the mass of the body and must take into

account the differences in bone formation and reabsorption rates (O'Flaherty 1993; O'Flaherty 2000). O'Flaherty developed separate derived bone volume relationships for individuals between the ages of 31 and 35, and for individuals older than 35 years (O'Flaherty 2000):

$$\begin{aligned} V_{Bone}(31-35) &= 0.8 \times V_{B(30)} + (0.2 \times V_{B(30)} \times (1 + (0.65 \times 1.188 \times V_{B(30)}) \\ &\times \left(\frac{-3 \times BW_C}{3 + Age}\right)\Big\{^{Age}_{0} \\ &- \left(\frac{600 \times \lambda \times BW_A^2}{600 \times \lambda \times BW_A + \lambda \times BW_A \times \exp\ (\lambda \times BW_A \times Age)}\right)\Big\{^{Age}_{0} \\ &- \left(0.006 \times Age \times 0.2 \times V_{B(30)}\right)\Big\{^{Age}_{0} \end{aligned} \tag{26}$$

$$\begin{aligned} V_{Bone}(36+) = \Bigg[& 0.8 \times V_{B(30)} \times (1 + (0.35 \times 1.188 \times V_{B(30)}) \times \left(\frac{-3 \times BW_C}{3 + Age}\right)\Big\{^{Age}_{0} \\ & - \left(\frac{600 \times \lambda \times BW_A^2}{600 \times \lambda \times BW_A + \lambda \times BW_A \times \exp\ (\lambda \times BW_A \times Age)}\right)\Big\{^{Age}_{0} \\ & - \left(0.004 \times Age \times 0.8 \times V_{B(30)}\right)\Big\{^{Age}_{0} \Bigg] \\ & + \Bigg[(0.2 \times V_{B(30)} \times (1 + (0.65 \times 1.188 \times V_{B(30)}) \\ & \times \left(\frac{-3 \times BW_C}{3 + Age}\right)\Big\{^{Age}_{0} \\ & - \left(\frac{600 \times \lambda \times BW_A^2}{600 \times \lambda \times BW_A + \lambda \times BW_A \times \exp\ (\lambda \times BW_A \times Age)}\right)\Big\{^{Age}_{0} \\ & - \left(0.006 \times Age \times 0.2 \times V_{B(30)}\right)\Big\{^{Age}_{0} \Bigg] \end{aligned} \tag{27}$$

where

- $V_{B(30)}$ = bone volume at the age of 30,
- BW_C = an estimate of the body weight of a child, held constant at 23 kg for males and 22 kg for females.
- λ = a logistic constant used to fit the expression defining growth to measured data. Held as 0.0095 $(kg\text{-}yr)^{-1}$ for men and 0.017 $(kg\text{-}yr)^{-1}$ for women.

- BW_A = the reference body weight for an adult, with a value of 50 kg for males and 34 kg for females (O'Flaherty 2000).

Skeletal kinetics is largely hormonally mediated, and the balance of hormones within the female body shifts during the period known as perimenopause (roughly 55-65 years of age for most women). For women between these ages, bone volume is given by (O'Flaherty 2000):

$$
\begin{aligned}
V_{Bone}(36+) = \Bigg[& 0.2 \times V_{B(30)} \times \left(1 + (0.35 \times 1.188 \times V_{B(30)}) \times \left(\frac{-3 \times BW_C}{3 + Age}\right)\right)\begin{cases} Age \\ 0 \end{cases} \\
& - \left(\frac{600 \times \lambda \times BW_A^2}{600 \times \lambda \times BW_A + \lambda \times BW_A \times \exp\ (\lambda \times BW_A \times Age)}\right)\begin{cases} Age \\ 0 \end{cases} \\
& - \left(0.006 \times Age \times 0.2 \times V_{B(30)}\right)\begin{cases} Age \\ 0 \end{cases} \\
& - \left(0.01 \times \left(Age - \frac{\cos\left(0.3 \times (Age - 55)\right)}{0.3}\right)\right)\begin{cases} Age \\ 0 \end{cases}\Bigg] \\
& + \Bigg[\left(0.8 \times V_{B(30)} \times \left(1 + (0.65 \times 1.188 \times V_{B(30)}\right)\right. \\
& \left.\times \left(\frac{-3 \times BW_C}{3 + Age}\right)\right)\begin{cases} Age \\ 0 \end{cases} \\
& - \left(\frac{600 \times \lambda \times BW_A^2}{600 \times \lambda \times BW_A + \lambda \times BW_A \times \exp\ (\lambda \times BW_A \times Age)}\right)\begin{cases} Age \\ 0 \end{cases} \\
& - \left(0.004 \times Age \times 0.8 \times V_{B(30)}\right)\begin{cases} Age \\ 0 \end{cases} \\
& - \left(0.01 \times \left(Age - \frac{\cos\left(0.3 \times (Age - 55)\right)}{0.3}\right)\right)\begin{cases} Age \\ 0 \end{cases}\Bigg]
\end{aligned}
\tag{28}
$$

The amount of material on the cortical bone surface depends on blood flow to the bone as with other organs, but also depends on the kinetics of the bone material itself. The

volume of the cortical surface of the bone and is assumed to be 0.2% of the total cortical bone volume, which is V_C (O'Flaherty 1991). The cortical bone resorption rate (R_{CR}) is sex- and age-dependent and is given by (O'Flaherty 2000):

$$R_{CR}(Age < 35) = 0.35 \times (1.188 \times 0.0168 \times BW^{0.188}) \times \frac{3 \times BW_C}{(3 + Age)^2} \times \frac{\exp(-\lambda \times BW_A \times Age)}{((1 + 600 \times \exp(-\lambda \times BW_A \times Age))^2)} \quad (29)$$

$$R_{CR}(Men\ Age > 35) = 0.35 \times (0.1 + (4 \times \exp(-4.4) + 4 \times \sin(4.4) + \exp(24)) \times (V_{B-35})) - \left(0.35 \times 1.188 \times 0.0168 \times BW^{0.188} \times \left[\frac{3 \times BW_C}{(3 + Age)^2} \times \frac{\exp(-\lambda \times BW_A \times Age)}{((1 + 600 \times \exp(-\lambda \times BW_A \times Age))^2)}\right]\right) + (0.004 \times 0.8 \times V_B) \quad (30)$$

$$R_{CR}(Women\ Age 55 - 65) = 0.35 \times (0.1 + (4 \times \exp(-4.4) + 4 \times \sin(4.4) + \exp(24)) \times (V_{B-35})) - \left(0.35 \times 1.188 \times 0.0168 \times BW^{0.188} \times \left[\frac{3 \times BW_C}{(3 + Age)^2} \times \frac{\exp(-\lambda \times BW_A \times Age)}{((1 + 600 \times \exp(-\lambda \times BW_A \times Age))^2)}\right] + (0.004 \times 0.8 \times V_B) + (0.01 + 0.01 \times \sin(0.3 \times (Age - 55)))\right) \quad (31)$$

V_{AFC} is the clearance of xenobiotic material from blood to bone during the mineralization of newly apposed cortical bone (L/yr) and is the product of the unitless fractional clearance of material from plasma to forming bone and the cortical bone formation rate (L/yr). Cortical bone formation rate depends on age and can be expressed as

(O'Flaherty 1991):

$$R_{F-C} = R_{BF} \times (0.35) \quad (32)$$

where 0.35 is a constant fraction of bone modeling or remodeling activity attributed to trabecular bone (O'Flaherty 1991) and R_{BF} is the total bone formation rate. The age dependence is also reflected in the total bone formation rate, which is represented by (O'Flaherty 1991):

$$R_{BF} = V_{Bone}(Age) \times R_{FBF} \quad (33)$$

where

$$V_{Bone}(Age \leq 35) = 0.0168 \times BW \times \exp 1.188 \quad (34)$$

up to the age of 35, which is generally accepted as the age of maximum cortical bone mass (O'Flaherty 1991). R_{FBF} is the fractional bone formation rate and is given by (O'Flaherty 1991):

$$R_{FBF} = (0.1 + (4 \times \exp(-4.4)) + 4 \times \sin(4.4) + \exp\big(0.6 \times (Age - 11)\big) \quad (35)$$

Trabecular bone follows the same equation formats as cortical bones with two important exceptions: the trabecular coefficient of bone volume is 0.2 rather than 0.8 as mentioned in the description of Equation 17, and the trabecular coefficient for bone formation and resorption is 0.65 rather than 0.35.

3.3.3. Respiratory System

The lung can be divided into two sub sections; namely the alveolar region of the lung and the blood region of the lung. Assumptions for developing the equations for this model are based on the ones presented by Kulkarni (2004), listed as follows:

1. Ventilation is continuous and not cyclic.
2. Conducting airways act as inert tubes, carrying vapor to pulmonary or gas exchange regions.
3. Diffusion of material across lung cell and capillary walls is nearly instantaneous when compared with blood flow through the lung.
4. All material from the inspired air appears in arterial blood (i.e. there is no significant storage of chemicals in the lung tissue and insignificant lung mass). Note that this assumption is not realistic for particulate inhalation.
5. Material concentrations in alveolar air and arterial blood with lung are related by the blood air partition coefficient (P_b). (e.g. $C_{alv} = C_{art}/P_b$)

Simulations of the human lungs are difficult both due to the complexity of biological structures and nonlinearities in the equations that describe fluid flows, such as the airflow in the human lungs.

The partitioning of a material from the air into the blood will depend on how much of the material is inhaled which is further dependent on the alveolar ventilation rate (Q_a) and the inhaled concentration (C_{inh}). By modeling the lungs as a well-mixed compartment with an average, one-directional airflow in the region of gas exchange (i.e., with air moving through the lungs with a constant flow rate equal to the alveolar ventilation rate, Q_P), and with rapid equilibration between lung air and blood in the lung alveoli, the concentration in the blood exiting the lungs (C_a), can be described as (Ramsey and Andersen 1984):

$$C_a = \frac{Q_P \times C_{inh} + Q_C \times C_{VEN}}{Q_C + {Q_P}/{P_b}} \tag{36}$$

where

- C_{VEN} = the concentration in the venous blood compartment,
- P_b = the blood : air partition coefficient,
- Q_C = the cardiac output,
- C_{inh} = the inhaled concentration of the material during the exposure and zero after the exposure ends.

While this equation is sufficient for inhalation of material in the gas phase, the behavior of particulate materials is somewhat more complicated. Analysis of particle transit within the airways must account for air flows, particle characteristics, particle clearance, and the probability that the particle will be deposited in the various airway regions.

Considering a given airborne material concentration, the proportion of inhaled particles that deposit in the head, ciliated regions of the lung, and alveoli is determined by the size of the particles and the individual's breathing rate. Generally, smaller particles will deposit deeper in the lung while coarser particles tend to be deposited in the head and ciliated regions where they are cleared by ciliary action or secretions and swallowed. Very small particles will, to a large extent, not interact with the walls of the respiratory system and will be exhaled. Particles in the range of 0.1-5 μm play an important role in both occupational and environmental exposure (Tsuda et al. 1994). Estimates of alveolar deposition based on ICRP formulae for CSP (Cigarette Smoke Particulate) typically of size 0.1-1 μm, under-predict the alveolar deposition fraction (Gower and Hammond 2007).

The most important mechanisms for deposition within the respiratory system are

inertial impaction, diffusion and gravitational settling (Brain and Valberg 1979). Coarse particles mainly deposit by impaction. Impaction occurs when the air changes direction and is therefore highest at the dividing point of the tracheal bifurcation and in the tracheobronchial region where the streamlines bend sharply at branching locations. Settling is most efficient in the narrow, horizontally oriented, airways further down in the lungs, and deposition by diffusion is the principal mechanism for particles with a diameter below 0.5 μm. Deposition by diffusion primarily takes place in small airways where residence time is long.

A useful term in describing the transport of a particle through human airways is the deposition efficiency, which is defined as the ratio of the number of particles depositing on a surface to the number of particles entering the airway region of that surface. The total deposition efficiency in the human airways is given by (Hinds 1999):

$$\eta = \eta_I + \eta_S + \eta_D - \eta_I\eta_S - \eta_S\eta_D - \eta_D\eta_I + \eta_I\eta_S\eta_D \qquad (37)$$

where the subscripts *I*, *S*, and *D* denote the deposition efficiency due to impaction, sedimentation, and diffusion, respectively. However, since deposition in the acinar airways is necessary for direct transition to systemic circulation, it is necessary to split the total deposition efficiency into separate efficiencies for each of the three lung regions.

Fractional deposition of particles in the airways of the respiratory tract may be estimated using theoretical or empirical models or some combination of the two. Most models of particulate deposition in the lung are based upon the classic work by Weibel (1963) in which the detailed morphology of the lung in terms of lung airway dimensions was first delineated. Weibel classified lung airways into 24 generations, beginning with the trachea (generation 0), and ending with the alveolar sacs (generation 23), and reported a

high degree of regular branching between generations. For simplicity in many models, it is assumed that the airway dimensions do not change during respiration (Tippayawong and Damrongsak 2003).

Deposition efficiency in the extrathoracic airways can be determined using the empirical equation presented by Cheng (2003).

$$\eta_0 = 1 - \exp(-20.4 \times D_B^{0.66} Q^{-0.31} - 2.78 \times 10^{-4} \rho d_p^2 Q) \qquad (38)$$

where

- Q = the mean respiratory flow rate in liters per minute,
- d_p = the particle diameter in microns,
- ρ = the density of the particle in grams per cubic centimeter.

D_B is the Brownian diffusion coefficient as expressed by (Choi and Kim 2007):

$$D_B = \frac{C_c kT}{3\pi\mu d_p} \qquad (39)$$

where

- k = the Boltzmann's coefficient,
- T = the temperature in Kelvins,
- C_c = the Cunningham Correction factor, used to account for the relative velocity of the air at the surface of the particle. For the purposes of this analysis, we allow C_c to remain constant at 1.168 for a 1 μm particle at 298 K.
- μ = the viscosity of air (Choi and Kim 2007).

Particles larger than 10 μm are generally deposited in the tracheobronchial region, and are rapidly cleared from the lungs (Hinds 1999). In this region velocities are high and heavy particles do not follow airstreams at the bifurcation of two bronchi and impact the airway walls at branching locations. These particles are then not available for diffusion into systemic circulation. For the conducting (tracheobronchial region) airways, the impaction, sedimentation, and diffusion depositions are each considered separately. Deposition due to impaction can be calculated by (Hinds 1999):

$$\eta_I = 1 - \frac{1}{(14.01 \times Stk^{1.977} + 1)} \tag{40}$$

Here, *Stk* is the unitless Stokes number, used to characterize curvilinear motion and defined by (Hinds 1999):

$$Stk = \frac{\rho d_p^2 C_c u}{18 \mu d} \tag{41}$$

where

- d = the airway diameter and
- u = the mean airflow velocity (Hinds 1999).

Deposition due to sedimentation is determined using (Choi and Kim 2007):

$$\eta_S = 1 - \exp\left(\frac{-2g\tau Al \sin\phi}{\sqrt{\pi a} Q}\right) \tag{42}$$

where

- A = the total cross sectional area of the airway generation,
- g = the gravitational acceleration constant,

- l = the length of the airway, a is the cross sectional area of the individual airway branch,
- φ = the gravity angle, or angle of airway inclination from the gravitational force vector.

The relaxation time, τ, is the time required for the particle to adjust its velocity as force conditions change and is given by (Hinds 1999):

$$\tau = \frac{\rho_p d_p^2 C_c}{18\mu} \tag{43}$$

Tracheobronchial deposition due to diffusion is determined using (Choi and Kim 2007):

$$\eta_D = 1 - 0.819 \times \exp\,(-14.63\Delta) - 0.0975\,\times \exp\,(-89.225\Delta) - 0.0325\,\times \exp\,(-228\Delta) - 0.0509\,\times \exp\,(-125.9\Delta^{2/3}) \tag{44}$$

where Δ is the diffusion parameter and is defined as (Choi and Kim 2007):

$$\Delta \equiv \frac{\pi D_B l}{4Q} \tag{45}$$

Deposition in the alveolar (acinar) region of the lungs depends on particle size, breathing frequency, and tidal volume. Particles smaller than approximately 2 μm have the potential to penetrate into the gas-exchange regions of the lung. Very small particles (< 100 nanometers) may pass through the lungs and into systemic circulation (Hinds 1999).

The average number of particles entering a single alveolus during inhalation is given by the expression (Choi and Kim 2007):

$$M_{1/2} = C_0 \int_{t_0}^{T/2} Q_A dt \tag{46}$$

where

- C_0 = the particle concentration in the airway leading to that alveolus,
- Q_A = the airflow into the alveolus,
- T = the breathing period.

The airflow in the alveolus can be described by (Choi and Kim 2007):

$$Q_A(t) = \frac{2}{T}\frac{V_T}{V_{FRC}} \times V_A(FRC) \tag{47}$$

where

- V_T = the tidal volume
- V_{FRC} = the functional residual capacity
- $V_A(FRC)$ = the volume of the alveolus at the end of a full inspiration.

Then the expression for the number of particles in the alveolus is (Choi and Kim 2007):

$$M_{1/2} = \frac{1}{2} C_0 V_a(FRC) \frac{V_T}{V_{FRC}} \left(1 + \cos\left(\frac{2\pi t_0}{T}\right)\right) \tag{48}$$

Alveolar deposition due to diffusion is determined using (Choi and Kim 2007):

$$\eta_D = 1 - \frac{6}{\pi^2} \sum_{n=1}^{\infty} \frac{1}{n^2} \times \exp\left(\frac{-4n^2\pi^2 D_B t}{d_{eq}^2}\right) \tag{49}$$

in which n is a variable that ranges from 1 to infinity. Because an alveolus is not completely spherical but has a portion open to the airway duct, we describe the volume of the space

using d_{eq}, the diameter of a sphere that has the same surface area as an individual alveolus. The equivalent diameter is then approximated to be 0.838 (Choi and Kim 2007; Weibel 1963).

Sedimentation deposition in the alveoli is (Choi and Kim 2007):

$$\eta_S = \left[1 + \min\left({}^{d_S}\!/_{d_{eq}}, 1\right)\right]^2 \times \left[1 - 0.5 \min {}^{d_S}\!/_{d_{eq}}, 1\right] - 1 \quad (50)$$

where d_s is the sedimentation distance and is expressed as (Choi and Kim 2007):

$$d_S = g\tau t \quad (51)$$

Deposition fraction is partly determined by the breathing pattern. Important parameters are tidal volume (TV), breathing frequency and flow rate. A large TV increases deposition. A high breathing frequency increases the efficiency of impaction and thus the deposition of particles larger than 1 μm, while the deposition of smaller particles is favored by a low frequency (Kim and Jaques, 2004).

Studies have shown that the ultrafine particles deposited in the alveolar region of the lungs are not easily phagocytized. However experiments conducted on rodents demonstrate that ultrafine particles can easily break the epithelial cell barrier and reach the blood/lymph circulation system. Inhaled particles may end up in systemic circulation and the lymphatic system once they reach the pulmonary interstitial sites following migration across alveolar epithelial cells (Oberdörster et al., 2005). For simplification, we will assume that all particles deposited in the alveolar surface are translocated to the interstitium, where they can be phagocytized by macrophages, transferred to the lymphatic system, or transferred to the systemic circulation. The amount of material in the blood

exiting the lungs (C_a) can then be described as (Kolanjiyil 2013):

$$M_{art} = M_{alv} \times K_{alv:bl} \tag{52}$$

where $K_{alv:bl}$ is the fractional mass transfer rate of the deposited material from the alveolar interstitial layer to the circulating blood.

3.3.4. Liver

The liver accepts input blood from the arterial blood supply (extraportal flow), the spleen, the pancreas, and the gut tissue via the hepatic portal vein. For the liver (LV), the above equation is modified to include input from the gut (GU), as well as to include a hepatobiliary clearance pathway (Péry et al. 2009):

$$V_{LV}\frac{dC_{LV}}{dt} = \tag{53}$$
$$Q_{EPORT} \times C_{art} + Q_{SPLEEN} \times \frac{C_{SPLEEN}}{K_{P,SPL}} + Q_{PAN} \times \frac{C_{PAN}}{K_{P,PAN}} + Q_{STOM} \times \frac{C_{STOM}}{K_{P,STOM}}$$
$$+ Q_{GU} \times \frac{C_{GU}}{K_{P,GU}} - Q_{LV} \times \frac{C_{LV}}{K_{P,LV}} - CL_{LV} \times C_{LV}$$

where CL_{LV} is the hepatic metabolic clearance (Péry et al. 2009). Total blood flow to the liver (Q_{LV}) is then the sum of the extraportal flow and the incoming flows from the gut, stomach, pancreas, and spleen (Péry et al. 2009):

$$Q_{LV} = Q_{EPORT} + Q_{GU} + Q_{ST} + Q_{PAN} + Q_{SPLEEN}. \tag{54}$$

Hepatobiliary clearance is the net result of material uptake into the liver cells, followed by biliary secretion. Hepatic clearance can be described using the venous equilibration model (Péry et al. 2009):

$$CL_{LV} = \frac{Q_{LV} \times f_U \times CL_{int}}{Q_{LV} + f_U \times CL_{int}} \tag{55}$$

where

- Q_{LV} is the hepatic blood flow,
- f_U is the unbound fraction of the material of interest,
- CL_{int} is the intrinsic hepatic clearance.

Hepatic intrinsic clearance can be estimated based on the well-stirred model and absence of any transmembrane barrier (Pang and Rowland 1977):

$$CL_{int} = \frac{CL_{bile} Q_{HV}}{(Q_{HV} - CL_{bile}) \times f_P} \tag{56}$$

where f_P is the fraction of the unbound xenobiotic concentration in plasma; CL_{bile} is the in vivo biliary clearance and Q_{HV} is the hepatic venous blood flow which is the sum of the flows of hepatic artery (Q_{HA}) and portal vein (Q_{PV}).

3.3.5. Renal System

For the kidneys (KD), the basic mass balance equation is modified to include the renal clearance, CL_{KD} (Pang and Rowland 1977):

$$V_{KD} \frac{dC_{KD}}{dt} = Q_{KD} \left(C_{art} - \frac{C_{KD}}{K_{P,KD}} \right) - CL_{KD} \times C_{KD} \tag{57}$$

In this equation, CL_{KD} can be modeled by (Rowland 1984):

$$CL_{KD} = (f_u \times GFR) \times (1 - F_r) \tag{58}$$

where GFR is the glomerular filtration rate, and F_r is the fraction reabsorbed, as given by (Jongeneelen and tenBerge 2011):

$$F_r = \int_{-\infty}^{x} \frac{\exp\left(-t^2/2\right)}{\sqrt{2\pi}} dt \quad (59)$$

Where

$$x = 2\,(\log(K_{OW}) + 0.5) \quad (60)$$

and K_{OW} is the octanol:water partition coefficient that is generally used to determine the other tissue partition coefficients.

The amount of material excreted in the urine, assuming no additional uptake by the urinary bladder or ureters, is then

$$V_{UR}\frac{dC_{UR}}{dt} = CL_{KD} \times C_{KD} \quad (61)$$

where volume of urine (in liters) at time t is computed as:

$$V_{UR}(t) = V_{UR}(0) + F_{UR} \times t. \quad (62)$$

For this model, $F_{UR}$is the urinary flow rate in liters per minute (Péry et al. 2009).

3.3.6. Gastrointestinal System

Although gastric emptying and small intestinal transit flow can influence the rate and extent of drug absorption after oral intake of a material, few of the previous PBPK models have fully considered these factors. A compartmental absorption and transit (CAT) model for estimating the fraction of dose absorbed and the rate of drug absorption was developed by Yu and Amidon (1999) and has been adopted for this study. In the Yu model, the gastrointestinal tract is divided into three segments: stomach, small intestine, and colon. The transit flow in the small intestine is described by seven compartments, where a

material transfers from one compartment to the next one in a first-order fashion. The assumptions for the CAT model include:

1. Absorption from the stomach and colon is insignificant compared with that from the small intestine;
2. Transport across the small intestinal membrane is passive;
3. A material moving through the small intestine can be viewed as a process flowing through a series of segments, each described by a single compartment with linear transfer kinetics from one to next, and all compartments may have different volumes and flow rates, but have the same residence times.

Under these assumptions, the absorption and transit in the gastrointestinal tract can be depicted as follows:

Stomach (Yu and Amidon 1999)

$$\frac{dM_{ST}}{dt} = -K_{ST}M_{ST} \tag{63}$$

The above equation assumes that any ingested material is immediately deposited in the stomach and that there is no absorption or loss in the mouth or esophagus.

Small intestine (Yu and Amidon 1999)

$$\frac{dM_n}{dt} = (CL_{LV} \times C_{LV}) + K_t M_{n-1} - K_t M_n - K_a M_n, \quad n = 1, 2, 3, \ldots, 7 \tag{64}$$

For the first small intestine compartment (n=1), $K_t M_0$ is replaced by $K_{ST}M_{ST,}$ the input from the stomach. If we let M_a be the amount of material absorbed, then the rate of material absorption from the intestine to the blood plasma is given by (Yu and Amidon 1999):

$$\frac{dM_a}{dt} = K_a \sum_{n=1}^{7} M_n \tag{65}$$

Large intestine (Yu and Amidon 1999)

$$\frac{dM_{Co}}{dt} = K_{t,n} M_n - M_{Co} K_{tCo} \tag{66}$$

where

- M_{ST} = the amount of xenobiotic in the stomach,
- M_{Co} = the amount of xenobiotic in the colon,
- M_n = the amount of xenobiotic in the *n*th compartment,
- t = the elapsed time,
- K_{ST}, K_t, and K_a are the rate constants of gastric emptying, small intestinal transit, and intrinsic absorption, respectively.

CL_{LV} and C_{LV} have been previously defined for hepatic clearance to the gut.

The rate constants for intestinal transit and intrinsic absorption can be determined by (Yu and Amidon 1999):

$$K_t = \frac{n}{T_{si}} \tag{67}$$

$$K_a = K_t \frac{1}{\sqrt[n]{1-F} - 1} \tag{68}$$

where

- F = the fraction of material absorbed,
- n = the number of compartments in the small intestine,
- T_{si} = the intestinal transit time.

3.3.7. Circulatory System

The final step in writing the mathematical model is to provide the equations for the heart-lung segment (HLS), venous (VEN), and arterial (ART) blood to establish the mass balance for the closed system (Brochot et al 2008):

$$V_{HLS}\frac{dC_{HLS}}{dt} = Q_{HLS}\left(C_{VEN} - \frac{C_{HLS}}{K_{P,HLS}}\right) \quad (69)$$

$$V_{VEN}\frac{dC_{VEN}}{dt} = \sum_{i=1}^{n} Q_i \times \frac{C_i}{K_{P,i}} - Q_{HLS} \times C_{VEN} \quad (70)$$

$$V_{ART}\frac{dC_{ART}}{dt} = Q_{HLS}\left(\frac{C_{HLS}}{K_{P,HLS}} - C_{ART}\right) \quad (71)$$

where

- *QHLS* = the cardiac output,
- *Qi*, = flow rate in the *i*th tissue
- *Ci*, = concentration in the *i*th tissue
- *KP,i* = the tissue-to-blood partition coefficients for the ith tissue.

While toxic metals are not eliminated from the blood by exhalation, many instead bind to (or diffuse into) red blood cells. Such chemicals are transported into tissues by concentration gradients in the plasma as opposed to the whole blood, and chemicals within the red blood cells are sequestered. If the relationship between chemical concentration in the blood and plasma is assumed to be linear (typically for free-diffusion), the following partitioning coefficient equation describes the relationship between whole blood, plasma, and red blood cell concentrations (Gerlowski and Jain, 1983):

$$K_{wbl/pl} = K_{rbc/wbl} \times Hc + (1 - Hc) \quad (72)$$

where

- $K_{wbl/pl}$ = the partition ratio of the material between whole blood (wbl) and plasma (pl);
- $K_{rbc/wbl}$ = the partition ratio of the material between red blood cells (rbc) and plasma
- Hc = the hematocrit (ratio of red blood cell volume to whole blood volume).

To convert a tissue/whole-blood partition coefficient to a tissue/plasma partition coefficient, it is multiplied by whole-blood/plasma partition coefficient.

3.4. Sensitivity Analysis

Sensitivity analysis in pharmacokinetics and pharmacodynamics (PD) is defined as the systematic investigation of the relationship between PK or PD model response(s) and perturbations occurring in the system structure and/or parameters (Nestorov 1999). Sensitivity analysis provides detailed information regarding the time course of the impact of each model parameter on model output(s) (Evans et al. 1994; Varkonyi et al. 1995; Spear et al. 1995). This information can be useful at the initial model specification stage in: (1) discriminating between which parameters that needs to be included and those that should be left out of the model (Nestorov et al. 1997); and (2) deriving an optimal PK or PD experimental design (e.g., sampling times, input doses, etc.) (Evans et al. 1994). At the model assessment and validation stage, the sensitivity analysis allows for the characterization of the degree of confidence in the final parameter estimates (Nestorov et al. 1997).

Sensitivity analysis methods can be classified as “Local” and “Global.” The Local methods depend on computation of analytical sensitivities; the partial derivatives of model output(s) with respect to model parameters (Clewell et al. 1994; Licata et al., 2001). The Global methods depend on Monte Carlo simulation techniques (Hetrick et al. 1991; Farrar et al. 1989; Portier and Kaplan 1989; Bois et al. 1990; Krewski et al. 1995). Briefly, in the Monte Carlo method, a probability distribution for each of the model input parameters is randomly sampled, and the model is run using the chosen set of parameter values. This process is repeated a large number of times until the probability distributions for the desired model outputs have been created. This method allows assessment of parameter uncertainty effect on the variability in the model output.

Despite the fact that the partial derivative methods don’t predict an overall model output variability, they allow ranking of model parameters according to their influence on the relative change in the model output. These methods don’t require the large numbers of simulations that are needed for the Monte Carlo methods, so they take significantly less computation time. For the Monte Carlo methods to be adequate, the input parameter distributions should reflect the true parameter variability. However, this information is usually not available (Clewell et al. 1994). Thus, partial derivative methods offer a simpler way to investigate parameter sensitivities than Monte Carlo methods.

There has sometimes been a tendency in model building to consider variability of a specific parameter, such as inhalation rate or the in vitro activity of a particular enzyme, as synonymous with the variability in dosimetry for in vivo exposures (Gentry and Clewell 2007). However, whether or not the variation in a particular physiological or biochemical parameter will have a significant impact on in vivo dosimetry is a complex function of

interacting factors. In particular, the structures of physiological and biochemical systems frequently involve parallel processes (e.g., blood flows, metabolic pathways, and excretion processes), leading to compensation for the variation in a single factor. Thus, it is often true that the variability in dosimetry may be more or less than the sum of the variability in each of the pharmacokinetic factors.

3.5. Test Case

Data available for model verification were reviewed to select the cases most suitable for this study. The criteria for selection included:

- Availability of well-documented assay data sets with multiple measurements, if possible;
- Study subject's age at time of intake known; and
- Quantity of radioactive material administered known.

Based on these criteria, data from a single case study was included for comparison to predicted values.

A 65-year-old male underwent myocardial perfusion imaging as part of an assessment of the severity and prognosis of ischemic heart disease. The patient had no known renal or hepatic insufficiency. An initial intravenous administration of 138.8 MBq ^{201}Tl in the form of thallous chloride was followed 3 hours later by a second intravenous administration of 34 MBq. Collection of 24-hour urine samples began two hours after the second administration. No chemical preparation was given to the samples prior to counting for 60 minutes on a high-purity germanium detector. Raw data as presented in the published study has been corrected for radiological decay (Blanchardon et al. 2005).

Chapter 4. DATA – PHYSIOLOGICAL CHANGES WITH ADVANCING AGE

Pharmacokinetics focuses on the concentration-time profile of a material and its metabolites within various body fluids and tissues and describes and allows the interpretation of the processes of absorption, distribution, metabolism and excretion (Gibaldi 1971). Two major aspects are involved in modulating the extent of ADME. The first one is physiochemical properties of the material of interest, such as molecular weight, lipophilicity, and pKa. The second is the gambit of biological/physiological factors of the body. It is the second of these two factors that is the main focus of this study.

Model parameterization refers to establishing plausible physiological, physicochemical, and biochemical parameters necessary for use in the model equations (Krishnan et al. 2001). Physiological properties include: body weight, organ weight, fractions of the body allocated to each compartment, tissue blood flow (i.e., blood flow to and from tissue), cardiac output, volume of tissues, and alveolar ventilation rate (Dixit et al. 2003; Reddy et al. 2005).

In many exposure assessment studies, doses are estimated for a hypothetical individual, often referred to as a "target" or "reference" individual, who is representative of a given population. In the case of a uniform exposure of an entire population, the doses to real people follow a distribution described by the variability in the population. The dose estimate to the target individual should actually be described by a range of values encompassing the true distribution (or the variability) of doses in the population. The importance and effects of the variability among individuals has been pointed out by IAEA (2008). In this section, the dependency of biokinetic parameters on age (within the adult age group) is explicitly investigated.

4.1. Body Composition and Structure

The distribution of materials within the body may be altered due to changes in body composition. Generally, there is a decrease in muscle mass and total body water and an increase in adipose tissue with age. An increase in body fat may increase the volume of distribution of lipophilic materials and prolong their elimination half-life and duration of action. The ICRP (1975) has recommended a reference human height of 176 cm for males and 163 cm for females, and a body weight of 70 kg for males and 58 kg for females. The ICRP values are based on the assumption that both males and females have attained their maximum height by the age of 18, and that adult body masses can be represented by and addition of 10% to the body mass of an 18 year-old male and a 16 year-old female (ICRP 2002). However, designation of reference body weights does not provide information on

Table 4.1. ICRP default body composition for males and females (ICRP 2001).

Parameter	Units	Reference Male Value	Reference Female Value
Body Mass	kg	73	60
Body Height	cm	176	163
Organ Masses			
Adipose Tissue	g	18,200	22,500
Adrenals	g	14	13
Blood	g	5,600	4,100
Bone	g	10,500	7,800
Brain	g	1,450	1,300
GI Tract			
Stomach	g	150	140
Small Intestine	g	650	600
Large Intestine	g	370	360
Heart	g	330	250

Table 4.2. (continued) ICRP default body composition for males and females (ICRP 2001).

Parameter	Units	Reference Male Value	Reference Female Value
Kidneys	g	310	275
Liver	g	1,800	1,400
Lungs	g	500	420
Lean Muscle	g	29,000	17,500
Pancreas	g	140	120
Skin	g	3,300	2,300
Spleen	g	150	130
Thyroid	g	20	17

the variability associated with body weight values. Stoudt et al. (1960) reported that the mean body weight for males was 71.7 ± 10 kg, and was 56.7 ± 8.6 kg for females. The ICRP default values for a reference male and female are presented in Table 4.2 (ICRP 2001).

4.1.1. Anatomy

Adipose tissue is known to be widely heterogeneous in both its composition and functional properties. Its general structure includes a rich, irregular vascular bed, with capillaries in contact with each adipocyte, or fat cell (Slavin 1985). The adipocytes, relatively large spherical cells containing lipid droplets that make up the bulk of each cell, are organized into a structure of lobules supported by connective tissue (Slavin 1985).

Skeletal muscle tissue is organized into distinct muscles, which perform lengthening, shortening, and stabilizing contractions across the joints of the body (McComas 1996). Muscle tendons form a musculo-skeletal junction which transfers contractile forces generated by the muscle cells to its origin and insertion points on the skeleton (Lieber 2010). This musculo-tendinous unit is composed of many muscle

fascicles bound together in a connective tissue fascia that tapers into a tendon. Each muscle fascicle is a bundle of muscle fibers enclosed in a sheath of connective tissue. While each fascicle spans the entire length of a muscle, each individual fiber within the fascicle may not (Lieber 2010).

4.1.2. Physiology

The major metabolic functions of adipose tissue include: the synthesis and storage of lipid in the form of triglyceride (Crandall and DiGirolamo 1990), the breakdown of triglyceride and the mobilization of lipid in the form of free fatty acids (Crandall and DiGirolamo 1990), and the uptake of fatty acids, glucose and amino acids (Slavin 1985).

Unlike many other organs, the adipose “organ" is located in multiple distinct depots throughout the body. Several studies have shown that there are pronounced differences in tissue composition, blood flow and metabolic activities across these depots (Crandall and DiGirolamo 1990; Crandall et al. 1997; Davidson and Beliles 1991; MacQueen et al. 1999; West et al. 1987), which suggests that a single perfusion-limited or diffusion- limited compartment may be insufficient to capture the behavior of adipose tissue as a whole. A possible modification to these models is the inclusion of many separate perfusion-limited or diffusion-limited compartments, each representing a distinct adipose depot and each with its own physiological parameters.

In addition to inter-depot differences in blood flow, metabolism and tissue composition, there are heterogeneities within each adipose depot itself. The sizes of individual fat cells greatly vary, as does the amount of lipid in each adipocyte, creating an uneven distribution of lipids across the depot (Hausman 1985).

It has been shown that the metabolic activities of adipose tissue are directly linked to its blood flow properties (Crandall and DiGirolamo 1990). As the metabolic process varies in different regions of tissue and in time, the perfusion of blood to those regions changes accordingly. Moreover, the blood flow to adipose tissue is affected directly by the local concentrations of substrates and hormones used in the process of metabolizing lipids (Crandall et al. 1997).

The functional status or functional capacity of a muscle (or a group of muscles), is a fitness measure determined by an ability to perform the tasks and necessary activities of daily living (Warburton et al. 2001; Starfield 2001). Strength, power, and endurance capacity are parameters of muscle functional capacity. A decline in any one of these can affect an individual's success in performing activities of daily living and lead to a loss of independence or disability (Warburton et al. 2001; Patterson et al. 2007).

4.1.3. Age-related changes

The rates of physiological changes that occur with age are highly individual, and there are also specific gender differences in body composition changes with age. In general, older people are shorter than younger people (Noppa et al. 1980). This is partly due to a secular trend in height, but also due to shrinkage of the spine with increasing age, ultimately caused by the loss in vertebral bone, kyphosis and scoliosis (Miller et al. 1988). Due to the increased rate of loss of bone mass after menopause in women, the decline in stature is larger in women than men (Cohn et al. 1986; Kuczmarski, 1989). Taren and Schler (1990) reported that the loss of height with age can reach up to 4.9 cm in women, almost twice that of men. Peak bone mass is usually reached by age 35 and decreases

thereafter.

Most studies show an increase in body weight from middle age to old age in healthy elderly subjects (Noppa et al. 1980). However, at very old age a decrease in body weight is observed (Steen et al. 1979). Maximum weight gain over the life span peaks at 35-55 years for men, whereas for women, peak weight gain occurs at approximately 55-65 years of age. Several cross-sectional studies illustrate an increase in body weight throughout early and middle adulthood (Guo et al. 1999; Chumlea et al. 2002; Carmelli et al. 1991; Lewis et al. 1997) until approximately age 60 at which point the weight trajectory begins to decline (Chumlea et al. 2002; Carmelli et al. 1991; Kyle et al. 2001). Longitudinal studies have confirmed these cross-sectional observations and have shown a decline in body weight in both sexes after 60 (Carmelli et al. 1991; Visser et al. 2003; Shimokata et al. 1989) or 70 (Gallagher et al. 2000; Raguso et al. 2006; Hughes et al. 2004) years of age.

The weight loss that occurs in older persons is likely not the same as the weight loss that is typically observed in younger individuals. In young and middle-aged persons, weight loss is often intentional (e.g., diet or exercise-induced) and represents improved body composition resulting in better health. Conversely, seniors that experience weight loss often do so unintentionally and this involuntary weight loss is often a marker of clinical and/or subclinical disease (Wannamethee et al. 2005). With advancing age the two major body tissues, skeletal muscle and fat, change in opposite directions. Skeletal muscle decreases (Doherty 2003) while there is a gradual increase in body fat (Villareal et al. 2005). Typically weight loss is observed when the loss of skeletal muscle exceeds the concurrent increase in body fat.

Muscle, bone, and water content remain relatively stable until the fifth or sixth

decade in life and then begin to decline (Going et al. 1995). Data from a study of elderly people ages 65-85 years indicates that these declines continue into the ninth decade of life and an average of 6-7% of these combine components may be lost over a 20-year span (Baumgartner et al. 1995). Wasting of appendicular skeletal muscle is the primary source of this decline, and accounts for approximately 60% of the lean tissue lost with aging (Baumgartner et al. 1998; Kirkendall and Garrett 1998).

Generally speaking, cross-sectional and longitudinal studies have shown that with advancing age there is an increase in fat mass and a decrease in muscle mass (Gallagher et al. 2000; Baumgartner et al. 1995; Forbes 1999; Hughes et al. 2002). Over the lifespan, women tend to have a lower percentage of lean body mass than men, with a preferential deposit of adipose tissue in the limbs and lower body, and more fat distributed subcutaneously than internally (Vogel and Friedl 1992). Gallagher and colleagues (Gallagher et al. 2000) demonstrated that after age 60 total skeletal muscle mass declined by 0.8 kg and 0.4 kg over a 5-year period in men and women, respectively. The corresponding values for changes in fat mass were a gain of 1.2 kg and a non-significant loss of 0.8 kg. These observations highlight the concurrent changes in these two major body tissues.

An absolute decline in muscle strength becomes most pronounced in the years following the sixth decade of life with losses of 1 – 1.5 % per annum reported in otherwise healthy adults (Skelton et al. 1994; Vandervoort 2002; Faulkner et al. 2007). Relative to young adults this decline eventually results in a 20 to 40% reduction in voluntary isometric strength by the seventh or eighth decade of life. Some evidence suggests that the lower body may experience greater declines in muscle mass, thickness, and strength with age

(Lynch et al. 1999; Janssen et al. 2000; Candow and Chilibeck 2005).

In addition to an increase in body fat, the distribution of fat also changes with age. Measurements of abdominal fat and fat around and within the muscles of thigh and upper arm made by magnetic resonance imaging or computed tomography show a redistribution of body fat with age. Elderly people tend to have relatively more fat accumulated around the abdomen and less fat at the extremities (Chien et al. 1975; Borkan and Norris 1977; Borkan et al. 1983; Enzi et al. 1986; Carmelli et al. 1991). In women total body fat and abdominal fat may increase especially after menopause, starting in the perimenopausal years (Svenden et al. 1995; Vogel and Friedl 1992).

A dehydrating effect has also been observed with aging. In the average normal subject, the body water comprises 60% of the body weight and 73% of the lean mass (Moore 1959). Fat and bone being relatively anhydrous, fatter individuals have a lower percentage of body water. Total body water decreases from 50% of total body weight in early adulthood to 45% in middle age (Going et al. 1995), and a possible loss of 4-6 liters by old age. Some studies indicate that there is no change in the water content of fat-free tissue due to proportional losses in both water and muscle (Deurenberg et al. 1989; Going et al. 1995), while others report slight increases in the water level of fat-free tissue with aging (Baumgartmener et al. 1991).

4.1.4. Data Summary

Body composition data were extracted from the 2005-2006 National Health and Nutrition Examination Survey (NHANES) databases, maintained at the Center for Disease Control and Prevention's (CDC) website (www.cdc.gov/nchs/about/major/nhanes/), as

presented below.

Table 4.3. American male population body composition means ± SD from the 2005-2006 NHANES data set.

Males

Age Groups	n	Body Mass (kg)	Height (cm)	Fat Free Mass (kg)	Total Body Fat (kg)	Percent Body Fat
10-19	1379	64.3 ± 17.1	168.7 ± 10.6	51.1 ± 10.9	13.2 ± 8.3	19.4 ± 7.4
20-29	1553	77.4 ± 17.3	173.8 ± 7.8	58.7 ± 10.0	18.8 ± 8.2	23.3 ± 6.5
30-39	1383	81.6 ± 17.0	174.8 ± 7.6	61.1 ± 10.3	20.5 ± 8.7	24.4 ± 6.2
40-49	1155	83.7 ± 16.7	174.3 ± 7.6	61.9 ± 10.2	21.8 ± 8.5	25.4 ± 5.8
50-59	792	84.1 ± 16.3	174.5 ± 6.9	62.0 ± 9.9	22.1 ± 8.3	25.6 ± 5.8
60-69	1055	81.7 ± 15.0	172.5 ± 7.1	59.9 ± 9.4	21.8 ± 7.7	26.1 ± 5.8
70-79	724	77.5 ± 14.1	171.2 ± 7.1	57.5 ± 9.1	20.0 ± 7.0	25.3 ± 5.8
80-89	472	72.6 ± 12.3	169.5 ± 6.8	54.5 ± 8.0	18.1 ± 6.6	24.4 ± 6.1
90-99	32	65.1 ± 12.1	167.1 ± 8.6	50.2 ± 8.0	15.0 ± 6.6	22.2 ± 7.2

Table 4.4 American female population body composition means ± SD from the 2005-2006 NHANES data set.

Females

Age Groups	n	Body Mass (kg)	Height (cm)	Fat Free Mass (kg)	Total Body Fat (kg)	Percent Body Fat
10-19	1448	59.5 ± 15.0	160.6 ± 7.2	40.3 ± 6.0	19.2 ± 9.9	30.6 ± 8.2
20-29	1511	66.4 ± 15.9	161.6 ± 7.0	42.6 ± 6.3	23.5 ± 10.7	34.1 ± 7.7
30-39	1632	73.0 ± 19.4	161.7 ± 7.1	45.1 ± 7.4	27.9 ± 13.1	36.6 ± 8.0
40-49	1248	74.7 ± 17.8	161.5 ± 6.6	45.4 ± 7.1	29.3 ± 11.7	38.0 ± 6.8
50-59	907	75.4 ± 17.9	160.8 ± 6.6	45.3 ± 7.1	30.1 ± 11.8	38.6 ± 7.0
60-69	1031	71.7 ± 15.6	159.0 ± 6.9	43.4 ± 6.5	28.2 ± 10.3	38.3 ± 6.6
70-79	817	68.2 ± 14.7	157.5 ± 6.6	42.4 ± 6.4	25.8 ± 9.6	36.8 ± 6.9
80-89	477	61.8 ± 11.7	155.1 ± 6.8	39.6 ± 5.3	22.2 ± 7.7	35.0 ± 6.9
90-99	44	53.7 ± 8.3	153.5 ± 5.2	37.1 ± 4.2	16.6 ± 6.1	30.1 ± 7.4

The above values support the general consensus in the literature that, for both females and males, height peaks in the third and fourth decades of life, followed by a very gradual decline (Figure 3.1). Lean body mass tends to peak in the fourth and fifth decades

before gradually declining in both sexes. Body fat percentage peaks somewhat later in the sixth decade. It is important to reiterate, however, that since these data come from a cross-sectional study, it is not possible to determine to what degree physiological processes are responsible for the variation, as opposed to secular trends within the population.

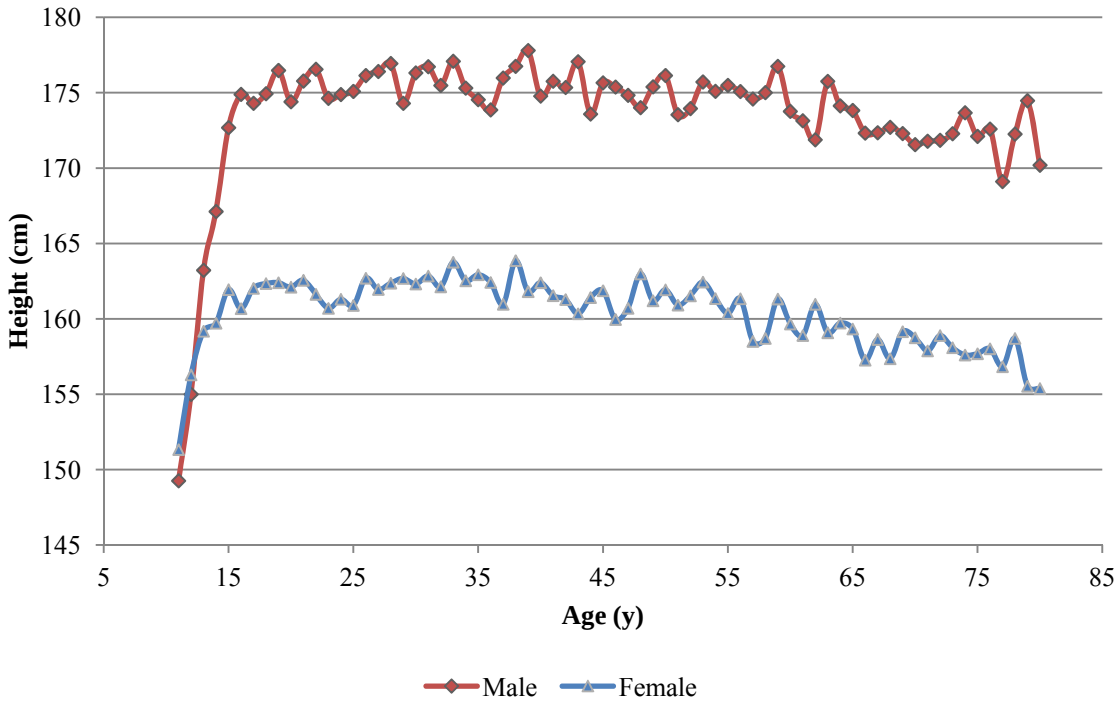

Figure 4.1. Variation in average height of the American population with respect to age. Data derived from the 2009 NHANES data set.

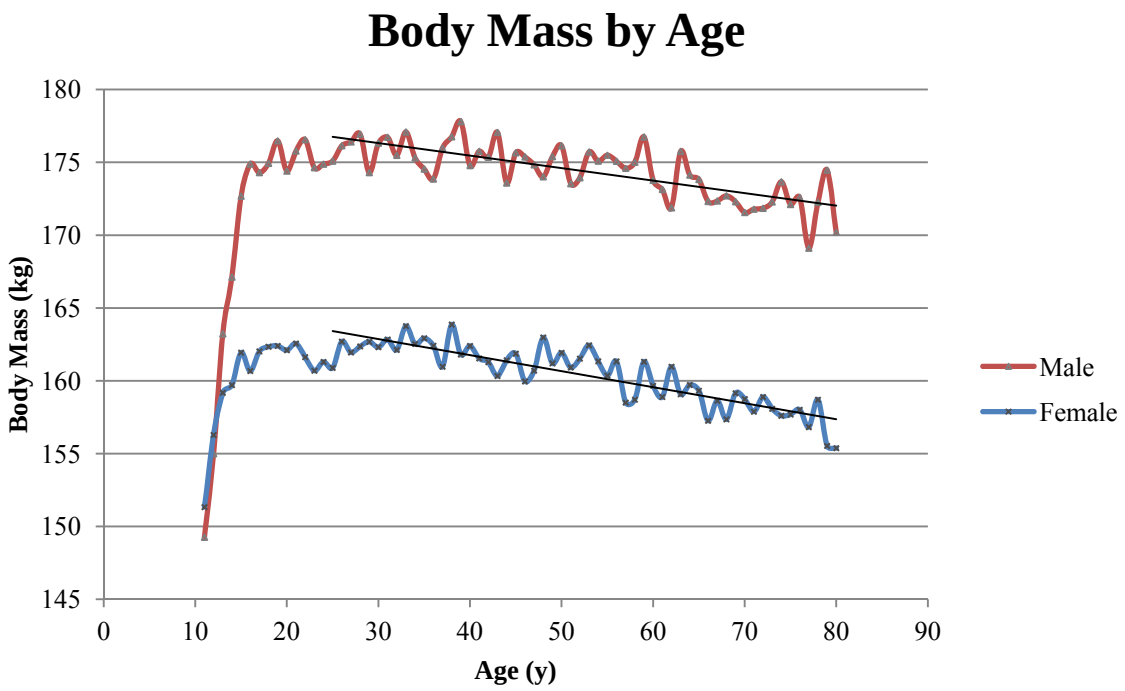

Figure 4.2. Variation in average body mass of the American population with respect to age. Data derived from the 2009 NHANES data set.

Quing He and colleagues have remarked that the degree to which organ and tissue mass change with age varies by organ and tissue (2009). Most reference data for organ weights have been derived from autopsy studies that have generally shown a linear decline in organ weight with increasing age for brain, liver, and kidneys, while the weight for heart increased with age. Young et al reviewed and summarized a total of 325 (192 male and 133 female) autopsy records to develop a meaningful set of organ mass data for various ages and body types (2009). The files were randomly accessed by hand to obtain organ weights, cause of death, and demographic information of age, body weight, height, and race. Using this data, Young devised a method to predict the masses of various organs based on gender and body mass using a polynomial of the form:

$$Y = X_0 Wt + X_1 Wt^2 + X_2 Wt^3 + X_3 Wt^4 + X_4 Wt^5 \qquad (73)$$

where

- *Y* is the organ mass in g and *Wt* is the total body mass in g (Young 2009).

This polynomial was used along with data from the NHANES 2007-2009 body measures data to determine age-specific masses for the spleen, kidney, lungs, adrenals, pancreas, thyroid, blood, and skin.

Table 4.5. Calculated masses of spleen, kidney, lungs, and adrenals as a function of age for males.

Age Groups	n	Spleen (g)	Kidney (g)	Lungs (g)	Adrenals (g)
ICRP Default		150	310	500 (ea)	14
19-20	144	212.7 ± 43.2	343.4 ± 191.6	1181.5 ± 201.9	15.4 ± 18.3
21-30	476	220.5 ± 39.6	342.6 ± 73.2	1223.7 ± 194.4	18.0 ± 6.3
31-40	482	236.9 ± 44.4	380.7 ± 141.5	1301.8 ± 205.1	19.9 ± 8.9
41-50	495	235.3 ± 40.5	369.3 ± 90.2	1296.0 ± 192.8	20.1 ± 7.5
51-60	488	232.5 ± 41.0	366.0 ± 100.9	1282.1 ± 194.5	19.5 ± 7.0
61-70	444	230.4 ± 40.8	361.5 ± 98.2	1272.3 ± 195.8	19.2 ± 7.0
71-80	454	217.2 ± 34.6	334.2 ± 57.6	1208.7 ± 172.3	17.1 ± 5.0

Table 4.6. Calculated masses of spleen, kidney, lungs, and adrenals as a function of age for females.

Age Groups	n	Spleen (g)	Kidney (g)	Lungs (g)	Adrenals (g)
ICRP Default		130	275	420 (ea)	13
19-20	124	160.4 ± 31.3	294.8 ± 33.8	976.3 ± 192.5	14.3 ± 4.4
21-30	546	174.2 ± 36.2	309.3 ± 37.4	1050.3 ± 191.8	16.2 ± 6.5
31-40	528	181.3 ± 34.4	317.0 ± 34.2	1090.2 ± 191.3	16.9 ± 6.5
41-50	568	178.5 ± 33.4	314.7 ± 35.1	1074.6 ± 174.8	16.2 ± 6.1
51-60	468	183.3 ± 31.7	319.9 ± 34.5	1102.3 ± 167.5	16.6 ± 9.1
61-70	432	181.4 ± 30.6	317.5 ± 30.0	1093.1 ± 164.4	16.5 ± 4.5
71-80	501	168.2 ± 30.2	304.2 ± 32.2	1023.5 ± 166.9	14.8 ± 4.1

Table 4.7. Calculated masses of human pancreas, thyroid, skin, and blood as a function of age and gender.

Male

Age Groups	n	Pancreas (g)	Thyroid (g)	Skin (g)	Blood (g)
ICRP Default		140	20	3300	5600
19-20	144	119.5 ± 33.7	19.5 ± 5.5	2699.8 ± 556.5	5227.1 ± 915.2
21-30	476	124.1 ± 27.9	20.3 ± 4.6	2784.7 ± 487.6	5384.4 ± 809.1
31-40	482	136.2 ± 34.3	22.3 ± 5.6	2986.9 ± 572.9	5721.2 ± 896.9
41-50	495	134.5 ± 29.8	22.0 ± 4.9	2962.8 ± 516.6	5687.0 ± 813.3
51-60	488	132.6 ± 30.4	21.7 ± 5.0	2928.5 ± 519.2	5631.1 ± 827.5
61-70	444	131.1 ± 29.9	21.4 ± 4.9	2905.3 ± 515.3	5588.9 ± 828.8
71-80	454	121.5 ± 23.8	19.9 ± 3.9	2738.2 ± 416.7	5320.2 ± 713.5

Female

Age Groups	n	Pancreas (g)	Thyroid (g)	Skin (g)	Blood (g)
ICRP Default		120	17	2300	4100
19-20	124	98.6 ± 26.5	16.1 ± 4.3	1967.7 ± 265.2	4549.9 ± 853.8
21-30	546	110.7 ± 34.0	18.1 ± 5.6	2089.8 ± 376.4	4930.5 ± 1010.1
31-40	528	116.4 ± 32.6	19.0 ± 5.3	2141.0 ± 368.0	5121.7 ± 958.1
41-50	568	114.0 ± 32.7	18.6 ± 5.3	2112.8 ± 364.0	5047.8 ± 946.0
51-60	468	117.8 ± 30.8	19.3 ± 5.0	2147.1 ± 342.8	5177.4 ± 895.6
61-70	432	115.6 ± 27.1	18.9 ± 4.5	2122.3 ± 304.8	5117.6 ± 838.9
71-80	501	104.5 ± 25.3	17.4 ± 8.4	2013.6 ± 250.6	4759.5 ± 819.5

Limitations associated with the use of autopsy data as a reference for in vivo organ mass were pointed out by Quing He et al. as including a significant loss of organ weight that occurs during the first 15 minutes after being removed from the surrounding tissue (He et al. 2009). To overcome measurement errors associated with organ desiccation following autopsy, He and colleagues acquired MRI scans of 36 men and 75 women between the ages of 19 and 88 years. The acquired data was used to derive the following regression

expression to correlate the masses of the brain, heart, and liver with an individual's gender, age, body mass, and height.

$$Y = X_0 + X_1 Age + X_2 Body\ Mass + X_3 Height + X_4 Gender \quad (74)$$

Within this expression, age is given in years, body mass and organ mass are in g, height is in meters, and gender is 1 for males and 0 for females. This expression was used long with the NHANES 2007-2009 body measures data to determine age-specific masses for the brain, and heart.

Table 4.8. Brain and heart masses calculated as a function of age and gender.

Male				Female			
Age Groups	n	Brain (g)	Heart (g)	Age Groups	n	Brain (g)	Heart (g)
ICRP Default		1450	330	ICRP Default		1300	250
19-20	144	1334.0 ± 25.4	355.4 ± 46.6	19-20	124	1168.2 ± 26.1	222.8 ± 36.4
21-30	476	1318.5 ± 27.8	364.3 ± 40.0	21-30	546	1146.7 ± 28.3	241.6 ± 46.8
31-40	482	1290.0 ± 29.1	384.6 ± 47.6	31-40	528	1124.9 ± 29.5	253.6 ± 45.0
41-50	495	1270.1 ± 28.3	386.2 ± 41.2	41-50	568	1102.5 ± 28.1	253.8 ± 45.0
51-60	488	1249.9 ± 25.9	387.2 ± 42.4	51-60	468	1077.6 ± 29.4	262.8 ± 42.4
61-70	444	1224.8 ± 26.3	388.6 ± 40.2	61-70	432	1054.4 ± 26.5	263.0 ± 38.2
71-80	454	1202.5 ± 24.7	379.8 ± 33.0	71-80	501	1030.6 ± 25.4	252.6 ± 34.6

4.2. Skeletal System

'Bone-seeking radionuclides' are those nuclides characterized by high affinity for bone, and are disposed in bone for prolonged periods of time while maintaining low systemic concentrations. The uptake of bone-seeking radionuclides is governed by two processes. A fraction of the amount that ends up in the skeleton is incorporated into the

bone mineral through bone formation. The remainder reaches the bone through the process of exchange. The exchange that occurs between the bone mineral and surrounding fluids represents the processes such as surface exchange, recrystallization, osteon formation and diffusion (Heaney 1963).

Although it appears to be inert and static, bone is a remarkable dynamic tissue which continuously repairs, renews and adapts in response to localized environmental changes, maintaining its function to provide structural support and a mineral reservoir (Parfitt 1994; Sommerfeldt and Rubin 2001). This dynamic behavior is achieved through the remodeling process (Frost 1986). Bone remodeling is a coupled process of bone resorption, carried out by osteoclasts, and bone formation, carried out by osteoblasts. The balance between the volume of resorbed and newly formed bone and the remodeling rate determines the integrity of the bone structure and strength throughout its life (Christiansen 2001; Seeman and Delmas 2006).

Positive balance and rapid remodeling cycles in healthy young individuals result in increasing bone mass and density, and therefore strengthen the bone. As juvenile growth ceases with epiphyseal closure, the remodeling rate decreases and the balance gradually shifts towards zero (Parfitt 2000). The balance in healthy adult bone is approximately zero and the mean activation frequency is about 0.33 per year for trabecular bone (Agerbaek et al., 1991; Eriksen et al., 1985, 1986a), where Eriksen et al. (1985) defines activation frequency as the formation rate of a new remodeling cycle at a particular point. Thus, remodeling of a point will occur every three years or so. The remodeling balance becomes negative throughout the aging process and disuse (Zaidi 2007), with bone loss beginning

between the ages of 18 and 30 years old, although the process is slow because the activation frequency is so low (Gilsanz et al. 1988).

4.2.1. Skeletal Anatomy and Physiology

The skeletal system plays both a biomechanical and metabolic role in the human body, and consists of a series of individual bones which are joined by softer connective tissues (Jee 2001). The skeleton provides structural support for the rest of the body, permits movement and locomotion by providing levers for the muscles, protects vital internal organs and structures, provides maintenance of mineral homeostasis, serves as a reservoir of growth factors and cytokines and provides the environment for hematopoiesis within the bone marrow spaces (Taichman 2005). Bone is the main constituent of the skeletal system and differs from connective tissue in terms of rigidity and hardness, enabling the skeleton system to maintain the shape of the body, protect the internal organs, supply the framework for the bone marrow and transmit the forces induced by muscular contractions during movement.

The four general categories of bones of the skeleton are long bones, short bones, flat bones and irregular bones. Flat bones are formed by membranous bone formation, whereas long bones are formed by a combination of endochondreal and membranous bone formation (Clarke 2008). The long bones are composed of a hollow shaft, or diaphysis; cone-shaped metaphyses below the growth plates; and rounded epiphyses above the growth plates

Cortical bone is a dense, solid mass with only microscopic channels. It accounts for approximately 80% of the skeletal mass in the adult human skeleton, forms the outer wall

of all bones and is responsible for the support and protection of the skeleton. Trabecular bone accounts for the remaining 20% and is located in the internal structure of bones (Clarke 2008). Cortical bones differ from trabecular bone in terms of their development, architecture, function, proximity to bone marrow, blood supply, rapidity of turnover time and magnitude of age-dependent changes and fractures (Jee 2001).

The composition of bone includes minerals, organic matrix, cells and water. Minerals account for 65% of bone and can be found within collagen fibers in the form of small crystals. The mineral is largely impure hydroxyapatite (Ca_{10} $(PO_4)_6$ $(OH)_2$), which contains traces of carbonate, citrate, magnesium, fluoride and strontium. These constituents are incorporated into the crystal lattice or absorbed onto the crystal surface (Gehron and Boskey 1996; Lian et al. 1999). The organic matrix accounts for the remaining 35% of bone and is made up of 90% collagen and about 10% of various non-collagenous proteins, and has a wide variety of functioned roles and determines the structural, mechanical and biochemical properties of the tissue (Gehron and Boskey 1996; Gorski 1998; Lian et al. 1999).

Bone cells include osteoblasts, osteoclasts, the immune regulatory system that supplies the precursor cells and regulates bone growth and maintenance, osteocytes, bone lining cells and cells of the marrow compartment (Jee 2001). Only osteoclasts, osteoblasts, bone lining cells and osteocytes are discussed in this chapter, as these are the most relevant cells to this study.

Osteoclasts are multinucleated giant cells which range in diameter from 20 to over 100 μm, with one osteoclast containing from 1 to more than 50 nuclei (Jee 2001). Osteoclasts are responsible for the resorption bone during the remodeling cycle.

Osteoblasts are responsible for building new bone by synthesizing and secreting unmineralized bone matrix, and also participate in the bone calcification (Jee 2001). They control the flow of calcium and phosphate in and out of bone and regulate bone resorption indirectly by interacting with osteoclastic cells (Jee 2001).

Bone lining cells are situated on the quiescent bone surface. Bone lining cells build three-dimensional networks with osteocytes. It is believed that these three-dimensional networks, in which the cells communicate with each other, are able to sense the stress and strain experienced within a bone, and subsequently transmit signals to the bone surface to initiate the remodeling process (Baron 1999; Burr 1997; Parfitt 1983; Roodman 1996).

Osteocytes are the most abundant cell type in mature bone, with about ten times more osteocytes than osteoblasts in healthy human bone. Osteocytes are formed from the osteoblasts deposited in the newly formed osteoid during bone formation (Bonewald 2004; Jee 2001).

4.2.2. Physiology - Bone Remodeling

Bone undergoes longitudinal and radial growth, modeling and remodeling during life. Longitudinal and radial growth occurs during childhood and adolescence. At growth plates, longitudinal growth occurs before subsequently undergoing mineralization to form primary new bone (Clarke 2008). Bone modeling on the other hand is the process by which bone changes its overall shape in response to physiologic influences or mechanical forces, leading to the gradual adjustment of the skeleton to the forces that it encounters (Clarke 2008).

Bone remodeling serves two closely linked purposes. First, some remodeling can be directed towards specific sites to repair fatigue damage, continuously replacing fatigued bone with mechanically competent new bone. So bone remodeling is necessary to maintain the mechanical strength and structural integrity of new bone. Secondly, through continuous bone resorption and formation, bone serves its metabolic functions as a storehouse of calcium and phosphorus. Therefore, bone remodeling plays a very important role in maintaining mineral homeostasis (Favus 2006; Heaney and Weaver 2005).

Bone formation begins *in utero* and continues throughout adolescence by "modeling" until skeletal maturity is reached (Einhorn 1996). After this point, bone remains a metabolically active organ that is able to adapt its structural and material properties to the mechanical demands placed upon it, via a localized process termed "bone remodeling" (Raisz 1999). The bone remodeling cycle consists of a series of highly regulated sequential steps involving the interactions of the various cell types described previously (Raisz 1999).

Remodeling is a continuous process of bone resorption performed by osteoclasts, followed by bone formation performed by osteoblasts, and occurs in the skeleton of vertebrates throughout their lifetime (Mundy 1999). This process occurs asynchronously at multiple spatially and temporally discrete sites of the skeleton in order to repair damaged portions or replace older bone with new bone (Pivonka et al. 2008).

The bone remodeling process is highly regulated by numerous local factors and systemic hormones (Fernandez-Tresguerres-Hernandez-Gil et al. 2006). Among them, estrogen is considered the most important hormone in maintaining normal bone turnover (Raisz 1999) It has a dual effect on bone remodeling: on one hand, it can increase bone

formation; on the other hand, it can reduce bone resorption (Fernandez-Tresguerres-Hernandez-Gil et al. 2006).

Studies with female humans and animals showed changes in bone remodeling during the menstrual cycle with monthly episodes of increased bone resorption (Chiu et al. 1999; Gass et al. 2008; Hotchkiss and Brommage 2000; Kalyan and Prior 2010).

The delicate balance between bone resorption and bone formation is essential for the maintenance of normal bone functions. Imbalance between the two can result in compromised bone renewal and change in bone mass; skeletal diseases will develop. Increased bone resorption or a relative decrease in bone formation compared to bone resorption can lead to osteoporosis. In contrast, increased bone formation or a relative decrease in bone resorption compared to bone formation can lead to osteopetrosis (Sommerfeldt and Rubin 2001).

4.2.3. Age-related Effects

Changes in the integrity of bone structural architecture and bone mineral density are a well established function of age. *In vivo* studies have shown decreases in cortical thickness, cancellous bone volume fraction, bone mineral density, trabecular number, structure model index and connectivity, and increases in trabecular spacing and porosity with advancing age in the spine, femur, and tibia (Halloran et al. 2002; Majumdar et al. 1997). With advancing age bone exhibits decreases in mass and area which may adversely affect its ability to support daily mechanical loads.

General population-based trends in skeletal status are commonly quantified with the use of densitometric techniques. All radiographic methods make use of distinct photon absorption properties of the bone mineral and soft tissue. Single and dual-energy absorptiometry utilizing gamma rays (SPA and DP A) or X-rays (SXA and DXA) are methods that are clinically most widely used.

To estimate general age-related trends of bone loss, results of numerous studies employing DXA, Quantitative Computed Tomography (QCT) and other related techniques were investigated. Notwithstanding the technical limitations of DXA (Bolotin 2004; Stepan 2000), there are numerous studies on bone mineral density using DXA which can contribute to the general model of bone metabolism. The main difficulty in formulating general trends in bone loss is that measurements are typically conducted on a limited number of skeletal sites. There are considerable differences between different sites in the skeleton regarding their composition, metabolic activity and loss, and this limits the predictive power of a model.

Bone loss is an inevitable age-related condition and is determined by the remodeling rate and the negative bone balance between bone resorption and formation (Seeman 2003). With advancing age there is a decrease in the number of bone forming osteoblasts and an increase in the number of marrow adipocytes. The rate of remodeling of cortical bone appears to reach a minimum in middle age and to increase again in older persons (ICRP 1995). The decline in bone density appears to begin between the ages of 18 to 30 years, with onset appearing after the rapid increase in remodeling evident during adolescence. This process is relatively slow because the overall remodeling rate is low (Gilsanz et al. 1988). Cortical bone loss measured at the forearm was found to be negligible

for men aged 20-30 years (Scopacasa et al. 2002). Loss commenced at about 40 years of age at an annual rate of 0.34%. At the age of 70 years, the cortical bone loss increased to 1.5 %/year. When stratified by age, the annual cortical bone loss was determined to be 0.22% for men younger than 50 years of age, and 0.60% in older men. Berntsen et al. (2001) also presented a 0.1 %/year decrease before the age of 50 and 0.6% /year in older men. Similarly, the results of a study by Riggs et al. (2004) showed that the cortical volumetric BMD remained at its maximum value until midlife, followed by a decline of approximately 18% over the next 45 years.

Osteoporosis refers to a condition when bone mass decreases to a critical level, below which fracture risk is substantially high (Riggs and Melton 1992). Although osteoporosis is characterized by decreased bone mass, the ratio of bone mineral to the organic matrix in osteoporosis normal, as opposed to a decreased ratio of bone mineral to the organic matrix in osteomalacia (Favus 2006; Lerner 2006).

Osteoporosis can be classified into primary osteoporosis and secondary osteoporosis, depending on whether or not an identifiable etiological mechanism is recognized (Kassem et al. 1996; Kleerekoper and Avioli 1990). In addition, osteoporosis can also be classified into juvenile osteoporosis and 'involutional osteoporosis', which includes postmenopausal osteoporosis and senile osteoporosis (Kassem et al. 1996). In 1982, Riggs characterized two distinct syndromes of involutional osteoporosis: high turnover and low turnover osteoporosis. High turnover osteoporosis occurs in postmenopausal women between the ages of 50 and 65 years old, and is pathologically related to estrogen deficiency. This hormonal deficiency leads to increased remodeling spaces and increased remodeling rates, i.e. both osteoclast and osteoblasts activities are

enhanced (Chambers 1998). However, due to estrogen deficiency, there is an imbalance between bone resorption and bone formation, resulting in a decrease in total bone mass (Simon 2007; Lerner 2006). The acceleration of bone loss tends to stop after about 4-8 years (Riggs et al. 2002). During that period bone is lost mainly due to loss of entire trabecular elements rather than due to generalized thinning of trabeculae (Aaron et al. 1987; Dempster 1995; Barger-Lux and Recker 2002).

This mechanism of bone loss is in sharp contrast to the overall thinning of trabeculae that occurs in aging men (Aaron et al. 1987; Seeman 1999), and due to mechanical disuse (Gardner et al. 2001). When the accelerated phase of bone loss in women stops, remodeling rates remain high (Garnero et al. 1996). Low turnover osteoporosis occurs in both men and women aged predominantly over 75, and affects both trabecular and cortical bone. It is caused by an age-related decline in osteoblast function and can lead to hip and vertebral fractures (Kanis 1996).

Peak trabecular mass is achieved at around 35 years of age (ICRP 1995). Adults normally lose 25-45% of the peak trabecular mass with aging, which translates into constant annual loss of 0.96% over the next 45 years. Clarke et al. (1996) reported a 40% decrease in the trabecular bone volume over approximately 60 years (equivalent to 0.85% /year on average). Riggs et al. (2004) found that the trabecular volumetric BMD begins to decline before midlife, with a total loss of 26-45% by the age of 90 years (or 0.8%/year). A linear decline of 0.94% /year in trabecular bone density starting in early adulthood was also reported by Russo et al. (2003), and this finding is supported by several other QCT and DXA studies.

Annual bone remodeling rates provided by the ICRP (1995) are equivalent to bone formation rates for adults younger than 60 years of age. In agreement with the data of the ICRP Report 70, Fatayerji and Eastell (1999) found that the activity of bone turnover markers is highest in young adult men, reaching a minimum in the third decade and increasing somewhat again in older men. Levels of bone formation and resorption markers were also highest in young men, and remained relatively constant with aging. Clarke et al. (1996) reported an age-related decrease in markers of osteoblastic activity, whereas markers specific to bone resorption did not change radically in aging men.

Bone turnover significantly increases at the time of menopause. This trend has been reported in numerous studies, including a study of bone turnover markers by Stepan et al. (1985) that detected levels in women very similar to those of men in the 29-45 year age group, followed by a significant increase in the 50-60 year age group and a relative decline in the 61-80 year age group. Elevated levels of bone turnover markers were reported for perimenopausal women by Chapurlat et al. (2000). The increase in the markers of bone resorption is rapid and seems to precede the increase in bone formation by a few months (Stepan 2000). The loss of bone during perimenopausal transition is believed to be primarily the result of increased bone resorption, followed by an increase in bone formation in the early postmenopausal years (Ebeling et al. 1996). The calcium kinetics study by Heaney et al. (1978) indicated that bone formation and resorption increase by 15 and 20%, respectively, across menopause.

4.2.1. Data Summary

The skeleton of a Reference Man is composed of 80% cortical bone and 20% trabecular bone (ICRP 1995). For adults older than 22 years of age, cortical and trabecular annual remodeling rates are normally in the range from 2-9% and 10-27%, respectively, but the adult values of 3 and 18% are typically assumed (ICRP 1995). A general decline in total skeletal mass up to the age of 60 years is presented in the ICRP Report 23 (1975). Simple linear extrapolation of the ICRP trend in bone mass from age 45 to 60 would result in bone loss of approximately 30% by 90 years of age. Based on the review of related published work, it is concluded that this rate of bone loss is unreasonably high for healthy older adults, and that the rate of bone loss must gradually decline in old age.

Data were extracted from the 2005 - 2006 NHANES databases, maintained at the Center for Disease Control and Prevention's website (www.cdc.gov/nchs/about/major/nhanes/), as presented below.

Table 4.9. American population bone mineral mass by age range, as extracted from the NHANES 2005-2006 data set.

Males			Females		
Age Groups	n	Bone Mineral Mass (g)	Age Groups	n	Bone Mineral Mass (g)
11-20	1095	2260.2 ± 621.5	11-20	1042	1983.9 ± 392.7
21-30	338	2814.9 ± 446.9	21-30	305	2202.2 ± 319.3
31-40	344	2785.6 ± 404.7	31-40	291	2249.4 ± 316.3
41-50	349	2761.3 ± 390.0	41-50	342	2263.9 ± 322.4
51-60	270	2739.5 ± 443.9	51-60	285	2086.8 ± 341.9
61-69	267	2633.6 ± 444.2	61-69	251	1992.0 ± 352.5

As the data in Table 4.9 demonstrates, there is a marked difference in total bone mineral mass throughout the life cycle. Men tend to reach their peak bone mineral content

in the third decade of life followed by a gradual decline. Women, on the other hand, do not achieve peak mineral content until the fifth decade, followed by a more rapid decline throughout the sixth and seventh decades of life.

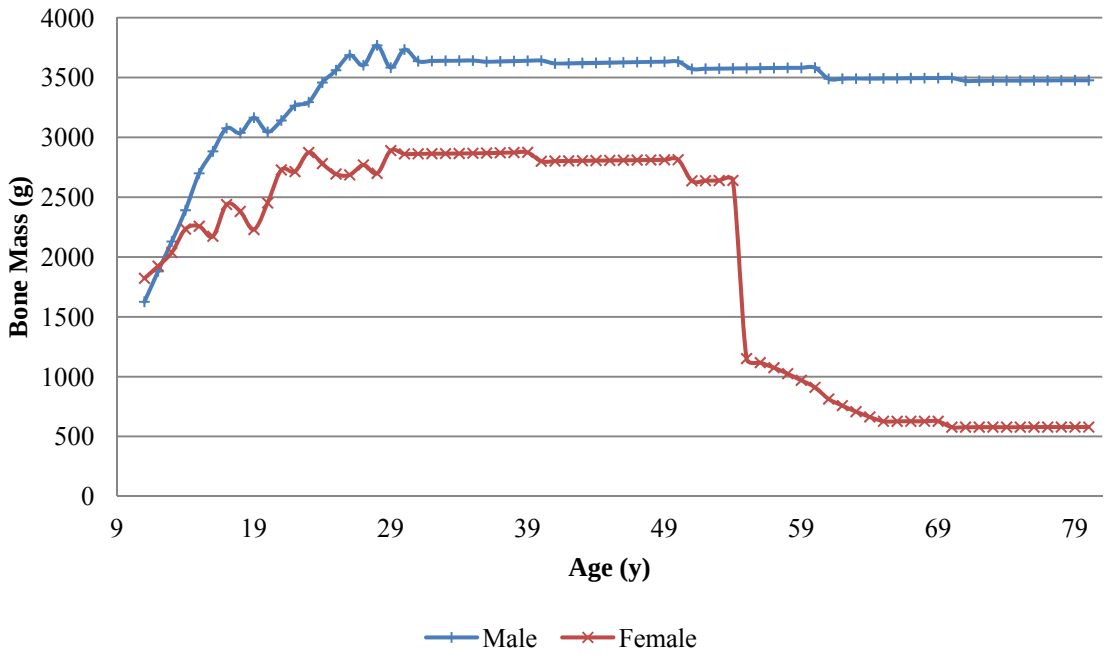

Figure 4.3. Variation of human bone mass with respect to age and gender.

It is well known that bone growth and mass are affected by many factors throughout the life cycle. Genetics may account for up to 80% of variability in BMD between individuals while environmental factors, such as physical activity and diet, may account for up to 35% of the variability. Other factors that have been shown to influence BMD and bone growth include hormonal fluctuations (sexual maturation) and growth factors (IGF-1). However, there is no direct way to measure the rate of bone turnover and mineralization in a human. Turnover must be estimated then by analysis of changes in BMD or the measurement of biochemical markers of bone turnover in urine or blood

samples.

The amount of mineral in a given area of bone determines its strength and susceptibility to fracture, and is measured to diagnose osteoporosis and other bone diseases (Sundberg et al. 2003). Areal bone mineral density (aBMD) can be assessed at specific sites using DXA (Sundberg et al. 2003). Dual energy x-ray absorptiometry may be limited, however, in that the aBMD is a two-dimensional projection of a three-dimensional bone. Thus, the density is not a true volumetric density and may under- or over-estimate measurements. DXA gives an accurate measure of aBMD which can be compared to a normative database in order to diagnose osteoporosis and fracture risk (Sundberg et al. 2003). Changes in volumetric bone-mineral density (vBMD) and bone mineral content (BMC) indicate changes in the ratio of bone resorption to formation. Cortical bone accounts for 80% of skeletal weight (ICRP 1995), but its contribution increases with advancing age because the age-dependent loss in trabecular bone is more pronounced than in cortical bone. Therefore, BMC loss is mainly determined by the loss of cortical bone mineral (Shagina et al. 2012).

Bone mineral density data were extracted from the 2009-2010 National Health and Nutrition Examination Survey databases, maintained at the Center for Disease Control and Prevention's (CDC) website (www.cdc.gov/nchs/about/major/nhanes/), as presented below.

Table 4.10. Bone mineral density measurements from the NHANES 2009 data set.

Males			Females		
Age Groups	n	BMD (g/cm^2)	Age Groups	n	BMD (g/cm^2)
11-20	775	1.009 ± 0.185	11-20	675	0.936 ± 0.141
21-30	431	1.082 ± 0.160	21-30	424	0.967 ± 0.128
31-40	414	1.054 ± 0.143	31-40	413	0.979 ± 0.123
41-50	436	1.046 ± 0.143	41-50	485	0.953 ± 0.136
51-60	429	1.028 ± 0.148	51-60	393	0.893 ± 0.140
61-70	398	1.001 ± 0.160	61-70	368	0.853 ± 0.127
71-80	398	0.994 ± 0.156	71-80	384	0.786 ± 0.147

Researchers have argued that the measurement of bone mass does not account for another important determinant of bone strength—bone quality (Briggs et al. 2007; McDonnell et al. 2007). Bone quality is independently influenced by parameters including bone architecture, bone turnover, microdamage, and mineralization (JAMA 2001). Rates of bone changes during remodeling depend mainly on bone turnover and balance per remodeling cycle. Variations in these variables are reflected in serum levels and renal excretions of specific biochemical bone markers, which may reflect bone resorption or bone formation.

Assessment of bone turnover using bone turnover markers has the advantages of relatively low cost and non-invasive sample collection compared to the evaluation of bone turnover rate by histomorphometry in bone biopsies from the iliac crest. Although bone biopsy may give direct evidence concerning the etiology, pathogenesis and progress of metabolic bone diseases, it has the disadvantage of being invasive and of giving information on bone turnover only concerning that specific skeletal region.

Bone biomarkers are proteins found in the blood and urine resulting from the

formation and resorption of bone. During this process of bone turnover, biomarkers spill over into systemic circulation, and measurement of these proteins are thought to reflect changes in bone mineral density (BMD). There are markers of bone formation and resorption. Osteocalcin (OC) is a small protein released by osteoblasts and is considered a sensitive, specific marker of osteoblastic activity and bone formation (Seibel 2003). Bone-Specific Alkaline Phosphatase (BAP) is a protein released into the circulation from the plasma membranes of osteoblasts and is a marker of bone formation (Avbersek-Luznik et al. 2007). Procollagen type I N-propeptide (P1NP) and type I collagen C-telopeptide (CTx) have been identified as the most promising turnover markers by the Joint International Osteoporosis Foundation International Federation of Clinical Chemistry and Laboratory Medicine Bone Marker Standards Working Group (Jenkins et al. 2013). P1NP is a propeptide that is released during the processing of type I procollagen into collagen. It is regarded as a bone formation marker, is synthesised by osteoblasts and correlates with histomorphometric parameters of bone formation. In contrast, CTx arises from collagen degradation and correlates with histomorphometric parameters of bone resorption (Jenkins et al. 2013). Levels of biomarkers found in the circulation may fluctuate with age, maturation, hormones, physical activity, and many other factors known to affect bone mass.

Studies involving healthy postmenopausal women have shown a general trend of reduced resorption markers corresponding to higher bone mass or decreased bone loss (Bass et al. 1999; Rauch et al. 1996; Rauch et al. 1994). These data suggest that lower rates of resorption contribute to increases in BMD. Formation markers have not given consistent results across this age group (Bass et al. 1999), but it is known that the increase in the

remodeling cycle after menopause is generally characterized by a small increase in formation and a larger increase in resorption of bone. It remains unclear, however, if these bone biomarkers accurately reflect the degree of bone formation and resorption occurring in the skeleton, and thus changes in BMD, during different stages of the lifecycle.

Table 4.11. Australian population median serum levels of bone turnover markers (condensed from Jenkins et al. 2013)

	Males			Females		
Age Groups	n	CTx (ng/mL)	P1NP (µg/L)	n	CTx (ng/mL)	P1NP (µg/L)
20-29	85	528	61	166	379	45
30-39	114	361	41	215	264	31
40-49	136	311	37	209	246	29
50-59	196	303	36	176	331	34
60-69	184	284	33	176	343	38
70-79	230	315	35	151	407	39
80 +	198	339	37	153	507	49

A study comparing serum levels to the iliac crest cortical samples obtained from subjects immediately postmortem showed variation in the age of peak osteocalcin levels by gender. Women's serum osteocalcin levels appear to peak in the sixth decade of life and men's in the eighth decade. Later in life, these levels decrease. This study also demonstrated that the actual bone osteocalcin were consistent with the serum osteocalcin measurements and therefore do reflect osteoblast levels (Vanderschueren et al. 1990).

While the analysis of bone formation and resorption markers in serum gives a qualitative measure of the rate of change of bone in humans, determination of the rates at which xenobiotic materials deposit in the skeletal mass requires knowledge of the actual rates of bone formation and resorption. To date, no method has been developed to link

serum measurements with histological measurements of actual formation and resorption rates. Few studies have presented detailed dynamic bone histomorphometry parameters by age and sex and, as shown below, those that have are based on limited population sets (ICRP 1995b; Clarke et al. 1996).

Table 4.12. Comparison of dynamic bone histomorphometry parameters from two resources by decade of life.

	ICRP 70			Clarke et al.		
Age Groups	n	BFR/BV (1/y)	MAR (μm/day)	n	BFR/BV (1/y)	MAR (μm/day)
20-29	49	0.067 ± 0.037	1.2 ± 0.6	7	0.180 ± 0.053	0.56 ± 0.08
30-39	52	0.018 ± 0.006	1.1 ± 0.36	7	0.133 ± 0.036	0.79 ± 0.05
40-49	53	0.037 ± 0.013	1.0 ± 0.33	9	0.120 ± 0.028	0.54 ± 0.04
50-59	63	0.036 ± 0.012	0.90 ± 0.30	5	0.097 ± 0.033	0.50 ± 0.05
60-69	37	0.040 ± 0.013	0.80 ± 0.26	9	0.129 ± 0.046	0.54 ± 0.07
70-79	23	0.044 ± 0.015	0.72 ± 0.20	5	0.081 ± 0.032	0.52 ± 0.12
80-89	-	-	-	2	0.037 ± 0.025	0.35 ± 0.15

BFR/BV is the total volume bone formation rate (mm^3 formed per mm^3 bone per year). MAR is the mineral apposition rate.

It is not possible to draw a direct comparison between the bone formation rates and mineral apposition rates presented in these two studies without significant background information as to how bone biopsies were taken, how tracers were administered, and bone selection sites. Additionally, the data presented by Clarke et al. is only for males, while the data presented in ICRP Publication 70 seems to be a composite of male and female data. Additionally, these authors do not draw a distinction between total bone formation rate, the amount of bone material created in a given period, and the bone growth rate, or the amount of material created in a given period relative to the amount of matrix material broken down in the same period.

It is generally understood that bone formation rate increases with age up until roughly thirty years of age, the age at which peak skeletal mass is attained. Bone resorption, however, is hormonally controlled and continues to vary across the entire lifespan and varies drastically in women around the time of perimenopause. Fortunately, for the sake of comparison of bone kinetic parameters with age, O'Flaherty has devised a differential model for bone formation rate and bone resorption rate that accounts for net bone loss after peak bone mass has been achieved in early adulthood (2000). The O'Flaherty model also makes a distinction between the rates of formation and resorption for cortical and trabecular bone volumes. A variation on this model was used to derive the bone formation and bone resorption rates presented here.

Table 4.13. Bone formation and resorption rates (in L/y) calculated using the methods presented in O'Flaherty 2000

Male	CBFR			TBFR			CBRR			TBRR		
21-30	0.172	±	0.512	0.319	±	0.950	0.163	±	0.450	0.309	±	0.831
31-40	0.180	±	0.690	0.335	±	1.281	0.180	±	0.692	0.334	±	1.283
41-50	0.180	±	0.690	0.335	±	1.281	0.180	±	0.690	0.334	±	1.281
51-60	0.180	±	0.690	0.335	±	1.281	0.180	±	0.690	0.334	±	1.281
61-70	0.180	±	0.690	0.335	±	1.281	0.180	±	0.690	0.334	±	1.281
71-80	0.180	±	0.690	0.335	±	1.281	0.180	±	0.690	0.334	±	1.281

Female	CBFR			TBFR			CBRR			TBRR		
21-30	0.151	±	0.632	0.280	±	1.328	0.144	±	0.526	0.272	±	1.148
31-40	0.180	±	0.921	0.335	±	1.647	0.177	±	0.935	0.329	±	1.680
41-50	0.180	±	0.921	0.335	±	1.647	0.180	±	0.921	0.334	±	1.647
51-60	0.180	±	0.921	0.335	±	1.647	0.219	±	0.905	0.373	±	1.631
61-70	0.180	±	0.921	0.335	±	1.647	0.186	±	0.941	0.340	±	1.666
71-80	0.180	±	0.921	0.335	±	1.647	0.180	±	0.921	0.335	±	1.647

4.3. Respiratory System

The regional deposition of xenobiotics in the lung depends on many factors, including the formulation properties (e.g., size, shape, density and charge), respiratory tract morphology and breathing pattern (e.g., inflow rate and tidal volume) (Gehr and Heyder 2000). Factors that most influence the amount of gas or vapor entering the human body are the alveolar concentration (Q_a), and the cardiac output (CO) of the individual as well as chemical specific parameters such as the chemical solubility and the blood:tissue partition coefficients for the chemical. For example, the blood flow rate into different organ systems of the human body will cause the gas concentrations in some compartments to rise sooner than in others. The total amount of chemical that passes through the body depends on the duration of exposure.

4.3.1. Pulmonary Anatomy

As a material absorption site, the lung can be divided into two functional regions: the conducting airways and the respiratory alveolar region. Airways start with trachea and continuously branch dichotomously into smaller children branches (Weibel 1963). The trachea is a flexible tube extending from the larynx. It is composed of 3 layers: 1) the mucosa made up of goblet cells and ciliated epithelium, 2) the submucosa which is a connective tissue, and 3) the adventitia, which is the outermost layer made of C-shaped rings of hyaline cartilage. The trachea bifurcates into the left and right bronchi which continue subdividing into the bronchioles.

The tissue walls of the bronchi and the bronchioles mimic that of the trachea. However, as the conducting airways become smaller, structural changes occur. The right

bronchus is wider in radius, shorter until it branches out at a steeper angle, which yields the asymmetry of the lungs. The main bronchi bifurcate in thousands of smaller bronchioles. There is a lack of cartilage support and increased amount of smooth muscle. Additionally, the epithelium is cuboidal without mucus-producing cells. The respiratory zone is defined by the presence of alveoli. The terminal bronchioles feed into the respiratory bronchioles which lead in to alveolar ducts, then to terminal clusters or alveolar sacs composed of alveoli. There are approximately 480 million alveoli in an adult human lung, which are arranged in clusters to form alveolar sacs (Mercer et al. 1994; Ochs et al. 2004). To make gas exchange possible, each alveolus is wrapped in a very dense mesh of thin capillaries carrying blood to the alveolar walls.

The conducting zone does not exchange gas with the blood, it merely transports the air. Due to many bifurcations in this region, the ratio of surface to volume increases drastically. The walls of the tubes have a mucus layer and very small hair, called cilia, to filter the air, cleaning it from dust and other particles. Through movement of the cilia, waste is transported back up to the pharynx or the nostrils, where it is either transported to the digestive system or blown out.

The airways bifurcate more than 17 times resulting in an enormous surface area of the alveolar region. A laborious study conducted by Weibel (1963) extracted the dimensions in different regions of the lungs. In many recent studies, the alveolar surface area of human adults was estimated to be ~100 m^2 (Thurlbeck 1967; Stone et al. 1992), which represents half a tennis court. The total lung capacity averages 6.7 and 4.9 liters in men and women, respectively (Stone et al. 1992). Of this volume approximately 10 percent is tissue, 10 percent is blood and 80 percent is air (Weibel and Cruz-Orive 1997). It

should be noted that under normal (tidal) breathing conditions the lungs are half empty. The conducting zone contains 4% of the inhaled air, and the alveoli the rest.

Two functional regions are supplied with two different circulatory systems. The bronchial and the pulmonary circulation loops supply the airways and alveolar region respectively (Staub 1989; Staub 1991). The bronchial circulation is a part of the systemic circulation and receives about 1% of cardiac output. The pulmonary circulation has an extensive vascular bed and receives the 100% of cardiac output, which perfuse the alveolar region to achieve an efficient gas exchange.

On the top of the lung mucosa there is a thin layer of surface lining fluid, which covers nearly 100% all surface area and generates a high humidity in the lung (Ehrhardt and Kim 2008; Tronde 2002). The thickness of the surface lining fluid is estimated to be 5–10 μm and gradually decreases with the airway generations. The surface lining liquid is composed of various types of surfactants mainly secreted by the alveolar type II cells. This liquid is generally comprised of a mixture of phospholipids, surfactant, and proteins (Staub 1991).

4.3.2. Pulmonary Physiology

The main function of the lung is to facilitate gas exchange including the uptake of oxygen and removal of carbon dioxide. The pulmonary circulation is a low pressure system which encompasses the entire right ventricular outflow tract; therefore pulmonary blood flow (PBF) is equivalent to cardiac output. Blood travels from the right ventricle into the pulmonary artery to pulmonary arterioles to the capillary bed where gas exchange occurs. The capillary bed merges to form pulmonary venules, which then form pulmonary veins,

and return blood to the left atrium of the heart. The capillaries lie in the alveolar walls and form a dense network around the alveoli. The capillary-alveolar boundary constitutes the blood-gas barrier in the lung. West describes the capillary-alveolar boundary as extraordinary due to its "extreme thinness, immense strength, and enormous area" (West 2003). This barrier consists of a single layer of alveolar epithelium, capillary endothelium, and an intervening extracellular matrix containing two basement membranes of the two cell layers. This boundary must remain very thin for passive diffusion of the gases to occur, while also maintaining a large area for diffusion (Maina and West 2005; West 2003).

Alveolar ventilation is in reality a cyclic process with inspiration and expiration cycles. However, for the purpose of this modeling, the alveolar ventilation is considered as a continuous process. This is because of an experiment conducted by Eger and described by Fiserova-Bergerova (1983) in which he studied the effect of respiratory rate and the rise of alveolar concentrations for an inert non-soluble gas. In this experiment he concluded that the rise in alveolar ventilation deviated very little for cyclic and continuous ventilation. This might be untrue in case of humans with some pathological conditions. However this assumption is still valid in this model because the model results are for healthy adult males and females.

To understand how the gas behaves with the blood and the lung tissue it is necessary to first know the definitions of some respiratory volumes (Thibodeau and Patton 2003). The amount of air that is inspired or expired in a single, resting breath is termed the tidal volume (TV), whereas the volume of air remaining in the lungs at the end of a normal, passive expiration is called the functional residual capacity (FRC). A stronger inspiratory effort will increase the amount of air inspired. The additional volume of the air taken in

beyond the tidal volume in a maximal inspiration is the inspiratory reserve volume (IRV). Expiratory reserve volume (ERV), by the name, is the volume of air expired by active effort beyond the passive expiration. The amount of air left in the lungs after a maximal expiratory effort is the residual volume (RV). The sum of the tidal volume and the IRV and ERV is called vital capacity (VC).

The respiration minute volume is the product of tidal volume and frequency of respiration per minute. In normal individuals this value represents the overall output of the respiration activity. The standard respiration minute volume for a normal, resting human is 6 - 8 L/min.

For many analyses, it is assumed that the alveoli are the only places where gas exchange occurs and the respiratory tubes carrying the inhalation and exhalation gas concentrations are inert tubes. This indicates that there is a certain amount of dead space in the respiratory airways. This dead space holds on to approximately 33% of the gas concentration that leaves the alveoli at the end of the previous expiration. In normal adult males, approximately 150 mL of alveolar air in dead space reenters the lung and mixes with approximately 350 mL of ambient air. During exhalation about 150 mL of ambient air retained in the dead space from the previous inspiration is exhaled first, followed by 350 mL of alveolar air; i.e. only about 2/3 of the effective tidal volume reaches the alveoli. The effective tidal volume is the tidal volume after subtracting the physiological dead space. The flow of ambient air that reaches the alveolar air in one minute is alveolar ventilation (Q_a). Alveolar ventilation (= effective TV * respiratory rate) accounts for about 2/3rd minute ventilation (= total TV * respiratory rate) under resting conditions. Hence the model uses alveolar ventilation instead of the minute ventilation to account for the

physiological dead space.

The retention and clearance of particles from the lung depends on the site at which the particles are deposited and the physicochemical characteristics of the particles. The clearance processes from the lung are region specific. Small particles of diameters below 1 μm remain suspended in the air and are exhaled. A small fraction of them reaches the deep lungs and deposit due to Brownian motion. Particle transit to the lower airways may be inhibited by deposition in the upper airways through impaction, sedimentation and diffusion (related to Brownian motion) (Edwards and Dunbar 2002). Clearance is rapid for particles that deposit in the upper airways compared to that for the particles that deposit in the gas exchange (alveolar) region of the lung. Particles with diameters larger than 5 μm deposit in the upper respiratory system (mouth, throat and tracheobronchial airways) due to inertial impaction. Insoluble particles that deposit on the surface of the tracheobronchial region are trapped in the mucus layer that covers the surface of the trachea and bronchi. Ciliated cells waft the mucus (mucociliary escalator) with trapped particles up to the pharynx where they are eventually swallowed. Soluble particles, on the other hand, are removed by the lymphatic system. The mucociliary escalator does not extend beyond the respiratory bronchioles and is depleted in the terminal bronchioles. Particles with diameters of 1-5 μm deposit in the deep lungs due to a combination of inertial impaction and sedimentation. Particles that are deposited in the terminal bronchioles and the alveolar region will be phagocytized by macrophages and transport them to the upper bronchioles for clearance through mucociliary escalator. Ultrafine particles can easily cross epithelial cell barrier and reach interstitial space. The free particles from the interstitium can easily

reach the lymphatic system or systemic system unless they are phagocytized by interstitial macrophages and transported back to the airways or to the lymphatic system.

4.3.3. Age-related Effects

The decline of pulmonary lung volume and function with age is a well-documented phenomenon (DeLorey and Babb 1999; Knudson et al. 1977). The vital capacity, the maximum amount of air that can be expired after a maximum inspiration, decreases with increasing age, because of the changes in the physical properties of the thorax-lung system and the diminished force-generating ability of the respiratory muscles. The residual air (the amount of air remaining in the lungs after a maximal forced expiration) increases with increasing age for similar reasons. A widely used and informative test is the measurement of the volume of air exhaled during the first second of a forced expiration. Beyond 25 years of age, the volume of air exhaled progressively decreases, because of the increased resistance to airflow in the bronchioles, the change in elastic properties of the lungs, and the decrease in the force generated by the respiratory muscles (Rossi et al. 1996).

Knudson et.al (1977) designed a study that attempted to eliminate and control for variables not solely related to age. Initial screening included over three thousand subjects from a longitudinal epidemiological study on obstructive lung. Stringent protocols eliminated all subjects that had any history of lung disease, smoking, or abnormal pulmonary functions. Final selection resulted in 73 eligible subjects with 51 full studies being completed. The subjects were placed into three different age groups delineated at 25-35, 36-64, and 65-75. Spirometry and plethysmographic studies were conducted to produce pressure volume curves and determine lung volumes. The results showed the loss

of elastic lung recoil existed with aging and was more significant (p=0.015) at higher rather than a lower lung volumes. The authors of this study concluded that while there was a statistically significant aging effect on lung function it was not profound and was less than half that reported by previous studies.

4.3.4. Data Summary

Values of ventilation rate may vary widely between published studies owing to the different target populations and measurement or calculation techniques employed. As such, a direct comparison of data from different studies and sources without significant background information is not possible. The U.S. EPA recognized that the tabulation of ventilation rates may be simplified for the purposes of intake/uptake dose modeling by examining human metabolism (EPA 2009). Metabolism can be quantified measured through energy expenditure (EE). The EPA builds upon Layton's (1993) approach for calculating ventilation rates as the product of EE (expressed in energy units per unit time—typically on a daily basis), oxygen uptake (H; the volume of oxygen consumed per energy unit), and ventilatory equivalent (VQ; a unitless ratio of inhaled air volume to H). To minimize uncertainty introduced by the use of a constant VQ for all individuals, the EPA calculates ventilation rate as a direct function of a person's oxygen consumption rate (VO_2). VO_2 was calculated as the product of EE (kcal/min) and H, the volume of oxygen consumed per unit of energy (L O_2/kcal) (EPA 2009):

$$VO_2 = EE \times H \tag{75}$$

where the value of H is held constant at 0.21 for males and 0.20 for females. Because energy expended depends on the type of activity being performed, EPA describes the idea

of metabolic cost given in units of "METS" or metabolic equivalents of work, an EE metric used by exercise physiologists and clinical nutritionists to represent activity levels. An activity's METS value represents a dimensionless ratio of its metabolic rate (EE) to a person's resting, or basal, metabolic rate (EPA 2009). For ease of comparison, the tabulated values for ventilation rate in this paper were calculated assuming a constant METS value of 1.5, the value for passive sitting. *EE* is then the product of the basal metabolic rate (BMR) and METS value.

The EPA calculates BMR using the Schofield equations, which express BMR as a function of body weight, gender, and age as follows:

Table 4.14 Equations from Schofield (1985) used to predict basal metabolic rate as a function of body weight (BW)

Age Category	Male	Female
10-17 years	BMR = 0.074 x BW + 2.754	BMR = 0.056 x BW + 2.898
18-29 years	BMR = 0.063 x BW + 2.896	BMR = 0.062 x BW + 2.036
30-59 years	BMR = 0.048 x BW + 3.653	BMR = 0.034 x BW + 3.538
60 years and older	BMR = 0.049 x BW + 2.459	BMR = 0.038 x BW + 2.755

Given that 1 MJ equals 238.846 kcal, BMR was converted from MJ/day to kcal/min as follows: BMR (kcal/min) = 0.16587 × [BMR (MJ/day)].

Data from 32 panel studies collected over a 25-year period by the same laboratory were fitted by multiple linear regression to yield an equation for ventilation rate that included both age and gender as independent variables (EPA 2009).

$$ln\left(\frac{V_E}{BM}\right) = b_0 + \left(b_1 \times \ln\left(\frac{VO_2}{BM}\right)\right) + (b_2 \times \ln(age)) + (b_3 \times gender) + e \quad (76)$$

where BM is body mass in kilograms, age is in years, gender is -1 for males and 1 for females, and the regression coefficients are presented in Table 4.15.

Table 4.15. Ventilation equation multiple linear regression parameter estimates using Adams (1995) data.

Age Category	n[a]	b_0	b_1	b_2	b_3	e
Less than 20 years	1085	4.4329	1.0864	-0.2829	0.0513	0.1444
20-33 years	3646	3.5718	1.1702	0.1138	0.0450	0.1741
34-60 years	1083	3.1876	1.1224	0.1762	0.0415	0.1727
61 years and older	457	2.4487	1.0437	0.2681	-0.0298	0.1277

[a] Number of subjects in Adams data for the specified age range

From Equation 76, ventilation rates for each decade of life were calculated using age, gender, and body mass data extracted from the 2009 NHANES databases as presented below.

Table 4.16. Estimation of daily average ventilation rate using data from the NHANES 2009-2010 data set.

Males			Females		
Age Groups	n	Ventilation Rate (m^3/day)	Age Groups	n	Ventilation Rate (m^3/day)
11-20	845	18.06 ± 3.53	11-20	789	15.01 ± 2.96
21-30	480	25.07 ± 3.94	21-30	548	21.15 ± 4.41
31-40	485	24.03 ± 3.57	31-40	529	19.15 ± 2.50
41-50	498	24.08 ± 3.10	41-50	572	19.02 ± 2.44
51-60	496	24.59 ± 3.49	51-60	469	19.79 ± 2.38
61-70	450	16.86 ± 2.61	61-70	439	12.66 ± 1.79
71-80	470	16.64 ± 2.62	71-80	511	12.60 ± 1.66

These data agree with findings from recent studies that suggest that daily ventilation peaks at around 25 years of age, followed by a decline. The calculated data

also present an increase in ventilation rate between the fourth and sixth decades of life, which corresponds to findings that older adults tend to breathe at higher lung volumes than younger subjects to compensate for increased elastic recoil of the chest wall in older subjects (Janssens 2005).

4.4. Cardiovascular System

The blood vessel is the channel interconnecting different organs and tissues of the body. Blood flow delivers xenobiotic molecules to tissue/organs for absorption, distribution, metabolism and excretion.

4.4.1. Cardiovascular Anatomy and Physiology

The human cardiovascular system serves to transport oxygen and nutrients to body tissues, where they are absorbed to provide energy, and to return carbon dioxide and other metabolic waste products to the lung and kidney for removal from the body. This system consists of two components: the heart and the circulatory loop. The heart functions as a pump, whereas the circulatory loop functions as a transport network.

Cardiac anatomy and function

The human heart has a weight of approximately 250-300 g and a size similar to a closed fist (Tortora and Grabowski 2003). This muscular organ is positioned in the thorax surrounded by a fibrous sac, the pericardium. The external layer of the heart tissue is called the epicardium and the innermost layer in connection to the ventricles the endocardium. The tissue between the two aforementioned layers, the myocardium, is responsible for

ventricular contraction and consists of muscular tissue. The heart is divided into a left and a right side by the septal wall. Each side of the heart consists of two chambers, the atrium and the ventricle, separated by an atrioventricular (AV) valve: the mitral and the tricuspid valves on the left and right sides, respectively. The ventricles are the major pumping parts of the heart, whereas the atria serve largely as antechambers for storing blood during the period when the ventricles are contracting and ejecting. The walls of left heart are quite muscular and when activated generate high pressures.

The ventricles have inlet and outlet valves. The inlet valve between the right atrium and the right ventricle consists of three cusps (tricuspid valve), whereas the inlet valve between the left atrium and left ventricle has two cusps (mitral valve or bicuspid valve). Each outlet valve has three cup-like cusps attached to the valve ring. This structure prevents regurgitation of blood into the ventricles when a brief reversal of blood flow toward the ventricles occurs at the end of ventricular ejection. As an approximation, the valves in the heart can be considered unidirectional and pressure operated. They prevent regurgitation when the pressure in the source chamber is not sufficient to open the valve, and once open, these valves maintain blood flow in a single direction under the positive pressure gradient imposed across the valves.

Blood circulation is maintained by the heart's application of pressure at key positions in the circulatory loop. The left side of the heart delivers oxygen-rich blood to the body (systemic circulation) passing through the aortic valve to the aorta, whereas the right side pumps blood through the pulmonary valve and the pulmonary artery for an oxygen refill in the lungs (pulmonary circulation). The four heart valves act as inlet and outlet check-valves for the ventricles, allowing unidirectional flow and preventing

backflow by being passively opened and closed due to pressure gradients. The plane that separates the ventricles from the atria is often referred to as the AV-plane, where all the valves of the heart are situated. Returning blood from the body flows to the right atrium through the inferior and superior vena cava, while blood from the lungs returns to the left atria through the pulmonary vein.

Several important indices are commonly used to assess cardiac function. The ventricular end-diastolic volume (EDV) is the amount of blood in the ventricle at the end of filling. Ventricular end-systemic volume (ESV) is the amount of blood in the ventricle at the end of ejection. Ventricular end-diastolic pressure is the pressure across the ventricular walls at the end of filling, and ventricular end-systolic pressure (ESP) is the pressure across the walls at the end of ejection.

The amount of blood ejected by a ventricle in each stroke is called stroke volume (SV), and is defined as the difference between EDV and ESV. Left ventricular ejection fraction (EF) is the ratio of the SV to the EDV. Ejection fraction is generally expressed as a percentage, with typical values ranging from 40-60% in normal, healthy individuals. The amount of blood pumped by the heart per minute is called the cardiac output (CO), and is simplistically described as the product of the heart rate (HR) and the SV (American Medical Association, 2003). In reality, CO is a function of many variables, including heart rate, total blood volume, venous resistance, and intrathoracic pressure (Keener and Sneyd 1998). A normal human subject at rest will have an end-diastolic ventricular volume of about 130mL and stroke volume of 70mL. Thus, the typical ejection fraction for human is about 60%. The average cardiac output of the human subject is about 5.0 L/min.

Vascular anatomy and function

Cardiac output affects the blood flow rate to the different compartments in a pharmacokinetic model. The blood flow rate in turn affects the concentration of chemical reaching the different compartments of the body. Hence one of the common ways to divide the organs into compartments and group specific organs together is based on their perfusion, i.e. the amount of blood flow that they receive. For example, organs such as the brain, the kidney, bone marrow and liver receive a large supply of blood, which means that the blood flow rate to these organs is very high (richly perfused organs). Hence in a number of PK/TK studies these organs are grouped in a single compartment. Only when specific organs in such a group are target organs or need to be studied in greater detail, are they separated from the grouping and considered individual compartments.

Receiving the output from the heart, the circulatory system serves to distribute and collect blood through its immense network of vasculature. The blood vessels in the cardiovascular system, estimated to have a total length of 100,000 km (Tortora and Grabowski 2003) can be classified according to their functions into elastic and muscular arteries, and resistance, exchange and capacitance vessels. All vessels, except for the exchange vessels, the capillaries, have the same basic structure. The vessel wall is arranged in three layers; tunica intima, tunica media and tunica adventitia. The tunica intima is the innermost layer, which is in direct contact with the blood. This layer consists of endothelial cells surrounded by a thin layer of connective tissue, providing the vessel with a smooth inner surface. In a young healthy individual, the intima does not contribute to the mechanical properties of the vessel. However, this can change with age, when the intima gets thicker and stiffer (Holzapfel et al. 2000).

The tunica media is the middle layer of the vessel wall, consisting of smooth muscle and elastic and collagen fibers in helically arranged medial layers. Tunica media is the principal determinant of the mechanical properties of the arteries. The media is connected to the intima and adventitia with elastic membranes, the internal and external elastic lamina (Witzleb 1989). The vessel is covered by loose connective tissue in its third layer, the adventitia. This layer consists of thick bundles of collagen fibrils arranged in helical structures which stabilize and strengthen the vessel. In larger arteries, this layer also contains a network of small blood vessels supplying the vessel, the vasa vasorum.

The elastic arteries are the largest arteries, i.e. the pulmonary artery, the aorta and their major branches. They are termed elastic arteries because elastic fibers are dominant in their vessel walls. The function of the elastic arteries is to transform the accumulated potential energy from the ejection phase into kinetic energy during diastole, in order to keep up a more continuous flow in the arteries. This function, called the Windkessel effect, is possible because the walls of an elastic artery easily expand and recoil. Arterial compliance is defined as the change in arterial volume divided by the associated distending pressure. Muscular arteries are located at more peripheral parts of the circulatory system and their main function is to distribute blood to different parts of the body. They are called muscular arteries, since they contain more smooth muscles and less elastic tissue than the elastic arteries. Small arteries and arterioles are termed resistance vessels, since they account for the greatest part of the resistance in the vasculature. The arterioles distribute and regulate the blood flow to the capillaries by adjusting the vessel diameter and thereby the resistance in the vessels. The smallest vessels in the cardiovascular system are the capillaries and their function is to exchange nutrients and gases between the blood in the

capillaries and the surrounding tissue. The capacitance vessels, the venules and veins collect and lead the blood back to the heart again. They work as a blood reservoir and thus can control the returning blood to the heart (Tortora and Grabowski 2003).

From the left ventricle, blood flows through the aorta, arteries, arterioles and capillaries. The capillaries then drain through venules into the veins and back to the right atrium. This is called the systemic circulation. From the right atrium, blood enters right ventricle and is pumped to the blood vessels in the lungs. The blood then is collected in the pulmonary veins and goes back to the left atrium. This part of the circulation is called the pulmonary circulation.

4.4.2. Age-related Changes

The Heart

Alterations in cardiovascular structure and function with age have been studied extensively in both humans and animals. While there seem to be differences between animals and humans with regard to changes in left ventricular structure with aging, both animals and humans undergo some degree of pathological hypertrophy with aging. Senescent rats develop moderate left ventricular hypertrophy in the form of chamber dilation with no increase in wall thickness (Lakatta and Sollott 2002). In healthy aged humans, however, ventricular hypertrophy is seen as an increase in relative wall thickness with little or no change in ventricular mass (Ganau et al. 1995). Mild ventricular hypertrophy is present even in subjects free of hypertension or other causes of increased afterload (Gerstenblith et al. 1977).

The conductile system of the heart also undergoes age-associated changes (Fleg et

al. 1988). After age 60 years, the number of cells in the SA node progressively declines. Some decrease in the resting heart rate with increasing adult age also occurs, and this appears to be due, in part, to a change in the SA node's pacemaker function. Some change with age also takes place in the AV node and its connection to the conductile system of the ventricles, causing a minor delay in the progression of action potentials from the atria to the ventricles. Increasingly common with increasing age are abnormal rhythms (arrhythmias) of the heart, such as a too rapid (tachycardia) or a too slow (bradycardia) heart rate, or the occurrence of pacemaker cells at sites other than the SA node.

It has been shown that aging alone has no significant effect on systolic function. In fact, under resting conditions, ejection fraction, stroke volume, and cardiac index are largely maintained with aging in the absence of disease and diastolic dysfunction (Rodeheheffer et al. 1984; Shivakumar et al. 2003). There is, however, a significant decline in systolic capacity with exercise. The decline in exercise capacity with aging is manifested as a decline in maximal oxygen uptake and maximum heart rate, and a decreased responsiveness to beta-adrenergic stimulation (Rodeheffer et al. 1984). It is widely believed that any alterations in resting cardiac function with age are related to diastolic dysfunction.

This is not to say, however, that the blood flow in an aged population should be expected to mimic that in a younger population. The pump function of the heart also changes with increasing age (Lakatta 1995). With aging, the blood flow into the left ventricle during diastole becomes slower, but this is compensated for by the increased amount of blood pumped by the left atrial contraction in late left ventricular diastole. Thus, at rest, the total amount of blood entering the left ventricle during diastole is similar for old

and young people of the same size and gender. The stroke volume in resting healthy people is similar for young and old of the same size and gender, as is the cardiac output. However, in the healthy young and old, there is one difference in the pump function of the left ventricle. The contraction of the left ventricle is prolonged with increasing age, and this prolongation helps the healthy elderly maintain a stroke volume similar to that of the young.

Diastolic dysfunction is increasingly recognized as a cause of heart failure in the aged population. It has been shown that left ventricular systolic function is preserved in up to 74% of patients with congestive heart failure (Burlew 2004), underlying the importance of diastolic dysfunction in heart failure. Diastolic dysfunction with aging is manifested as alterations in both early (Benjamin et al. 1992) and late (Kuo et al. 1987) left ventricular filling which is likely associated with both active and passive diastolic function.

For several years disparate results existed regarding changes in left ventricular mass with advancing age. Relatively new technologies such as two-dimensional (2D) Doppler ultrasound imaging suggested that, in women but not in men, there was a modest but significant increase in cardiac mass with advancing age (Shub et al. 1994). In a follow-up study Park et al compared the results of calculated left ventricular mass according to American Society of Echocardiography guidelines with autopsy results from those same individuals (Park et al. 1996). Due to the inclusion of papillary muscle tissue in the Doppler images there was a tendency to overestimate the actual left ventricular mass as assessed on autopsy. However, because this error does not appear to be affected by sex it is unlikely to explain the previous observations in aging patients.

Around this same time, Olivetti et al conducted a gross anatomic and histological

investigation to determine the changes in myocardial cell mass and apoptosis with aging and how this might mitigate potential changes in cardiac mass with aging, which appear to be sex-specific (Olivetti et al. 1995). In hearts from 106 women and men (n=53 in each group) between the ages of 17 and 95 they found that females maintained their myocardial mass, average cell volume and diameter. In contrast, men lost approximately 1g/year of myocardial tissue and had larger cell volumes and diameters with increasing age, suggesting compensatory hypertrophy of the remaining cells (Olivetti et al. 1995). More definitive evidence using improved imaging technology came in 2002 when Hees et al examined this question using magnetic resonance imaging (MRI) techniques to study not only the myocardial mass but also its geometry (Hees et al. 2002). When examining 336 individuals on MRI it was found that the heart shortens along its long axis and thus the left ventricle becomes less of a hemi-ellipsoid and more of a hemi-spheroid shape (Hees et al. 2002). Interestingly, women also thicken their ventricular wall to preserve overall mass in the face of this long-axis shortening whereas men do not, potentially accounting for the sex differences in left ventricular mass observed in previous studies.

It is clear that there is a reduction in the peak cardiac output with aging in women and men (Ogawa et al. 1992; Fleg et al. 1995; Hageberg et al. 1985; Hossack and Bruce 1982). This is largely driven by a reduction in peak exercising heart rate in both sexes (Lakatta and Levy 2003) and this reduction is not modifiable by training. Between the ages of 20 and 85 there is an approximately 30% reduction in peak exercising heart rate (Fleg et al. 1995) or approximately 0.7 beats/min/year (Tanaka et al. 2001), and as cardiac output is the product of stroke volume and heart rate, this severely limits the cardiac output reserve in older individuals. The mechanisms behind this reduction in peak heart rate are likely a

reduction in sinoatrial node responsiveness to beta-adrenergic stimulation and reduced conduction velocity of cardiac neural tissue (Fleg et al. 1994), and a decreased intrinsic heart rate (Christou and Seals 2008).

Peak exercise stroke volume also falls in old age in both master athletes and sedentary individuals (Ogawa et al. 1992; Revera et al. 1989). As stroke volume is the integrated output of several determinants both intrinsic to the myocardium such as Frank-Starling mechanism dependent increases in contractility, and extrinsic to the myocardium such as afterload it becomes very difficult to parse the relative impact of each of these influences during any given condition. Previous studies investigating the effect of unloading the aged heart during exercise in an attempt to improve cardiac function have utilized a "balanced vasodilator" (equal effects on venous capacitance and systemic vascular resistance reduce preload *and* afterload simultaneously) such as sodium nitroprusside (Chantler et al. 2011; Nussbacher et al. 1999). This was found to reduce the work of the heart during exercise yet stroke volume and cardiac output remained the same as control exercise bouts due to a concomitant reduction in end-systolic and end-diastolic volume.

The Vasculature

Aging is associated with changes in several structural characteristics of the arterial tree. In a large-scale study of cadaveric aortae from two occidental (Australia and the United States, n=192) populations and a population with low prevalence of atherosclerosis (China, n=80) Virmani et al characterized age-associated morphologic changes (Virmani et al. 1991). They found, in samples from normotensive individuals, that when accounting

for height and weight there was an age-associated increase in aortic diameter that was maximal at the ascending aorta and present in women and men (Virmani et al. 1991). More recently, others have found that the aorta lengthens and becomes more tortuous with age and that this lengthening is primarily confined to the ascending portion (Sugawara et al. 2008). Without any further structural changes, this dilation of the aorta would increase wall tension according to the Law of LaPlace:

$$T = \frac{(P \times R)}{M} \tag{77}$$

where

- T = wall tension
- P = transmural pressure
- R = vessel radius
- M = wall thickness.

Likely in order to normalize wall tension, the thickness of the arterial wall increases with advancing age. In the same cadaveric aorta study cited above, it was found that aortic wall thickness increased with aging and this was due to hyperplastic growth of the intima (Virmani et al. 1991). More recently, research in both non-human primates (Qui et al. 2007) and humans (Wang et al. 2007) has shown increases in intima-medial thickness (IMT) are due to growth of both the intima and medial layers. It is well established from large-scale non-invasive studies that IMT, while highly variable among individuals, increases with age in humans (Lakatta and Levy 2003). Clinically, this is generally assessed in the carotid artery via 2D ultrasound and increased IMT has been shown to be associated with hypertension (Hughes et al. 1993), diabetes (Chen et al. 2010), severity of

atherosclerosis (Bonithon-Kopp et al. 1996) and hypercholesterolemia (Wendelhag et al. 1992). Brachial artery IMT thickness increases similarly with age along the length of the vessel, including both predominantly elastic proximal regions as well as more muscular conduit distal regions (Bjarnegard and Lanne 2010). Finally, femoral artery IMT increases with age in healthy control (Tanaka et al. 2000) and hypertensive subjects as well (Gariepy et al. 1993) and thus the overall literature suggests this is a ubiquitous finding in both central elastic and large conduit arteries of both the upper and lower limbs.

Age-associated functional changes in the arterial vasculature, driven by the aforementioned structural changes as well as biochemical differences between the young and aged (altered production of or response to dilator and constrictor substances, vasoregulatory receptor makeup, bioavailability of dilatory and constrictor substances, etc.) is a broad and prodigious literature. A truly comprehensive review of the functional changes in the arterial vasculature with aging would constitute an expansive work and is beyond the scope of this dissertation. However, a brief discussion of changes in arterial function with aging appears below.

Flow-mediated dilation (FMD) is the dilatory response of a vessel when given an increase in shear force at the endothelium. This property of regulation of arterial caliber was characterized in dog femoral arteries in 1970 (Lie et al. 1970) and later in human brachial arteries (Sinoway et al. 1989). Since that time it has been demonstrated that FMD declines with age in a sex-specific manner. Celermajer et al found that, in men, FMD begins to decline progressively after the age of 40 and in women function is preserved until the early 50s, after which their rate of decline is significantly greater than men (Celermajer et al. 1994). This same study found that in both sexes the response to sublingual glyceryl

trinitrate (GTN, an endothelium-independent vasodilator) did not decline with aging, suggesting a deficit in the ability to sense or respond to shear at the endothelium may underlie this difference and not a loss of ability for arteries to dilate when given nitric oxide. In a follow-up investigation Parker et al. examined both the brachial and popliteal arteries of older women to determine if there is limb-specificity in this functional decline with aging (Parker et al. 2006). When normalizing the percentage dilation to shear rate to more appropriately account for the dilatory response exhibited per unit of stimulus delivered, Parker et al found that there is not limb-specificity in the decline in FMD in older women (Parker et al. 2006) and normalization may abolish the decrease in FMD in older men (Wray et al. 2006).

Gender has been shown to be a contributing factor in decreases observed in measures of arterial function with advancing age. Loss of estrogen at the menopause is associated with a significant increase in overall cardiovascular disease mortality risk (Kannel et al. 1976; Gordon et al. 1978; Guthrie et al. 2004). It has been suggested that there is a linear increase in central elastic and/or peripheral muscular artery pulse wave velocity that is consistent with that found in men (Tanaka et al. 1998; Segers et al. 2007). Other groups have suggested a non-linear increase in this parameter with advancing age, with the slope of the regression line increasing after the common age of the menopause (Takahashi et al. 2005; Zaydun et al. 2006). Regardless of the specific model that best applies, it is clear that vascular stiffness, as indexed by PWV, increases with age in both sexes and may be accelerated by the change in hormonal milieu after the menopause.

4.4.3. Data Summary

Cardiac output is the volume of blood pumped by the heart per minute (L blood/min) and is a function of heart rate and stroke volume. The most widely used methods for measuring cardiac output are the invasive methods of thermodilution, which, involves the danger of inserting a SwanGanz catheter into the circulatory system, and the Fick Method, which requires the measurement of oxygen consumption via the insertion of a pulmonary artery catheter equipped with a fiber optic bundle (Lavdaniti 2008).

Starr derived a method to estimate stroke volume using blood pressure that correlates well with measurements obtained using the other measurement methods (1954). To avoid the need for invasive testing, cardiac output for this study is estimated using the Starr (1954) method and using measurements of the heart rate, pulse pressure, and end diastolic pressure via the following relationships:

$$CO = HR \times SV \tag{78}$$

$$SV = (93 + 0.62 * PP - 0.45 * EDP - 0.61 * age) * 0.001\ L/cm^3 \tag{79}$$

where

- *HR* = the heart rate in beats per minute
- *PP* = the pulse (systolic) pressure in mmHg
- *EDP* = the end diastolic pressure in mmHg
- age is given in years.

Heart rate, pulse pressure, and end diastolic pressure data used in this calculation were extracted from the 2009-2010 NHANES databases and results are presented in Table 4.17 below.

The cardiac output rates determined using the Starr method overestimate the measured cardiac output values presented in Williams (1994) by more than 20% in males and up to nearly 50% in females. However, the calculated data and measured data do both reflect the overall tendency for cardiac output to peak in the late teens to early twenties and then decline with age. The principal drawback of the Starr method for calculating cardiac output is that it does not take into account the degree of venous compliance to the pressures generated by the heart, and so may not reflect the true heart rates in those with varying degrees of atherosclerosis (Starr 1954).

Table 4.17 Estimation of cardiac output values using the NHANES 2009-2010 heart rate, age, and blood pressure data sets.

Males			Females		
Age Groups	n	Cardiac Output (L/min)	Age Groups	n	Cardiac Output (L/min)
11-20	751	9.17 ± 1.61	11-20	751	9.66 ± 1.55
21-30	454	8.49 ± 1.49	21-30	519	8.93 ± 1.42
31-40	459	8.02 ± 1.40	31-40	484	8.28 ± 1.35
41-50	485	7.70 ± 1.45	41-50	539	7.83 ± 1.39
51-60	478	7.49 ± 1.50	51-60	458	7.72 ± 1.34
61-70	437	7.28 ± 1.56	61-70	414	7.62 ± 1.53
71-80	454	6.88 ± 1.45	71-80	491	7.49 ± 1.48

Williams presents a different regression method for calculating cardiac output based on oxygen consumption. For males, cardiac output (in liters per minute) can be estimated by

$$CO = 4.0 + 10 \times VO_2 \quad (80)$$

and females by

$$CO = 4.1 + 8.4 \times VO_2 \quad (81)$$

where VO_2 is the oxygen consumed in liters per minute. This regression equation does not have a visible age coefficient because oxygen consumption is age-dependent and the coefficient is included in the determination of oxygen consumption for each age group. As shown in Table 4.18, the cardiac output values derived using this method still follow the general pattern of a peak in the second to third decades of life, followed by a gradual decline with age.

Table 4.18. Calculated cardiac output based on oxygen consumption rates and using data from the NHANES 2009-2010 data set.

Males			Females		
Age Groups	n	Cardiac Output (L/min)	Age Groups	n	Cardiac Output (L/min)
11-20	845	8.51 ± 0.90	11-20	789	6.99 ± 0.60
21-30	480	9.06 ± 0.78	21-30	548	7.40 ± 0.69
31-40	485	9.04 ± 0.73	31-40	529	7.21 ± 0.38
41-50	498	9.01 ± 0.64	41-50	572	7.18 ± 0.39
51-60	496	8.94 ± 0.70	51-60	469	7.19 ± 0.37
61-70	450	8.24 ± 0.66	61-70	439	6.95 ± 0.40
71-80	470	8.01 ± 0.63	71-80	511	6.81 ± 0.36

The values derived using oxygen consumption rates are still markedly higher than those determined by direct, invasive sampling. However, the calculated values assume an oxygen consumption rate that corresponds to light-to-medium exertion, whereas direct sampling is generally conducted with the subject relaxed and in a recumbent position (Williams, 1994).

Change in regional blood flow varies with organ, with the most pronounced changes being evident in the kidneys (Ritschel 1988). However, these changes are generally proportional to changes in organ mass, such that the regional blood flow rate in mL of fluid per mass of tissue per hour is unchanged.

4.5. Gastrointestinal System

Absorption is one of the processes that influence the kinetics of a radionuclide. Pharmacokinetic models have traditionally used first order absorption assumptions to describe the oral absorption rate of drugs from the gastrointestinal tract. However, oral drug absorption is a complex process affected by physicochemical properties of the drug, drug formulation, and gastrointestinal physiology factors. Several parameters need to be studied to define and model the events involved in gastrointestinal tract absorption of nutrients and non-nutrients. These include anatomical and physiological features of the gastrointestinal tract such as surface area, vascularity, transit time/motility and enterohepatic circulation (DeSesso and Jacobson 2001). There are also the physicochemical properties of the digested material and the functional ingredients of interest in it such as lipophilicity, chemical and/or enzymatic stability, solubility, particle size, density, diffusivity, pKa and crystal form. Other factors are the type of membrane transport mechanism (described in Section 2.2.4.1), pH and stomach emptying (Idkaidek and Abdel- Jabbar 2001).

The duration of absorption and of excretion will influence the duration of efficacy of a drug (Theeuwes 1985). The former cannot be longer than the residence time of the dosage form in the region of absorption. This residence time is itself dependent on the rate

of gastric emptying of the formulation, and so, gastric emptying rather than permeation is prospectively the primary rate-limiting step in drug absorption (Gibaldi 1981). Thus, factors that affect gastric emptying could markedly influence drug absorption.

4.5.1. Anatomy

The GI tract consists of the mouth, esophagus, stomach, small intestine (duodenum, jejunum, and ileum), the liver and gallbladder, and the large intestine (cecum, colon, and rectum). The GI tract not only serves as a region in the body where digestion of ingested food and absorption of necessary nutrients to maintain life occur, but it also prevents potentially harmful xenobiotics from entering the systemic circulation by acting as a barrier (Guyton, 1996). Furthermore, it excretes any unabsorbed GI contents from the body. The diversity in structure and environment of the GI tract is a reflection of the many essential functions that this part of the body performs.

Food enters the stomach from the mouth in the form of a food bolus (a soft wet ball of food made after the mouth has chewed and moistened it). The stomach then acts as a short-term storage reservoir to allow large meals to be consumed quickly and then processed over a period of time. The stomach performs the function of mixing and grinding the digesting food with gastric secretions, resulting in a food form suitable to be presented to the small intestine. The stomach serves as a temporary reservoir for ingested food and is not considered to be a major site of absorption for most drugs due to its small surface area.

Peristaltic waves originate from the stomach wall and spread toward the antrum, mixing and forcing the antral contents toward the pylorus. The pylorus contracts to slow gastric emptying and results in further mixing of gastric contents (Kong et al., 2008).

During this time, the stomach transforms its contents into a multiphase slurry called chyme. The chyme is a combination of separate phases of aqueous solutions, fats, and solids. More intense peristaltic waves promote antral emptying, which allows gastric contents, mainly fluid mixed with small particles, to pass through the pylorus and enter the duodenum in the small intestine. The particle size of the food emptied through the pylorus is less than 1 to 2 mm during the fed state (Thomas 2006). The typical gastric contents in the stomach have a viscosity roughly in the range 0.01 to 2 Pa*s and a density close to that of water (Marciani et al. 2000; Abrahamsson et al. 2005).

The small intestine is the predominant site for absorption in the GI tract due to its large surface area. The small intestine is loosely divided up into three parts (duodenum, jejunum, and ileum) and the mean total length is said to be 285 cm. The mean length of the duodenum is approximately 25 cm and the jejunum and ileum combined are approximately 260 cm (Ganong 2005). The average length of the human small intestine will vary depending on sex, height, weight and method of measurement (Ganong 2005). The diameter of the intestine gradually decreases from the proximal to the distal end. Finger-like projections, known as villi and microvilli which are located on the walls of the small intestine greatly increase the small intestine surface area. The small intestine is the major area of absorption of water, nutrients and electrolytes.

The structure of the liver is comprised of liver cells, called hepatocytes, arranged in thin layers in a radial pattern around a central vein. Hexagonal blocks of such layers are called lobules. Spaces, called sinusoids, exist between the layers of hepatocytes and are supplied by two sources of blood. First, the liver is supplied by arterial blood from the hepatic artery. Second, the liver is supplied by the hepatic portal vein, which transports

blood from the gastrointestinal tract and spleen. This physiological feature prevents contaminants from entering systemic circulation directly and is called the “first-pass effect." Combined, these two supplies carry approximately 25% of systemic circulation to the liver at any given time (Garnett 2007).

Orally deposited xenobiotics need to traverse the gut wall, enter into enterocytes, diffuse into intestinal portal blood, and reach the liver. A distinct intestinal blood flow pattern has been observed for various tissue layers of the intestine: the mucosa, submucosa and muscular layer versus the serosa which lies inferior to the muscular layer (Granger et al. 1980; Cong et al. 2000). The majority (approximately 70% to 90%) of the intestinal blood flow perfuses the non-absorptive, non-metabolic serosal region whereas only 10% to 30% of the blood flow reaches the enzyme- and transporter-rich enterocyte region at the mucosal layer (Mailman 1978; Granger et al. 1980; Schurgers et al. 1984; Cong et al. 2000). As a result, orally deposited materials are more accessible to intestinal enzymes and transporters compared to intravenously administered materials. This blood flow pattern has been incorporated into the “segregated-flow model” of the intestine in describing “route dependent metabolism” (Cong et al. 2000).

Bicarbonate is released from the pancreas to help neutralize acidic contents that are emptied from the stomach and prevent ulceration from occurring in the duodenal wall. Bile is made in the liver and stored in the gall bladder and is secreted into the duodenum. It contains bile salts (sodium and potassium salts of bile acids which are synthesized from cholesterol) that emulsify dietary fat into small droplets to increase surface area for lipase activity (Ganong 2005). Re-absorption of most of the secreted bile salts occurs in the ileum for re-use. The acidic intestinal contents entering from the stomach are neutralized by a

bicarbonate secretion from the pancreas that enters the duodenum to obtain the appropriate pH for small intestinal enzymes (Minekus et al. 1995). Pancreatic juice is also secreted into the duodenum and contains a complex mixture of enzymes. The pancreatic juice is alkaline and neutralizes the gastric acid, raising the pH of the duodenal contents to 6.0 – 7.0. The powerful protein-splitting enzymes of the pancreatic juice are secreted into the small intestine (Ganong 2005). Approximately 1500 mL of pancreatic juice and 500 mL of bile is secreted per day.

The large intestine, or colon, is the portion of the digestive system most responsible for absorption of water from the indigestible residue of food. The human colon is about 1.5m long and is generally described in several parts: appendix, cecum, ascending colon, transverse colon, descending colon, sigmoid colon, rectum and anus. Material passes through the ascending, transverse, descending and sigmoid portions of the colon and finally enters into the rectum. From the rectum, the waste is expelled from the body (U.S. National Library of Medicine, 2008 - www.nlm.nih.gov). The large intestine removes about 90% of the fluid; it converts 1000-2000 mL of isotonic chyme that enters it each day from the ileum, to about 200-250 mL of semisolid feces.

4.5.2. Physiology

The processing of food by the gastrointestinal system involves the following activities: motor activity of the gastrointestinal tract; glandular secretion; digestion; and absorption of substances from the lumen of the gastrointestinal tract into the blood or lymph. It is generally assumed that radionuclide intakes via oral routes have an emptying pattern similar to food. Thus, liquid formulations behave as simple liquids, and show an

exponential emptying pattern (Jenkins et al. 1983). Solid particulates and larger solids will have a similar exponential pattern of emptying, after an initial dissolution lag phase (Hunter et al. 1981).

The emptying of stomach contents predominantly occurs in a pulsatile manner and is a well coordinated event between the stomach, pylorus, and duodenum. The coordination is especially apparent during Phase III of the migrating motor complex (MMC), a multi-phase cycle of intense contractile activity that occurs during the fasted state. When the antrum contracts during Phase III, the pyloric sphincter relaxes and the duodenal bulb briefly stops contractile activity to accept a bolus from the stomach. Once a bolus is emptied from the stomach the pyloric sphincter contracts preventing further flow of contents into the duodenum and Phase III contractile activity resumes in the duodenum (Horowitz et al. 2001).

Physical properties of the gastric contents such as volume, caloric content, viscosity, density, and particle size can influence gastric emptying rates (Gentilcore et al. 2003). Major differences exist in the gastric emptying patterns of digestible solids and non-nutrient liquids. Solids empty relatively slowly in an overall linear fashion, while non-nutrient liquids empty rapidly in an overall exponential fashion. As the caloric content of liquids increases, emptying slows and approximates a linear pattern (Collins et al. 1983; Gentilcore et al. 2003). The emptying pattern of digestible solids is typically characterized by a lag time of approximately 20-60 minutes.

In addition to the physical properties of the gastric contents, the gastric emptying rate is influenced by gastrointestinal motility in the fasted state. In a study that investigated the human gastric emptying rate of 50 mL and 200 mL of water during different phases of

the MMC, it was found that the gastric emptying of liquids can be greatly influenced by the different phases of the MMC (Oberle et al. 1990). The mean gastric emptying rate for 50 mL of water increased with increasing contractile activity. The gastric emptying half lives for 50 mL of water were 61 min, 17 min and 9 min for Phase I, Phase II and Late Phase II/Phase III, respectively. The gastric emptying lag time for 50 mL of water also depended on the phases of the MMC and decreased with increasing contractile activity.

The gastric emptying lag times for 50 mL of water were 19 min, 7.6 min, and 4 min for Phase I, Phase II and Late Phase II/Phase III, respectively. The gastric emptying of 200 mL of water was influenced differently by the phases of the MMC than 50 mL of water. During Phase I and Phase II the gastric emptying rates were found not to be statistically different from each other. The gastric emptying half lives for 200 mL of water were 14 min, 10 min, and 5 min for Phase I, Phase II and Late Phase II/Phase III, respectively. The gastric emptying lag times for 200 mL of water were 7 min, 4 min, and 2 min for Phase I, Phase II and Late Phase II/Phase III, respectively. The results of the study suggest that the gastric emptying of small volumes of liquid are more sensitive to stomach motility changes than larger volumes of liquid. However, both 50 mL and 200 mL of liquid had significantly increased rates of gastric emptying during Late Phase II/Phase III activity.

Other physiological factors known to alter gastric emptying include stress (Cann et al. 1983), posture (Hunt et al. 1965), and sex of the subject (Notivol et al. 1984). A relationship has been shown between gastric emptying and the phase of the menstrual cycle (Wald et al. 1981), and also the presence of pregnancy (Munro and Eckerman 1998).

Recent research indicates that gastric emptying is controlled so that about 2 to 4 kcal/min (8.4 to 16.8 kJ/min) caloric content is delivered to the duodenum through a

negative feedback mechanism mediated by the duodenal receptors. Meals with similar energy content are emptied from the stomach at similar rates which has been shown using magnetic resonance imaging studies (Faas et al. 2002; Gentilcore et al. 2006).

The manner of movement within the small intestine depends on the volume and composition of food, although little is known about these characteristics in each region of the intestine. It is known that duodenal contents are more voluminous and less viscous than ileal contents. Non-propulsive contractions serve to mix and locally circulate the contents by rhythmic segmentation, causing movements at the oral and distal ends, but no net propulsion. Propulsive contractions, or peristalsis, propel the intestinal contents toward the colon over varying distances, but cause little mixing (Bayliss and Starling 1899).

The duration of transit of a substance through the small bowel will influence the extent of absorption (Johansson 1975). A comprehensive study of small intestine transit times in a number of subjects between the ages of 1-25 years reported mean transit times of 2.75-3h (Lonnerblad 1951). Unlike the stomach, the small intestine does not differentiate between solids and liquids, and both materials move through the intestine at the same rate (Malagelada et al. 1984). However, liquids reach the colon faster than solids, when considering stomach to cecum transit, due to the difference in gastric emptying.

The digestive system is unique in that veins converge from the stomach, small intestine and large intestine to form the portal vein, which brings venous blood to the liver instead of the right atrium of the heart. Thus substances that are absorbed from the GI tract and enter the portal vein must pass through the liver before entering the systemic circulation. The liver is a highly perfused organ. Approximately 25% of its blood supply comes from the hepatic artery, which provides oxygenated blood, and 75% is provided by

the portal vein, which is enriched in nutrition and xenobiotics (Bernareggi and Rowland 1991; Kawai et al. 1994). The highly branched capillary vessels, together with the discontinuous (fenestrated) endothelium, allow dissolved molecules within the blood space to come into contact with the hepatocyte directly for metabolism and biliary excretion (Horn et al. 1986).

Water-soluble nutrients leave the GI tract in the blood and travel via the portal vein, first to the liver where some nutrient metabolism occurs (chemical reaction to break down or build the chemicals) and then to the heart. Fat-soluble nutrients enter the lymphatic system. Unlike blood, the lymphatic system has no pump for fat-soluble nutrients and instead these nutrients eventually enter the vascular system, though they bypass the activity of the liver (Insel 2004).

The large intestine receives unabsorbed material from the small intestine and stores it before it is excreted. During the time that unabsorbed material stays in the large intestine most of the remaining water is absorbed to compact the material into feces. It has been commonly thought that drug absorption in the colon is low due to a low surface area and tighter tight junctions compared to the small intestine. However, studies that evaluated regional permeabilities in rats using an Ussing chamber technique showed that some drugs may be absorbed well in the colon. It was found that hydrophilic compounds had decreased permeabilities in the colon compared to the jejunum. However, hydrophobic compounds had similar or increased permeabilities in the colon compared to the jejunum (Ungell et al. 1998). This study suggests that significant absorption of hydrophobic drugs can occur in the colon.

All segments of the colon have the capacity both to propel and prevent too rapid a progression of contents. This storage function facilitates digestion, reabsorption of ileal fluids and production of fecal mass. Furthermore, this property makes it more appropriate to measure colon transit time in days rather than in hours (Hinton et al. 1969). Early studies have suggested that stools are retained in the right half of the colon (Edwards and Beck 1971), although a more recent study suggests that the transverse colon is the primary site of storage (Krevsky 1986).

Table 4.19. Residence times of material in each of the four primary segments of the human gastrointestinal tract.

Section of GI Tract	Approximate Residence Time
Mouth	A few seconds to a few minutes (Dean and Ma 2007)
Stomach	A solid substance varies from 15 minutes to about 2 hours (Banker and Rohodes 2002)
Small Intestine	Transit time is 2.5 hours +/- 78 minutes (Yu et al. 1996)
Large Intestine	12-25 hours (Matont et al. 1993)

4.5.3. Age-related Effects

In the healthy elderly, changes in swallowing are minor and do not cause significant functional difficulties. However, swallowing difficulties can arise with age-associated diseases that adversely affect motor nerve control of the swallowing process; these include: stroke, Parkinson's disease, amyotrophic lateral sclerosis, and myasthenia gravis. In addition, reduced compliance of the upper esophageal sphincter is more common in the elderly, which interferes with the passage of the food bolus from the throat down into the esophagus. Heartburn is the result of reflux of stomach contents through the lower esophageal sphincter up into the esophagus. Such reflux increases with age and may lead to serious complications such as ulceration of the esophagus.

Early studies suggested that there is a positive correlation between advancing age and the retardation of gastrointestinal physiological functions (Horowitz et al. 1984). Gastric emptying of both liquids and solids was long believed to slow with advancing age. However, using advanced technologies, recent studies indicate that there is no clear evidence that these changes are clinically significant (O'Mahony et al. 2002).

Small intestinal transit times may be measured by a variety of techniques, including breath tests, transit scintigraphy and manometry (Hsu et al. 2012). Small bowel motility is essentially unchanged with normal aging (O'Mahoney et al. 2002).

The elderly frequently complain of constipation. However, this is commonly the result of increased and prolonged intake of constipating drugs, reduced intake of dietary fiber, and relatively low levels of physical exercise rather than an intrinsic effect of the physiological changes that accompany aging. Opioid analgesics are among the most widely prescribed drugs in elderly people. For centuries, constipation has been a well known adverse effect of opioids, being mediated principally through reduced colonic propulsive activity (O'Mahoney et al. 2002). Studies utilizing objective measures of constipation indicate that it does not occur more frequently in the elderly than in the young (Lovat 1996).

The elderly also frequently complain of diarrhea, but the healthy elderly do not suffer from diarrhea. When diarrhea poses a serious problem for the elderly, it is related to some disease. The elderly are more prone to fecal incontinence than the young because of both higher rectal pressures, when the rectum is distended by a fecal mass, and reduced force of the anal sphincters. These studies have concluded that most of the problems the elderly suffer in evacuating as well as the increasing prevalence of fecal incontinence with

increasing age are likely the result of mechanical changes and decreased muscle strength (Lovat 1996). In anatomical terms, increasing age is accompanied by a thinning of the external anal sphincter and a thickening of the internal anal sphincter (O'Mahoney et al. 2002).

There is relatively little measured data on the effects of aging on gastrointestinal motor function in humans. There is a growing body of data that suggests there are effects (particularly slowing effects) on colonic transit in women during different stages of the menstrual cycle (Stubbs 1992). Analyses performed in 2004 showed that advanced age did not influence gastric emptying, postprandial frequency of antral contractions or small intestinal transit rate, although the older subjects had a longer colonic mean transit time than young subjects (Madsen and Graff 2004).

4.6. Kidneys

The primary function of the kidney is the maintenance of internal homeostasis of fluids, excretion of metabolic wastes, conservation of nutrients and regulation of acid/base balance (McCance and Huether, 2006).

4.6.1. Renal Anatomy and Physiology

Like the liver, the kidneys receive a considerable amount of cardiac output (approximately 25%), or approximately 1.2-1.3 liters of blood per minute. The functional unit of the kidney is the nephron, which are small tufts of blood capillaries. These capillaries have small fenestrations which allow glomerular filtration of blood with transit across Bowman's Capsules. Afferent arterioles bring blood to the nephrons, which then

filter the blood, actively secrete substances from the blood, and finally reabsorb water and electrolytes, and eliminate waste as urine. Through the different membranes of the glomerulus, proximal tubule, Loop of Henle, and distal tubule, via both active and passive transport, wastes are excreted and nutrients conserved, and electrolyte balance is maintained. When damage occurs within the nephron, wastes are no longer cleared from the body, fluid is retained, and nutrients are no longer conserved. The kidney functions as a filter for wastes from the body. When the kidney fails to clear the wastes from the body, they accumulate. The health of the kidney directly impacts an individual's overall health. The ability of the kidney to filter waste products directly impacts any medications prescribed or diagnostic procedure.

GFR cannot be measured directly, but must be calculated by measuring a substance that is eliminated at a constant rate by the kidneys. Creatinine meets this criterion and is routinely used to estimate GFR by calculating the rate at which the kidneys eliminate it from systemic circulation. This estimation is known as creatinine clearance. Recent guidelines of the National Kidney Foundation propose to use an estimation of GFR as the best index of the level of kidney function. The level of GFR should be estimated from prediction equations that take into account the serum creatinine concentration and some or all of the following variables: age, gender, race, and body size (National Kidney Foundation 2002).

Besides renal function, the health of the kidneys is reflected by its size. Factors affecting renal size and function include age, gender, body weight, but also hypertension and diabetes mellitus (Culleton et al. 1999; Emamian et al. 1993).

4.6.2. Age-related Effects

Structural and functional changes occur in the kidneys with increasing age during adult life (Lindeman 1995). Advancing age is associated with progressive loss of renal mass. Renal weight decreases 20 to 30 per cent between the age of 30 and 90 years (Tauchi et al. 1971; Brown 1986). Renal length diminishes by 2 cm between the age of 50 and 80 years (McLachlan 1987). The loss of renal mass is primarily cortical, with relative saving of the renal medulla.

There is a progressive reduction in renal plasma flow of approximately 10% per decade (Vestal 1997). The decrease in renal blood flow is associated with significant increases in both the afferent and efferent arteriolar resistance (McDonald et al. 1951). Studies looking at the relationship between renal plasma flow and cardiac output, suggest that the major determinants of reduced renal blood flow with age are the primary anatomical and/or functional alterations in the renal vasculature and not the changes in cardiac output (Lee et al. 1966). Much of the decrease stems from the constriction of the kidney arterioles, which increases the resistance to blood flow through the kidneys.

Aging is associated with subtle losses of glomeruli due to vascular ischemia and scarring. The fall in the total number of identifiable glomeruli with age is roughly in accordance with the changes in renal weight (Dunnill and Halley 1973; McLachlan et al. 1977). The proportion of sclerotic glomeruli identified on light microscopy increases from 1-2% during the third to fifth decade, to 12% after age 70 and is as high as 30% in some apparently healthy 80-years-old people (Kaplan et al. 1975). Glomerular basement membranes are patchily reduplicated and, in general, thicker than in the young (Steffes et al. 1983). However, despite these changes, studies of glomerular filtration characteristics

show no differences in glomerular permeability with aging.

Loss of glomeruli leads to an almost inevitable loss of glomerular function measured by decreasing glomerular filtration rate. Multiple studies have shown that most persons experience at least some decline in glomerular filtration rate of approximately 0.75 mL/min/year after age 40 (Lindeman and Goldman 1986; Lindeman et al. 1985).

The first longitudinal study to look at glomerular filtration rate over time in older individuals was a cross-sectional study of 548 healthy volunteers published from the Baltimore Longitudinal Study on Aging (Rowe et al. 1976a). The study demonstrated a progressive linear decline in creatinine clearance of 0.9 mL/min/1.73m²/year. This study also showed that 254 normal subjects followed longitudinally had a decline in GFR with age, with a main decrease of 0.75 mL/min/1.73m²/year. However, 36% of the subjects did not show an absolute decrease in creatinine clearance (Lindeman et al. 1985), suggesting that age-related loss of glomerular function is not a universal phenomenon, and that dietary, metabolic, hormonal or hemodynamic factors may play a major role in modulating the age-related decrease in renal function (Lindeman et al. 1985; Fliser et al. 1997).

The naturally occurring substance which correlates best with kidney function across all ages has historically been creatinine. Creatinine is a byproduct of muscle mass and dietary protein intake. Theoretically a constant amount is produced and a constant amount is filtered out of the serum by the kidney. However, the decrease in GFR with aging is usually not accompanied with an elevation in serum creatinine concentration (Rowe et al. 1976b). Since muscle mass, from which creatinine is derived, falls with age at approximately the same rate as GFR, the age-related loss of renal function is not reflected by an increase in the serum creatinine (Hadj-Aissa et al. 1990). Thus, the serum creatinine

level usually underestimates the decline in GFR in the elderly (Cameron and Macias-Nunez 1998).

More robust descriptive observational data is reported from the Baltimore Longitudinal Study, but looking at longer periods of time by Robert Lindeman from data collected between 1958 and 1981 (Lindeman et al. 1985). These data were derived from 446 men who were included in the study who had at least five creatinine clearance determinations during the study period. The study sample was primarily well educated, middle class Caucasian men who volunteered to participate. When subjects with possible renal or urinary tract diseases or on antihypertensive or diuretic medication therapy were removed from the study sample, 254 subjects remained who were considered to have "normal" renal function. The mean decrease in creatinine clearance was 0.75 mL/min/year. One third of the subjects had no absolute decrease in function and there was a small group of subjects who showed a statistically significant increase in creatinine clearance with age.

Equations for estimating GFR based on creatinine clearance were first proposed by Cockcroft and Gault in 1976 (Cockcroft & Gault 1976). The purpose was to develop an easy method to predict renal function from common, easily obtainable serum biochemistry. The best method for measuring renal function at the time was 24 hour creatinine clearance, so the estimating equation measured how closely it could predict the creatinine clearance produced by a 24 hour creatinine clearance. In 1999, Andrew Levey and colleagues followed a similar pathway to produce a simpler estimating formula which involves more easily obtained variables and developed the Modified Diet in Renal Disease (MDRD) estimation formula (Levey and Bosch 1999).

The Cockcroft/Gault formula uses the variables of serum creatinine, weight, gender

and age to predict creatinine clearance (Cockcroft and Gault 1976). The authors developed and tested the equation on 236 mostly male (96%) inpatients at the Queen Mary Veteran's Hospital in Montreal, Quebec. All subjects who were participants in the study had at least two measured 24 hour urinary creatinine clearances that were stable over time (defined by the authors as not differing by more than 20% from one measurement to the next). The subjects did not have known renal disease. The authors compared the measured 24 hour creatinine clearance of each subject to the predicted creatinine clearance from four different equations, two equations by Jelliffe (1971; 1973), one by Edwards and Whyte (1959) and the last determined from multiple regression of variables based on a separate sample of 249 patients. The resulting equation has since been known as the Cockcroft/Gault equation for estimating creatinine clearance. This equation had the highest correlation with 24 hour creatinine clearance of any formula to date with a correlation coefficient of 0.83. Cockcroft and Gault speculated that the reasons for their improved accuracy over any prior formula are due to the inclusion of age and weight as variables. They suggest that the inclusion of these variables may help to capture the decline in muscle mass that occurs with aging.

The second most popular equation was developed in the 1990s by a large group studying the impact of dietary protein intake on renal disease (Levey and Bosch 1999). The scientists performed a multiple regression on 1628 subjects who had known renal disease. They compared their estimations to inulin clearance instead of creatinine clearance. The initial equation included gender, race (Black or not Black), age, serum creatinine, serum albumin and serum urea nitrogen. The formula was later abbreviated and albumin and urea nitrogen were dropped. This equation is easier for laboratories to use to produce an

estimated GFR (eGFR) because weight is not a variable in this equation; all the other variables besides creatinine are demographic. The weakness of this equation is that the subjects in the sample from which the regression equation was drawn were middle aged (subjects' mean age was 50.6 years) and not elderly subjects. Also all the subjects in the sample had known advanced kidney disease.

Amit Garg and associates published a secondary analysis of 5,248 subjects 60 years of age and older who were participants in the National Health and Nutrition Examination Survey III which is reflective of data gathered from 1988-1994 (Garg et al. 2001). Their study was intended to answer the question of whether renal insufficiency was associated with malnutrition, independent of relevant demographic, social and medical conditions. Using the MDRD formula, estimated GFR less than 30 was present in 2.3% of men and 2.6% of women. These participants demonstrated low protein and energy intake and higher serum markers of inflammation. Thirty-one percent of individuals with malnutrition had GFR less than 60. GFR less than 30 was independently associated with malnutrition in this study.

One of the most extensive studies to date done in an elderly population was published in 2004 by Garg and colleagues. The study is important because the sample included 9,931 long term care residents who were at least 65 years of age. This study was a cross-sectional analysis of NHANES III data. The researchers compared the estimates of GFR produced by the Cockcroft/Gault and MDRD formulas. They found that the Cockcroft/Gault formula produced a consistently lower estimate than did the MDRD, which was most pronounced in the oldest subjects (Garg et al. 2004).

Pedone, Corsonello, and Incalzi (2006) studied 7,747 acute care geriatric ward

patients whose mean age was 77.8. They compared estimated GFR by Cockcroft/Gault and by MDRD 1 and MDRD 2. MDRD 1 includes serum albumin and BUN in addition to all other variables. MDRD 2 is abbreviated and only requires demographic variables with serum creatinine. They found mean eGFR by Cockcroft/Gault to be 51.2, by MDRD 1 to be 54.9 and MDRD 2 to be 64.7. They concluded that although the formulas have good agreement, they cannot be used interchangeably in individual patients or populations.

4.6.3. Data Summary

Glomerular filtration cannot be measured directly, so the Cockcroft/Gault formula, as shown below, was used to estimate the mean value for each decade of life.

$$eGFR = \frac{(140 - Age) \times Body\ Mass\ (kg) \times\ 0.85(if\ female)}{72 \times Serum\ Creatinine\ (in\ ^{mg}/_{dL})} \quad (82)$$

Creatinine data and body mass were extracted from the 2009 National Health and Nutrition Examination Survey databases, maintained at the CDC website (www.cdc.gov/nchs/about/major/nhanes/), as presented below.

Table 4.20 American population glomerular filtration rate estimated using the Cockroft/Gault formula and data from the NHANES 2009 data set.

Males			Females		
Age Groups	n	GFR	Age Groups	n	GFR
11-20	671	156.33 ± 53.58	11-20	591	142.75 ± 43.65
21-30	443	144.13 ± 41.29	21-30	504	150.09 ± 56.39
31-40	446	145.23 ± 43.60	31-40	498	140.17 ± 46.33
41-50	467	128.06 ± 35.62	41-50	540	121.57 ± 39.02
51-60	456	111.49 ± 33.00	51-60	429	106.88 ± 32.22
61-70	414	92.76 ± 27.88	61-70	405	90.76 ± 27.11
71-80	428	66.10 ± 21.59	71-80	448	60.48 ± 22.33

4.7. Liver

The liver is the largest gland in the human body and is located in the upper right section of the abdominal cavity. It lies below the diaphragm, to the right of the stomach, and above the right kidney and intestines. In adult males the liver weighs from 1.4 to 1.6 kg and in adult females from 1.2 to 1.4 kg. It is relatively much larger in the fetus than in the adult, constituting, in the former, about one-eighteenth, and in the latter about one thirty-sixth of the entire body weight.

Structurally the gland has two lobes: a larger right lobe and a smaller left lobe, which are further subdivided into lobules. These lobules are held together by an extensively fine areolar tissue, in which ramify the portal vein, hepatic ducts, hepatic artery, hepatic veins, lymphatics and nerves. The entire structure is invested by a serous and a fibrous coat. Lobules constitute the chief mass of the hepatic structure. Each lobule consists of a mass of hepatic cells, arranged in irregular radiating columns between which run the blood channels (sinusoids) and minute bile capillaries. Each lobule measures approximately 1 to 2.5 mm in diameter.

The liver performs numerous functions for the body: it produces proteins, bile, and cholesterol; it stores glucose; and it regulates amino acid concentrations. Most importantly for this study, the liver metabolizes toxins to water-soluble substances that the kidneys excrete in urine. The cells within the liver that perform these functions are called hepatocytes. Only 60% of the liver's cells are hepatocytes; the remainder is mostly vascular tissue.

The liver connects to the rest of the body via four routes: the hepatic artery, the portal vein, the hepatic vein, and the hepatic duct. The hepatic artery and portal vein supply

blood to the liver. The hepatic vein takes blood from the liver. The hepatic duct takes bile from the liver to the gall bladder.

The hepatic artery connects the liver directly to the heart and lungs and hence supplies blood rich in oxygen. Approximately 30% of the liver's blood flow is attributable to the hepatic artery. However, the liver metabolizes only 25% of this blood. The remaining blood from the hepatic artery either nourishes the liver or passes straight through. The portal vein supplies the remaining 70% of the liver's blood supply. The blood from the portal vein passes first through the alimentary tract, spleen, or pancreas before entering the liver. This blood is poor in oxygen but rich in nutrients. The liver acts on all blood entering through the portal vein. This allows the liver to examine and filter ingested substances before it enters other parts of the body. Hence the liver has the opportunity to metabolize only 30% x 25% + 70% = 77:5% of the blood that enters it.

The hepatic artery and portal vein branch as they enter the liver lobes into what we respectively call arterioles and venules. The branches pair up into portal tracts though their blood does not mix until it reaches the actual hepatocytes. This newly mixed blood must squeeze between the hepatocytes. These passages are not vascular; blood is seeping through the hepatocytes in the same way water seeps through soil. The pathway is barely large enough for blood to pass. This tightness provides the blood better contact with the hepatocytes which gives the substances greater opportunity to pass from the blood to the hepatocytes where the metabolism actually occurs. The breaks between hepatocytes through which blood passes are called sinusoids. In a sense sinusoids are the capillaries of the liver; they are regions where passages are tightest and the exchange between blood and tissue occurs. After blood passes through the hepatocytes, it enters a central vein. These

central veins anastomose and empty into the hepatic vein as the blood leaves the liver. The hepatic vein empties into the vena cava which leads to the kidneys.

The biliary network is the conduit between the hepatocellular parenchyma of the liver and the lumen of the small intestine. Microscopic ductules are called bile canaliculi which are spaces of 0.5-2 μm wide formed between the neighboring hepatocytes (Ludwig et al. 1998; Boyer et al. 2006). A bile canaliculus is a dilated intercellular space between adjacent hepatocytes. Hepatocytes secrete bile into the canaliculi and bile flows parallel to the sinusoids but in the opposite direction of blood. At the ends of the canaliculi, bile flows into bile ducts. Bile duct is lined with simple cuboidal epithelium and collects the bile directly from the hepatocellular parenchyma via the canals of Herring (Takasaki and Hano 2001). Small bile ducts converge into larger ductules and larger ducts eventually forming the common bile duct which dumps bile into the gall bladder. This is a sac-like structure adhering to the liver which has a duct that leads directly into the common bile duct.

4.7.1. Physiology

The liver is a complex organ that has pivotal roles in metabolism, synthesis and storage of carbohydrates, lipids, vitamins and proteins as well as blood filtration from bacteria, bacterial endotoxins, antigen-antibody complexes and other toxic substances by specific detoxification mechanisms then excreted (Boyer et al. 2006). The liver receives blood containing substances absorbed or secreted by the viscera including the spleen, gastrointestinal tract and pancreas and uses these substances as raw materials and modifies them or synthesizes new chemicals. These substances are then returned to the blood stream or to the bile for elimination (Bacon et al. 2006).

From a metabolic point of view, the functional unit of the liver is the hepatic acinus. The axis of hepatic acinus is a portal tract and its boundary is described by an imaginary line connecting the neighboring terminal hepatic venules (central veins). Every hepatic acinus is subdivided into three zones of hepatocytes. Each zone has different levels of oxygen supply and metabolic function (Bacon et al. 2006). Zone I (periportal cells) are supplied with blood rich in oxygen, hormones and substrates. Zone II (mid-zonal cells) and zone III (perivenous cells) are supplied by blood poor in oxygen but rich in carbon dioxide and metabolic products (Gebhardt 1992; Katz 1992).

Nearly 75% of the blood entering the liver is venous blood from the portal vein. All venous blood returning from the small intestine, stomach, pancreas and spleen pour into the portal vein (Bacon et al. 2006). Therefore, the liver comes in contact with nearly all absorbed nutrients from the gastrointestinal tract. The hepatic artery provides the liver with highly oxygenated blood and this represents approximately 25% of the liver blood supply. Terminal branches of both portal vein and hepatic artery mix as they enter the hepatic sinusoids in the liver (McCuskey 2008). Blood flows through the sinusoids and pours into the central vein of each hepatic lobule. Central veins coalesce into hepatic veins which leave the liver on the dorsal surface and join the inferior vena cava (Boyer et al. 2006).

4.7.2. Age-related effects

The liver decreases in size with increasing age and liver metabolism function can also change with age advancement. The process of liver clearance of xenobiotics is primarily impacted by hepatic blood flow, intrinsic clearance (i.e. liver enzyme capacity and liver mass) and protein binding. It is established that elderly people can have up to 40%

reduction in liver blood flow and a similar decrease in liver mass (Le Couteur and McLean 1998), which is considered as the major contributing factor causing impaired hepatic clearance of medications. There are still controversies regarding whether or not intrinsic activities of common CYP450 enzymes will decline with age. In a study of 226 patients, the cytochrome P450 enzymes in liver biopsy samples decreased by approximately 30% in patients over 70 years of age (Sotaniemi et al. 1997), but many other in vitro and in vivo studies suggested that the intrinsic function of CYP450 enzymes keep intact with age advancement.

4.7.3. Data Summary

In a retrospective study of liver weights performed by Chouker et al. (2004), autopsy records from the Institute of Legal Medicine, Ludwig-Maximilians University, Munich, Germany, were reviewed over 18 months between 2001 and 2002. From 1410 autopsies, 682 subjects were excluded from analyses because of various factors, including; putrification, major abdominal and liver trauma, jaundice, macroscopic liver steatosis, and cirrhosis and age outside the range of 16 or 70 years of age. A total of 728 data files were finally included the study. In these autopsies the following variables were determined: gender, age, body weight, body height, calculated body mass index (BMI), body surface area (BSA), and native liver weight measured ex situ on a balance (Chouker et al. 2004).

Necropsy data were subjected to stepwise multiple linear regression analyses separately for younger (16–50 years, n = 418) and elderly (51–70 years, n = 310) subjects. From the data, the following equations were derived to correlate liver mass to body mass and age:

- For ages 16-50:

$$LW\ (g) = 452 + (16.34 \times BW) + (11.85 \times AGE) + (-166.5 \times gender) \quad (83)$$

- For ages 51-70:

$$LW\ (g) = 1390 + (15.94 \times BW) + (-12.86 \times AGE) \quad (84)$$

where body weight (BW) is in kg, age is in y, and gender is 0 for male and 1 for female.

Using the above regression formulas and the age-associated body mass data from the 2009-2010 NHANES data set, liver masses for each decade of life were calculated as presented in Table 4.21.

Table 4.21. Liver mass derived using the Chouker (2004) formulae and with data from the 2009 NHANES data set.

Males			Females		
Age Groups	n	Liver Mass (g)	Age Groups	n	Liver Mass (g)
16-20	374	1958.12 ± 343.09	16-20	374	1579.49 ± 293.60
21-30	443	2129.61 ± 318.31	21-30	504	1814.52 ± 383.36
31-40	446	2374.42 ± 373.26	31-40	498	1991.61 ± 367.61
41-50	467	2475.23 ± 331.70	41-50	540	2083.41 ± 362.86
51-60	456	2109.69 ± 332.81	51-60	429	1933.45 ± 307.75
61-70	414	1963.52 ± 325.35	61-70	405	1797.58 ± 287.66
71-80	428	1717.80 ± 271.62	71-80	448	1535.16 ± 282.26

Chapter 5. RESULTS AND DISCUSSION

5.1. Model Parameter Sensitivity Analysis

A sensitivity analysis was implemented to evaluate the influence of each model parameter on the predicted urine concentration-time profile. The sensitivity function (*S(t)*) was obtained using the partial derivatives of predicted urine concentration-time profile with respect to model parameters (Clewell et al. 1994; Licata et al. 2001). The *S(t)* was calculated using the central difference method:

$$S(t) = \frac{\partial C_{out}^{tot}(\theta_i, t)}{\partial \theta_i} \cong \frac{C_{out}^{tot}(\theta_i + \Delta\theta_i, t) - C_{out}^{tot}(\theta_i - \Delta\theta_i, t)}{2\Delta\theta_i} \quad (85)$$

where

- $C_{out}^{tot}(\theta_i, t)$ is the total urine concentrations predicted at the i^{th} parameter θi and time t
- $\Delta\theta i$ is the change in parameter θi (5% was used for all parameters).

While parameter θ_i was investigated, all other parameters were held constant. The lognormalized *S(t)* is given by (Clewell et al. 1994):

$$NS(t) = \frac{\partial C_{out}^{tot}(\theta_i, t)}{\partial \theta_i} \cong S(t) \times \frac{\theta_i}{C_{out}^{tot}(\theta_i, t)} \quad (86)$$

and determines the relative change in $C_{out}^{tot}(\theta_i, t)$, caused by a small relative change in θ_i (Clewell et al. 1994; Licata et al. 2001). A *NS(t)* that is near zero indicates that the corresponding θ_i has only little influence on the plasma concentration response. A θ_i that has *NS(t)* further away from zero, in the positive or the negative side, is associated with a greater influence on $C_{out}^{tot}(\theta_i, t)$. Note that a negative value for *NS(t)* indicates that the

measured output value decreases with an increase in the parameter value. The highlighted and bolded values in Table 5.1, Table 5.2, and represent the greatest and second greatest sensitivities for each of the outputs listed, respectively.

Table 5.1. Parameter sensitivity analysis for concentration in urine, concentration in liver, concentration in kidney, and concentration in bone at the end of a 3-minute intravenous simulation.

Parameter	NS(t) Urine	NS(t) Liver	NS(t) Kidney	NS(t) Bone
CBFR	-1.74×10^{-09}	-1.58×10^{-08}	3.41×10^{-06}	-3.71×10^{-08}
TBFR	-7.64×10^{-09}	-8.49×10^{-09}	-6.73×10^{-06}	-5.12×10^{-07}
CBRR	-1.56×10^{-09}	-2.00×10^{-08}	5.13×10^{-06}	-4.68×10^{-11}
TBRR	-1.77×10^{-10}	-2.26×10^{-09}	5.80×10^{-07}	-5.29×10^{-12}
GFR	$1.87 \times 10^{+01}$	$-1.87 \times 10^{+01}$	$-2.06 \times 10^{+01}$	$-1.40 \times 10^{+01}$
BF Adipose	$-8.76 \times 10^{+00}$	$7.93 \times 10^{+00}$	$7.66 \times 10^{+00}$	$1.89 \times 10^{+00}$
BF Bone	$-1.77 \times 10^{+01}$	$-9.27 \times 10^{+00}$	$-9.09 \times 10^{+00}$	$-1.15 \times 10^{+02}$
BF Heart	$-1.66 \times 10^{+02}$	$-7.09 \times 10^{+01}$	$-6.96 \times 10^{+01}$	$-1.13 \times 10^{+02}$
BF Hepatic Artery	$-1.05 \times 10^{+02}$	$5.08 \times 10^{+02}$	$-4.41 \times 10^{+01}$	$-7.15 \times 10^{+01}$
BF Kidney	$-3.21 \times 10^{+03}$	**$-2.50 \times 10^{+03}$**	**$-1.35 \times 10^{+03}$**	$-3.32 \times 10^{+03}$
BF Liver	$6.21 \times 10^{+02}$	$-1.85 \times 10^{+04}$	$2.80 \times 10^{+02}$	$4.45 \times 10^{+02}$
BF Lung	**$3.07 \times 10^{+03}$**	$1.43 \times 10^{+03}$	$1.40 \times 10^{+03}$	**$2.22 \times 10^{+03}$**
BF Muscle	$-6.75 \times 10^{+01}$	$4.68 \times 10^{+00}$	$5.03 \times 10^{+00}$	$-1.22 \times 10^{+01}$
BF Pancreas	$-2.39 \times 10^{+01}$	$1.16 \times 10^{+02}$	$-1.00 \times 10^{+01}$	$-1.64 \times 10^{+01}$
BF Skin	$-2.01 \times 10^{+01}$	$-7.19 \times 10^{+00}$	$-6.80 \times 10^{+00}$	$-1.15 \times 10^{+01}$
BF Spleen	$-3.32 \times 10^{+02}$	$1.61 \times 10^{+03}$	$-1.40 \times 10^{+02}$	$-2.27 \times 10^{+02}$
BF Stomach	$-2.51 \times 10^{+01}$	$1.22 \times 10^{+02}$	$-1.05 \times 10^{+01}$	$-1.72 \times 10^{+01}$

Table 5.2. Parameter sensitivity analysis for concentration in urine, concentration in liver, concentration in kidney, and concentration in bone at the end of a 3-minute ingestion simulation.

Parameter	NS(t) Urine	NS(t) Liver	NS(t) Kidney	NS(t) Bone
CBFR	2.75×10^{-05}	4.15×10^{-04}	-1.22×10^{-01}	-1.01×10^{-04}
CBRR	1.80×10^{-05}	2.48×10^{-04}	-7.68×10^{-02}	1.67×10^{-05}
GFR	$1.83 \times 10^{+03}$	$-1.88 \times 10^{+03}$	$-3.04 \times 10^{+03}$	$-2.53 \times 10^{+04}$
BF Adipose	$-1.26 \times 10^{+03}$	$-4.09 \times 10^{+03}$	$1.33 \times 10^{+03}$	$-7.80 \times 10^{+04}$
BF Bone	$-1.48 \times 10^{+03}$	$-5.85 \times 10^{+03}$	$-6.64 \times 10^{+03}$	$1.40 \times 10^{+06}$
BF Gut	$-3.51 \times 10^{+04}$	$6.25 \times 10^{+05}$	$-1.81 \times 10^{+05}$	$-2.35 \times 10^{+06}$
BF Heart	$-1.65 \times 10^{+04}$	$-5.91 \times 10^{+04}$	$-6.74 \times 10^{+04}$	$-1.04 \times 10^{+06}$
BF Hepatic Artery	$-1.03 \times 10^{+04}$	$1.38 \times 10^{+05}$	$-4.65 \times 10^{+04}$	$-6.50 \times 10^{+05}$
BF Kidney	$-3.18 \times 10^{+05}$	**$-1.50 \times 10^{+06}$**	$-1.46 \times 10^{+06}$	$-2.60 \times 10^{+07}$
BF Liver	**$8.01 \times 10^{+04}$**	$-6.94 \times 10^{+06}$	$3.71 \times 10^{+05}$	$4.79 \times 10^{+06}$
BF Lung	$3.18 \times 10^{+05}$	$1.13 \times 10^{+06}$	**$1.41 \times 10^{+06}$**	**$1.99 \times 10^{+07}$**
BF Muscle	$-9.21 \times 10^{+03}$	$-2.83 \times 10^{+04}$	$-3.50 \times 10^{+04}$	$-5.51 \times 10^{+05}$
BF Pancreas	$-2.37 \times 10^{+03}$	$3.15 \times 10^{+04}$	$-1.02 \times 10^{+04}$	$-1.49 \times 10^{+05}$
BF Skin	$-2.17 \times 10^{+03}$	$-6.79 \times 10^{+03}$	$-7.87 \times 10^{+03}$	$-1.33 \times 10^{+05}$
BF Spleen	$-3.28 \times 10^{+04}$	$4.38 \times 10^{+05}$	$-1.47 \times 10^{+05}$	$-2.07 \times 10^{+06}$
BF Stomach	$-2.50 \times 10^{+03}$	$3.32 \times 10^{+04}$	$-1.07 \times 10^{+04}$	$-1.57 \times 10^{+05}$
TBRR	-2.14×10^{-05}	-2.95×10^{-04}	9.11×10^{-02}	-1.99×10^{-05}
TBFR	-5.75×10^{-06}	-1.02×10^{-04}	2.82×10^{-02}	-1.50×10^{-03}

Table 5.3. Parameter sensitivity analysis for concentration in pulmonary regions at the end of a 3-minute inhalation simulation.

Parameter	NS(t) ET Region	NS(t) TB Region	NS(t) Alv Region
ALV Deposition Fraction	$0.00 \times 10^{+00}$	$0.00 \times 10^{+00}$	2.62×10^{-05}
CBFR	$0.00 \times 10^{+00}$	$0.00 \times 10^{+00}$	$0.00 \times 10^{+00}$
CBRR	$0.00 \times 10^{+00}$	$0.00 \times 10^{+00}$	$0.00 \times 10^{+00}$
ET Deposition Fraction	8.98×10^{-09}	-2.30×10^{-05}	-4.11×10^{-05}
GFR	$0.00 \times 10^{+00}$	$0.00 \times 10^{+00}$	$0.00 \times 10^{+00}$
Ventilation Rate	-4.90×10^{-01}	$1.25 \times 10^{+03}$	$2.47 \times 10^{+03}$
BF Adipose	$0.00 \times 10^{+00}$	$0.00 \times 10^{+00}$	$0.00 \times 10^{+00}$
BF Bone	$0.00 \times 10^{+00}$	$0.00 \times 10^{+00}$	$0.00 \times 10^{+00}$
BF Brain	$0.00 \times 10^{+00}$	$0.00 \times 10^{+00}$	$0.00 \times 10^{+00}$
BF Gut	$0.00 \times 10^{+00}$	$0.00 \times 10^{+00}$	$0.00 \times 10^{+00}$
BF Heart	$0.00 \times 10^{+00}$	$0.00 \times 10^{+00}$	$0.00 \times 10^{+00}$
BF Hepatic Artery	$0.00 \times 10^{+00}$	$0.00 \times 10^{+00}$	$0.00 \times 10^{+00}$
BF Kidney	$0.00 \times 10^{+00}$	$0.00 \times 10^{+00}$	$0.00 \times 10^{+00}$
BF Liver	$0.00 \times 10^{+00}$	$0.00 \times 10^{+00}$	$0.00 \times 10^{+00}$
BF Lung	$0.00 \times 10^{+00}$	$0.00 \times 10^{+00}$	$8.98 \times 10^{+03}$
BF Muscle	$0.00 \times 10^{+00}$	$0.00 \times 10^{+00}$	$0.00 \times 10^{+00}$
BF Pancreas	$0.00 \times 10^{+00}$	$0.00 \times 10^{+00}$	$0.00 \times 10^{+00}$
BF Skin	$0.00 \times 10^{+00}$	$0.00 \times 10^{+00}$	$0.00 \times 10^{+00}$
BF Spleen	$0.00 \times 10^{+00}$	$0.00 \times 10^{+00}$	$0.00 \times 10^{+00}$
BF Stomach	$0.00 \times 10^{+00}$	$0.00 \times 10^{+00}$	$0.00 \times 10^{+00}$
TBRR	$0.00 \times 10^{+00}$	$0.00 \times 10^{+00}$	$0.00 \times 10^{+00}$
TB Deposition Fraction	$0.00 \times 10^{+00}$	9.93×10^{-09}	7.61×10^{-03}
TBFR	$0.00 \times 10^{+00}$	$0.00 \times 10^{+00}$	$0.00 \times 10^{+00}$

Table 5.4. Parameter sensitivity analysis for concentration in urine, liver, kidney, and bone at the end of a 3-minute inhalation simulation.

Parameter	NS(t) Kidney	NS(t) Bone	NS(t) Liver	NS(t) Urine
ALV Deposition Fraction	3.44×10^{-11}	-4.93×10^{-11}	6.36×10^{-11}	5.67×10^{-12}
CBFR	-9.27×10^{-08}	-7.70×10^{-12}	3.57×10^{-10}	3.58×10^{-11}
CBRR	1.88×10^{-04}	-1.96×10^{-09}	-7.26×10^{-07}	-7.32×10^{-08}
ET Deposition Fraction	-2.29×10^{-05}	-2.30×10^{-05}	-2.29×10^{-05}	-2.31×10^{-05}
GFR	8.71×10^{-02}	-3.38×10^{-03}	-5.42×10^{-03}	6.40×10^{-03}
Ventilation Rate	$2.45 \times 10^{+03}$	$2.47 \times 10^{+03}$	$2.43 \times 10^{+03}$	$2.47 \times 10^{+03}$
BF Adipose	$-1.69 \times 10^{+01}$	-8.96×10^{-03}	6.92×10^{-02}	1.82×10^{-03}
BF Bone	$-6.19 \times 10^{+00}$	6.85×10^{-03}	1.76×10^{-02}	-3.67×10^{-03}
BF Brain	$-4.95 \times 10^{+01}$	-1.70×10^{-01}	2.10×10^{-01}	-7.74×10^{-02}
BF Gut	$-6.65 \times 10^{+01}$	-2.81×10^{-01}	6.81×10^{-01}	-1.32×10^{-01}
BF Heart	$-1.32 \times 10^{+01}$	-1.01×10^{-01}	6.23×10^{-02}	-5.21×10^{-02}
BF Hepatic Artery	$-2.72 \times 10^{+01}$	-6.44×10^{-02}	2.02×10^{-01}	-2.56×10^{-02}
BF Kidney	$1.49 \times 10^{+02}$	**$-2.60 \times 10^{+00}$**	-5.01×10^{-01}	**$-1.17 \times 10^{+00}$**
BF Liver	$1.14 \times 10^{+01}$	4.14×10^{-01}	**$-2.76 \times 10^{+00}$**	2.13×10^{-01}
BF Lung	$4.06 \times 10^{+00}$	$1.81 \times 10^{+00}$	-5.35×10^{-02}	$1.10 \times 10^{+00}$
BF Muscle	$-1.36 \times 10^{+02}$	-5.19×10^{-02}	6.07×10^{-01}	2.27×10^{-02}
BF Pancreas	$-3.47 \times 10^{+00}$	-1.46×10^{-02}	3.52×10^{-02}	-6.89×10^{-03}
BF Skin	$1.76 \times 10^{+01}$	-1.18×10^{-02}	-6.07×10^{-02}	-1.38×10^{-02}
BF Spleen	$-2.34 \times 10^{+00}$	-2.05×10^{-01}	3.17×10^{-01}	-1.14×10^{-01}
BF Stomach	$-3.65 \times 10^{+00}$	-1.54×10^{-02}	3.70×10^{-02}	-7.25×10^{-03}
TBRR	1.70×10^{-04}	-1.77×10^{-09}	-6.57×10^{-07}	-6.63×10^{-08}
TB Deposition Fraction	-1.58×10^{-06}	-5.16×10^{-06}	-1.38×10^{-06}	-2.79×10^{-06}
TBFR	-9.88×10^{-06}	-1.25×10^{-10}	3.81×10^{-08}	3.84×10^{-09}

5.2. Statistical Comparison of Default Values with Age-Specific Data

Data for each physiological parameter considered are expressed as mean ± SD for each decade of life. Student's t-test was used to compare the ICRP Reference Man physiology values to the means of age-specific data. Means were considered significantly different at $p \leq 0.05$.

Recent studies have suggested that, during the past decades, there have been considerable changes in body weight and body composition, as well as the introduction of new in vivo technologies of body composition analysis (Later et al. 2010). With this in mind, the Student's t-test was also used to compare the mean values for various age ranges to the mean values of both the entire adult age range and the age range from which ICRP reference values were derived.

5.2.1. Body Composition

Reference values for height are central estimates based on data collected for European populations. The values for adult males and females are based on data for 18-year-old males and females, respectively, on the basis of results of longitudinal studies indicating that both genders have attained virtually their maximum height by age 18 years.

Reference values for body mass are also based on the European data on body growth, together with consideration of the long-term increase in body mass after the apparent end of the growth period. Specifically, the reference value for body mass in the adult male is 10% greater than the central value determined for European males at age 18 years, and the reference value for adult females is 10% greater than that determined for European females at age 15 years.

Table 5.5. Comparison between average population height estimates using NHANES 2009-2010 data [mean ± SD] and a reference individual [mean]. Grayed out cells indicate the age data used for evaluation.

Males			ICRP = 176		21-30 year old mean = 175.7		21-80 year old mean = 172.9	
Age Groups	n	Height (cm)	Percent Change	p-value	Percent Change	p-value	Percent Change	p-value
21-30	476	175.733 ± 7.558	0.152	0.442			1.621	<0.005
31-40	482	175.773 ± 8.201	0.129	0.544	0.023	0.914	1.644	<0.005
41-50	495	175.405 ± 7.960	0.338	0.097	0.187	0.359	1.431	<0.005
51-60	488	174.832 ± 7.707	0.663	<0.005	0.513	0.010	1.100	<0.005
61-70	444	172.963 ± 7.914	1.726	<0.005	1.576	<0.005	0.019	0.930
71-80	454	171.396 ± 7.262	2.616	<0.005	2.468	<0.005	0.887	<0.005
21-80	3680	172.930 ± 9.426	1.744	<0.005	1.595	<0.005		

Females			ICRP = 163		21-30 year old mean = 162.2		21-80 year old mean = 160.5	
Age Groups	n	Height (cm)	Percent Change	p-value	Percent Change	p-value	Percent Change	p-value
21-30	546	162.231 ± 6.619	0.472	0.007			1.091	<0.005
31-40	528	162.866 ± 7.078	0.082	0.665	0.392	0.040	1.487	<0.005
41-50	568	161.553 ± 6.409	0.888	<0.005	0.418	0.012	0.668	<0.005
51-60	468	161.080 ± 6.838	1.178	<0.005	0.710	<0.005	0.373	0.059
61-70	432	159.372 ± 6.740	2.226	<0.005	1.762	<0.005	0.691	0.001
71-80	501	156.714 ± 6.518	3.856	<0.005	3.401	<0.005	2.347	<0.005
21-80	3819	160.481 ± 7.181	1.546	<0.005	1.079	<0.005		

Table 5.6. Comparison between average population weight estimates using NHANES 2009-2010 data [mean ± SD] and a reference individual [mean]. Grayed out cells indicate the age data used for evaluation.

Males			ICRP = 73		21-30 year old mean = 83.9		21-80 year old mean = 83.5	
Age Groups	n	Weight (kg)	Percent Change	p-value	Percent Change	p-value	Percent Change	p-value
21-30	476	83.855 ± 18.835	14.350	<0.005			0.455	0.660
31-40	482	92.009 ± 23.176	14.870	<0.005	9.724	<0.005	10.223	<0.005
41-50	495	90.867 ± 20.136	26.040	<0.005	8.362	<0.005	8.854	<0.005
51-60	488	89.601 ± 20.569	24.475	<0.005	6.852	<0.005	7.338	<0.005
61-70	444	88.601 ± 20.214	22.741	<0.005	5.660	<0.005	6.140	<0.005
71-80	454	82.101 ± 16.078	21.372	<0.005	2.091	0.021	1.646	0.069
21-80	3680	83.476 ± 22.344	12.468	<0.005	0.453	0.303		

Females			ICRP = 60		21-30 year old mean = 75.2		21-80 year old mean = 73.5	
Age Groups	n	Weight (cm)	Percent Change	p-value	Percent Change	p-value	Percent Change	p-value
21-30	546	75.213 ± 22.938	25.354	<0.005			2.280	0.088
31-40	528	78.937 ± 22.055	31.561	<0.005	4.952	<0.005	7.344	<0.005
41-50	568	77.312 ± 22.147	28.854	<0.005	2.792	0.024	5.135	<0.005
51-60	468	79.946 ± 20.760	33.243	<0.005	6.293	<0.005	8.716	<0.005
61-70	432	78.441 ± 18.709	30.736	<0.005	4.293	<0.005	6.670	<0.005
71-80	501	70.667 ± 16.943	17.778	<0.005	6.044	<0.005	3.902	<0.005
21-80	3819	73.536 ± 21.334	22.560	<0.005	2.229	<0.005		

Adipose tissue reference values for adults given in ICRP 89 are based on estimates for age 35 years. The reference values for body fat include interstitial fat and yellow bone marrow, whose masses are included in specific organs and tissues (ICRP 2002).

5.2.2. Skeletal System

A value of 3% per year is estimated as the average rate of remodeling of compact bone in adult humans, based on histological data and estimates of the rate of turnover of radionuclides in adult humans. A value of 18% per year is estimated as the average rate of remodeling of trabecular bone in adult humans, based on histological data, estimates of the rate of turnover of radionuclides in adult humans, and the presumption that the amount of remodeling per unit area of bone surface is the same in trabecular as in compact bone. Remodeling rates vary substantially with age during adulthood; the indicated typical values for adults are estimated averages during adulthood.

Table 5.7. Cortical bone turnover rates as a function of sex and age: comparison to ICRP default values.

Male	n	Mean	St Dev	ICRP	Percent Change	p-value
21-30	431	3.43E-02	7.57E-01	0.03	1.44E+01	0.905
31-40	414	3.48E-02	4.95E+01	0.03	1.59E+01	0.998
41-50	436	3.46E-02	3.06E+01	0.03	1.54E+01	0.997
51-60	429	3.45E-02	4.73E+01	0.03	1.50E+01	0.998
61-70	398	3.44E-02	6.98E+01	0.03	1.47E+01	0.999
71-80	398	3.43E-02	1.01E+02	0.03	1.45E+01	0.999

Female	n	Mean	St Dev	ICRP	Percent Change	p-value
21-30	424	3.43E-02	7.57E-01	0.03	1.43E+01	0.907
31-40	413	3.48E-02	4.95E+01	0.03	1.59E+01	0.998
41-50	485	3.46E-02	3.06E+01	0.03	1.53E+01	0.997
51-60	393	6.10E-02	4.73E+01	0.03	1.03E+02	0.990
61-70	368	1.32E-01	6.98E+01	0.03	3.40E+02	0.978
71-80	384	1.39E-01	1.01E+02	0.03	3.62E+02	0.983

Table 5.8. Trabecular bone turnover rates as a function of sex and age: comparison to ICRP default values.

Male	n	Mean	St Dev	ICRP	Percent Change	p-value
21-30	431	1.29E-01	4.13E+01	0.18	2.83E+01	0.980
31-40	414	1.29E-01	4.36E+01	0.18	2.82E+01	0.981
41-50	436	1.29E-01	3.56E+01	0.18	2.85E+01	0.976
51-60	429	1.28E-01	3.30E+01	0.18	2.88E+01	0.974
61-70	398	1.28E-01	2.79E+01	0.18	2.90E+01	0.970
71-80	398	1.28E-01	2.16E+01	0.18	2.91E+01	0.961

Female	n	Mean	St Dev	ICRP	Percent Change	p-value
21-30	424	1.29E-01	6.36E+00	0.18	2.86E+01	0.868
31-40	413	1.29E-01	9.94E+01	0.18	2.82E+01	0.992
41-50	485	1.28E-01	1.25E+02	0.18	2.86E+01	0.993
51-60	393	2.15E-01	9.25E-01	0.18	1.94E+01	0.454
61-70	368	4.87E-01	6.78E+00	0.18	1.70E+02	0.386
71-80	384	5.14E-01	1.54E+03	0.18	1.86E+02	0.997

5.2.3. Respiratory System

Data from publications of biometric and respiratory data were used in regression analyses against age in years (A), mass in kg (W), and standing height in m (H). The resulting regression equations for respiratory volumes and air flows in healthy adult Caucasian subjects are given in Tables B.1 and B.2 in Annex B of the HRTM. Ventilation rates based on these data are presented for four different activity categories: resting (sleeping), sitting awake, light exercise, and heavy exercise. Reference values are then given for sedentary workers and heavy workers, with 8 hours allotted for respiration at a sleeping rate, 8 hours for occupational tasks, and 8 hours for non-occupational tasks (ICRP 1994; ICRP 2002).

Table 5.9. Comparison between daily ventilation rate estimates using NHANES 2009-2010 data [mean ± SD] and a reference individual [mean]. Grayed out cells indicate the age data used for evaluation.

Males			ICRP = 22.9		21-30 year old mean = 25.07		21-80 year old mean = 21.98	
Age Groups	n	Ventilation Rate (m^3/day)	Percent Change	p-value	Percent Change	p-value	Percent Change	p-value
21-30	480	25.07 ± 3.94	9.49	<0.005			14.06	<0.005
31-40	485	24.03 ± 3.57	4.94	<0.005	4.16	<0.005	9.32	<0.005
41-50	498	24.08 ± 3.10	5.13	<0.005	3.98	<0.005	9.52	<0.005
51-60	496	24.59 ± 3.49	7.37	<0.005	1.94	<0.005	11.85	<0.005
61-70	450	16.86 ± 2.61	26.34	<0.005	32.72	<0.005	23.27	<0.005
71-80	470	16.64 ± 2.62	27.32	<0.005	33.62	<0.005	24.28	<0.005
21-80	2879	18.73 ± 0.81	4.01	<0.005	12.32	<0.005		

Females			ICRP = 18.5		21-30 year old mean = 21.15		21-80 year old mean = 17.56	
Age Groups	n	Ventilation Rate (m^3/day)	Percent Change	p-value	Percent Change	p-value	Percent Change	p-value
21-30	548	21.15 ± 4.41	14.30	<0.005			20.42	<0.005
31-40	529	19.15 ± 2.50	3.50	<0.005	9.45	<0.005	9.04	<0.005
41-50	572	19.02 ± 2.44	2.79	<0.005	10.07	<0.005	8.30	<0.005
51-60	469	19.79 ± 2.38	6.95	<0.005	6.43	<0.005	12.68	<0.005
61-70	439	12.66 ± 1.79	31.57	<0.005	40.13	<0.005	27.90	<0.005
71-80	511	12.60 ± 1.66	31.88	<0.005	40.40	<0.005	28.23	<0.005
21-80	3068	17.13 ± 0.49	5.09	<0.005	16.96	<0.005		

5.2.4. Cardiovascular System

ICRP reference values for cardiac output as a function of age and gender were derived as trimmed means of data collected from more than 50 studies involving healthy subjects who were resting in the recumbent position at the time of measurement (Williams

1994). For a reference value, ICRP has selected those values that correspond to a 34 year-old male and female (ICRP 2002).

Table 5.10. Evaluation of differences in cardiac output estimated using NHANES 2009-2010 data [mean ± SD] and values for a reference individual [mean]. Grayed out cells indicate the age data used for evaluation.

Males			ICRP = 6.5		31-40 year old mean = 9.04		21-80 year old mean = 8.73	
Age Groups	n	Cardiac Output (L/min)	Percent Change	p-value	Percent Change	p-value	Percent Change	p-value
21-30	480	9.06 ± 0.78	39.35	<0.005	0.17	0.66	3.79	<0.005
31-40	485	9.04 ± 0.73	39.11	<0.005			3.61	<0.005
41-50	498	9.01 ± 0.64	38.59	<0.005	0.37	0.24	3.22	<0.005
51-60	496	8.94 ± 0.70	37.59	<0.005	1.09	<0.005	2.47	<0.005
61-70	450	8.24 ± 0.66	26.80	<0.005	8.85	<0.005	5.57	<0.005
71-80	470	8.01 ± 0.63	23.16	<0.005	11.47	<0.005	8.28	<0.005
21-80	2879	8.73 ± 0.81	34.27	<0.005	3.48	<0.005		

Females			ICRP = 5.9		31-40 year old mean = 7.21		21-80 year old mean = 7.13	
Age Groups	n	Cardiac Output (L/min)	Percent Change	p-value	Percent Change	p-value	Percent Change	p-value
21-30	548	7.40 ± 0.69	25.47	<0.005	2.63	<0.005	3.80	<0.005
31-40	529	7.21 ± 0.38	22.26	<0.005			1.14	<0.005
41-50	572	7.18 ± 0.39	21.68	<0.005	0.47	0.04	0.66	<0.005
51-60	469	7.19 ± 0.37	21.91	<0.005	0.28	0.23	0.85	<0.005
61-70	439	6.95 ± 0.40	17.74	<0.005	3.70	<0.005	2.60	<0.005
71-80	511	6.81 ± 0.36	15.45	<0.005	5.57	<0.005	4.50	<0.005
21-80	3028	7.13 ± 0.49	20.88	<0.005	1.13	<0.005		

5.2.5. Kidneys

ICRP 89 reports an approximate relative value for glomerular filtration rate for the average adult human as extracted from Guyton (1982).

Table 5.11. Comparison of glomerular filtration rate between estimates using NHANES data [mean ± SD] and a reference individual [mean]. Grayed out cells indicate the age data used for evaluation.

Male

			ICRP = 125		21-30 year old mean = 144.13		21-80 year old mean = 115.29	
Age Groups	n	GFR (mL/min)	Percent Change	p-value	Percent Change	p-value	Percent Change	p-value
21-30	443	144.13 ± 41.29	15.30	<0.005			25.01	<0.005
31-40	446	145.23 ± 43.60	16.22	<0.005	0.80	0.58	26.01	<0.005
41-50	467	128.06 ± 35.62	2.45	0.06	11.15	<0.005	11.08	<0.005
51-60	456	111.49 ± 33.00	10.81	<0.005	22.64	<0.005	3.30	<0.005
61-70	414	92.76 ± 27.88	25.79	<0.005	35.64	<0.005	19.54	<0.005
71-80	428	66.10 ± 21.59	47.12	<0.005	54.14	<0.005	42.67	<0.005
21-80	2654	115.29 ± 44.71	7.77	<0.005	20.01	<0.005		

Female

			ICRP = 125		21-30 year old mean = 150.09		21-80 year old mean = 113.60	
Age Groups	n	GFR (mL/min)	Percent Change	p-value	Percent Change	p-value	Percent Change	p-value
21-30	504	150.09 ± 56.39	20.07	<0.005			32.13	<0.005
31-40	498	140.17 ± 46.33	12.13	<0.005	6.61	<0.005	23.39	<0.005
41-50	540	121.57 ± 39.02	2.75	<0.005	19.01	<0.005	7.01	<0.005
51-60	429	106.88 ± 32.22	14.50	<0.005	28.79	<0.005	5.91	<0.005
61-70	405	90.76 ± 27.11	27.39	<0.005	39.53	<0.005	20.10	<0.005
71-80	448	60.48 ± 22.33	51.62	<0.005	59.70	<0.005	46.76	<0.005
21-80	2824	113.60 ± 49.81	9.12	<0.005	24.31	<0.005		

5.2.6. Liver

The mass of the normal liver has been determined in several autopsy studies and age-specific data from multiple studies are compared in Fig. 6.4 of ICRP 89 (ICRP 2002). From this table, it appears that ICRP has chosen the mean liver masses for a 21 year-old male and female as their reference masses for an adult.

Table 5.12. Comparison of liver mass between estimates using NHANES data [mean ± SD] and a reference individual [mean]. Grayed out cells indicate the age data used for evaluation.

Males

			ICRP = 1800		21-30 year old mean = 2129.61		21-80 year old mean = 2135.82	
Age Groups	n	Liver Mass (g)	Percent Change	p-value	Percent Change	p-value	Percent Change	p-value
21-30	443	2129.61 ± 318.31	18.31	<0.005			0.29	0.68
31-40	446	2374.42 ± 373.26	31.91	<0.005	11.50	<0.005	11.17	<0.005
41-50	467	2475.23 ± 331.70	37.51	<0.005	16.23	<0.005	15.89	<0.005
51-60	456	2109.69 ± 332.81	17.20	<0.005	0.94	0.20	1.22	0.09
61-70	414	1963.52 ± 325.35	9.08	<0.005	7.80	<0.005	8.07	<0.005
71-80	428	1717.80 ± 271.62	4.57	<0.005	19.34	<0.005	19.57	<0.005
21-80	2654	2135.82 ± 411.97	18.66	<0.005	0.29	0.44		

Females

			ICRP = 1400		21-30 year old mean = 1814.52		21-80 year old mean =1868.48	
Age Groups	n	Liver Mass (g)	Percent Change	p-value	Percent Change	p-value	Percent Change	p-value
21-30	504	1814.52 ± 383.36	29.61	<0.005			2.89	<0.005
31-40	498	1991.61 ± 367.61	42.26	<0.005	9.76	<0.005	6.59	<0.005
41-50	540	2083.41 ± 362.86	48.81	<0.005	14.82	<0.005	11.50	<0.005
51-60	429	1933.45 ± 307.75	38.10	<0.005	6.55	<0.005	3.48	<0.005
61-70	405	1797.58 ± 287.66	28.40	<0.005	0.93	0.24	3.79	<0.005
71-80	448	1535.16 ± 282.26	9.65	<0.005	15.40	<0.005	17.84	<0.005
21-80	2824	1868.48 ± 380.73	33.46	<0.005	2.97	<0.005		

5.3. Comparison of Sex- and Age-Specific Values in PBPK Model

Mean data for each variable parameter was categorized by both sex and decade of age. These parameters were then used as inputs for the Simulink model constructed using the pharmacokinetic equations described earlier. Each division was run as a separate simulation and concentration of the radionuclide within a given compartment at the end of the simulation was reserved as an output value. Output data was sorted and compiled into an Excel spreadsheet for easier comparison. The variation in strontium concentration within 2000 mL of urine at the end of a 3-hour simulation is presented for males and females in Figure 5.1 and Figure 5.2, respectively.

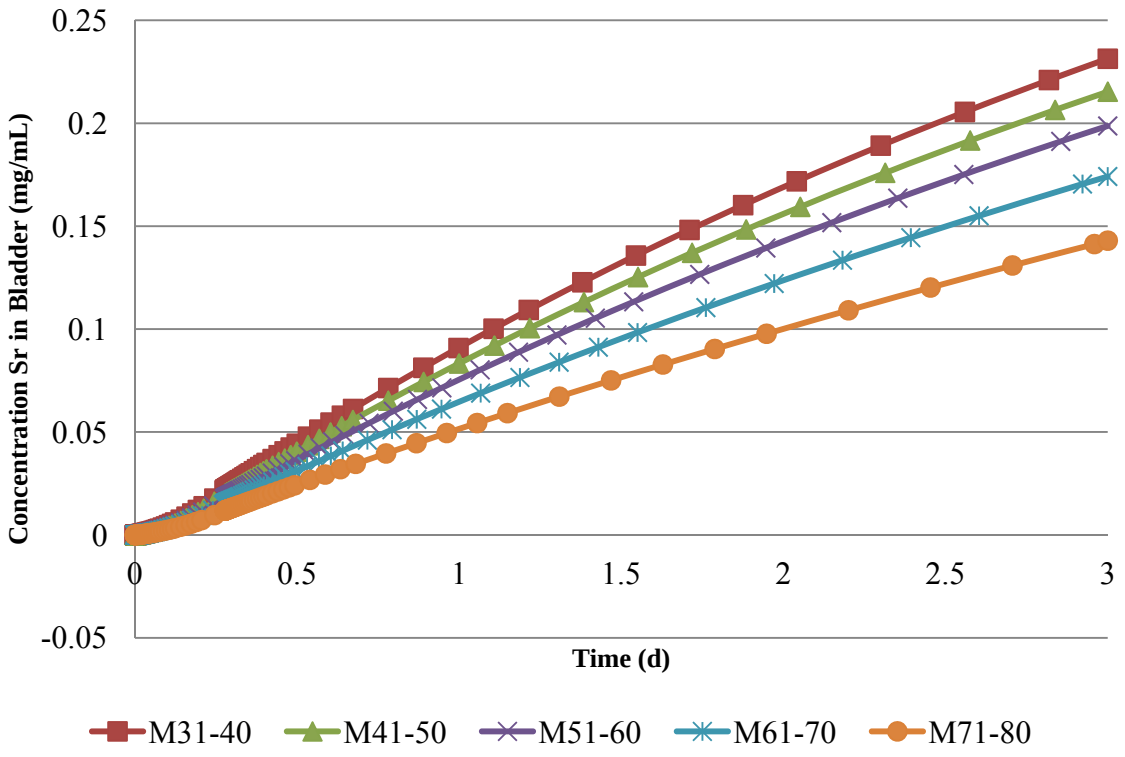

Figure 5.1 Variation of strontium concentration in urine with respect to age in human males.

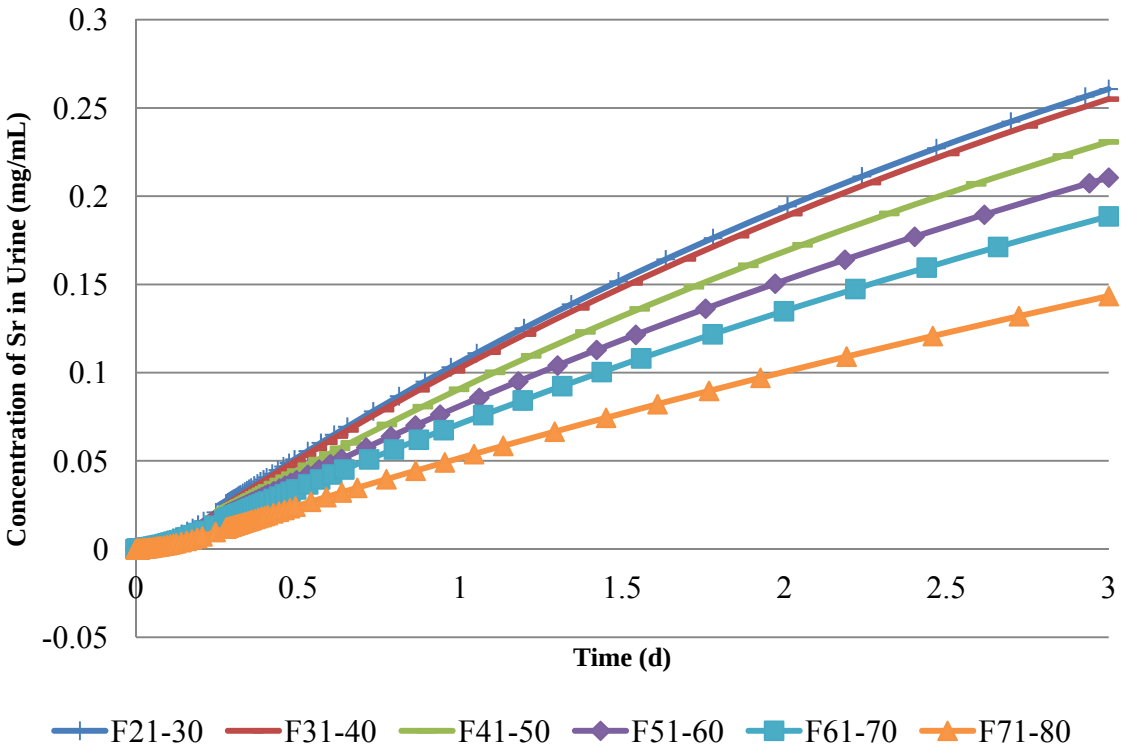

Figure 5.2 Variation of strontium concentration in urine with respect to age in human females.

The variation in strontium concentration within human mineralized bone at the end of a 3-day simulation is presented for males and females in Figure 5.1 and Figure 5.2, respectively.

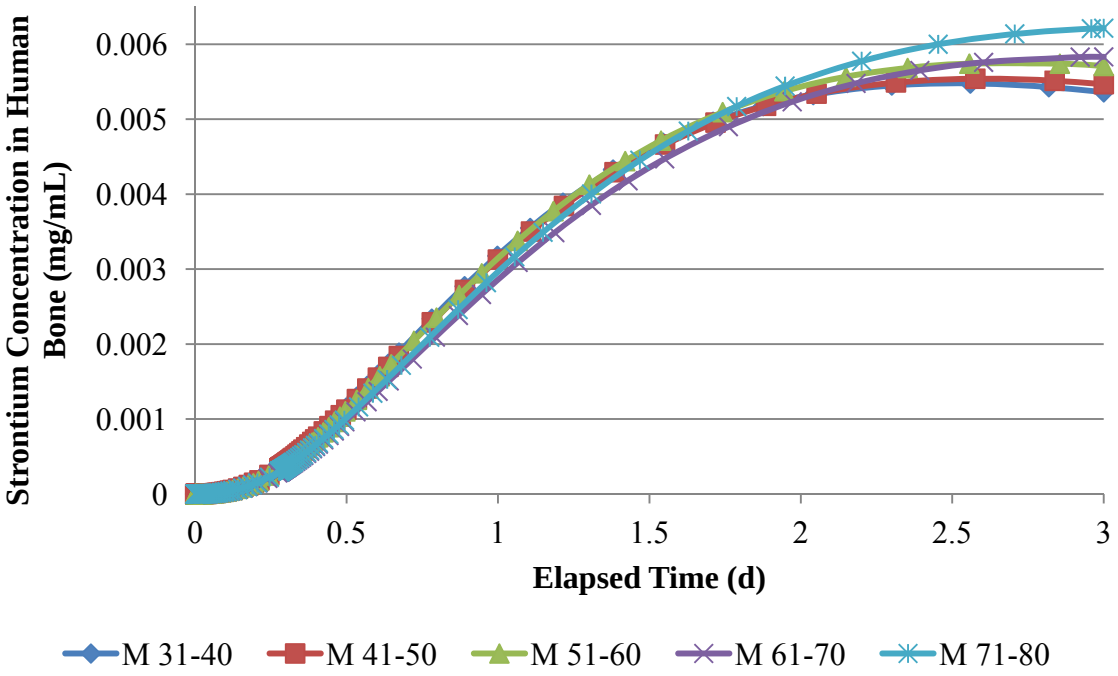

Figure 5.3. Variation of strontium concentration in formed bone with respect to age in human males.

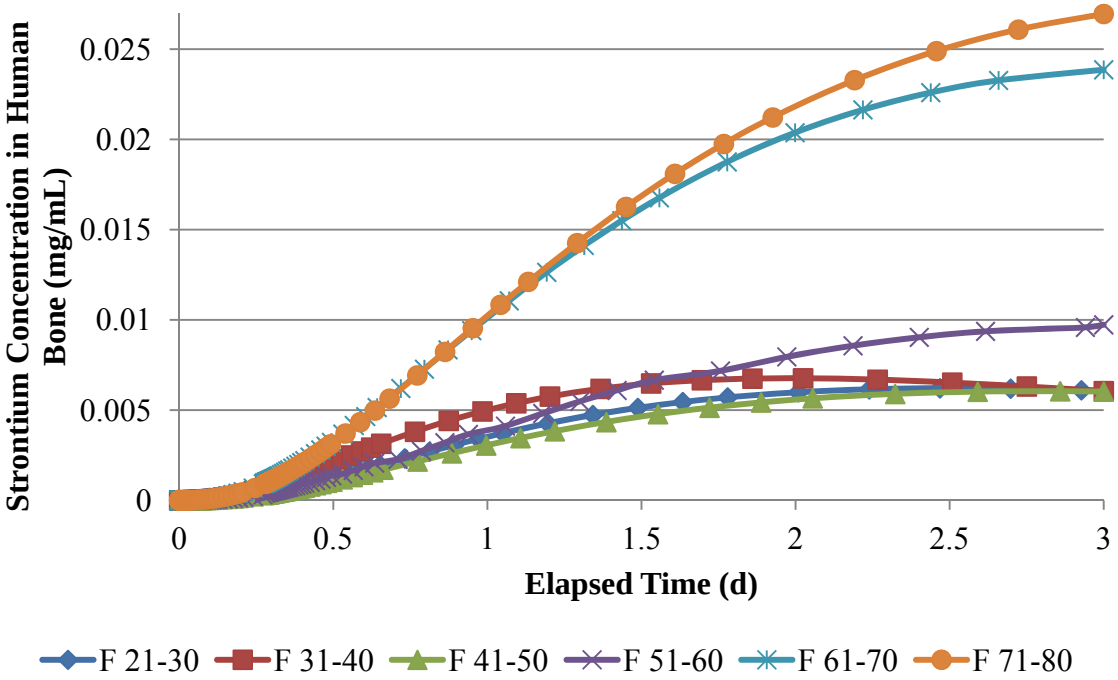

Figure 5.4. Variation of strontium concentration in formed bone with respect to age in human females

Qualitatively, it appears that there is a wide variation in the outputs depending on whether reference parameters or age-specific parameters were used. A Mann-Whitney U test was used to quantify whether or not there was a statistical difference in the predicted outputs between models built using age-specific data and Reference Individual data. In all cases, the difference was considered significant if $p \leq 0.05$.

Table 5.13. Significance of variation in model outputs as determined using the Mann-Whitney U test.

	Age 51-60	Age 61-70	Age 71-80
Liver	$p = 0.37$	$p = 0.59$	$p = 0.02$
Kidney	$p = 0.32$	$p = 0.59$	$p = 0.02$
Urine	$p = 0.15$	$p = 0.06$	$p = 0.01$
Bone (f)	$p < 0.005$	$p < 0.005$	$p < 0.005$

Comparison of the simulated liver concentration, kidney concentration, and urine concentration output values using age specific parameters to outputs derived using reference man parameters shows that for the 51-60 year age range and the 61-70 year age range, these two sets of parameters are consistent within the 95% probability interval. At the 71-80 year age range, the age-specific outputs were found to be statistically different than those acquired using reference male parameters. Bone concentration outputs were found to be statistically different for all three age ranges from those determined using reference female parameters.

5.4. Comparison of Measured Data to Predicted Data

A 65-year old male received an initial intravenous administration of 138.8 MBq ^{201}Tl in the form of thallous chloride, followed 3 hours later by a second intravenous administration of 34 MBq. Collection of 24-hour urine samples began two hours after the second administration. No chemical preparation was given to the samples prior to counting for 60 minutes on a high-purity germanium detector. Raw data as presented in the published study has been corrected for radiological decay (Blanchardon et al. 2005). These data, measured and reported by Blanchardon et al. (2005), were compared to model predictions for the same age and activity administration by calculating a value for percent median absolute performance error based on estimated performance error as shown below (Ruiz et al. 2010):

$$PE = \left(\frac{C_{measured} - C_{predicted}}{C_{measured}}\right) \times 100 \quad (87)$$

where,

- $C_{measured}$ = the concentration in urine from the measured data
- $C_{predicted}$ = the concentration in urine as predicted by the model

From the estimated performance errors, the accuracy of the model prediction across the total time of the experiment was measured by root mean square performance error (Ruiz et al. 2010):

$$RMSPE\ (\%) = \sqrt{\frac{\sum_{i=1}^{n} PE^2}{n}} \quad (88)$$

where,

- n = the number of measurement points, and;

- PE = the performance error as calculated in Equation 87.

The results of the performance error measurements are presented in Table 5.12. Comparison of the calculated urine activities using both reference parameters and age-specific parameters to the measured urine activity shows that the age-specific calculated results are a better fit to the observed data than the estimates using ICRP data.

Table 5.12. Comparison of model-predicted data with data measured by Blanchardon et al. (2005). Grayed out cells indicate a time that was not reported by the simulation.

	Measured	PBPK 60-70 y		ICRP	
Time (d)	Activity (Bq)	Activity (Bq)	Percent Difference	Activity (Bq)	Percent Difference
1	1.70E+06	2.20E+06	29.70	1.45E+06	-14.71
2	1.35E+06	1.27E+06	-5.76	1.05E+06	-22.22
3	9.44E+05	9.62E+05	1.96	7.69E+05	-18.54
4	8.59E+05	7.30E+05	-15.04	5.61E+05	-34.69
5	4.64E+05	5.55E+05	19.64	4.10E+05	-11.64
6	3.90E+05	4.23E+05	8.58	3.00E+05	-23.08
7	2.30E+05	3.23E+05	40.57	1.61E+05	-30.00
8	1.08E+05			1.18E+05	9.26
19	8.13E+03	8.92E+03	9.71	5.59E+03	-31.24
24	2.79E+03	1.81E+03	-35.26	1.27E+03	-54.48
30	4.49E+02	2.98E+02	-33.58	2.26E+02	-49.67
RMSPE			23.91		32.13

Chapter 6. SUMMARY AND CONCLUSIONS

6.1. Summary and Discussion of Results

The aging process is characterized by structural and functional changes affecting all organ systems and results in reduced homeostatic capacity. There is an increasing understanding of the relationship among the aging process, age-related diseases, and the effects of aging on pharmacokinetics. Even so, the clinical trial evidence base for the physiological impact on absorption, distribution and elimination in older people remains small.

The data collected indicate an overall decline in body weights with age. Generally, women have a higher proportion of body fat than men within the same age range, and in both genders the fat percentage increases with age. In women, there appears to be a postmenopausal acceleration of this trend. Generally, the maximum age for fat accumulation was shown to be around the sixth decade of life, with a plateau phase and a subsequent reduction in the amount and proportion of body fat occurring in the seventh and eighth decades of life.

There is a marked difference in total bone mineral mass throughout the life cycle. Men tend to reach their peak bone mineral content in the third decade of life followed by a gradual decline. Women, on the other hand, do not achieve peak mineral content until the fifth decade, followed by a more rapid decline throughout the sixth and seventh decades of life.

Daily ventilation was shown to peak at around 25 years of age, followed by a decline. The calculated data also present an increase in ventilation rate between the fourth and sixth decades of life, which corresponds to findings that older adults tend to breathe at

higher lung volumes than younger subjects to compensate for increased elastic recoil of the chest wall in older subjects (Janssens 2005). Change in regional blood flow varies with organ, with the most pronounced changes being evident in the kidneys (Ritschel 1988). However, these changes are generally proportional to changes in organ mass, such that the regional blood flow rate in mL of fluid per mass of tissue per hour is unchanged. Renal blood flow decreases with increasing age, and the age-related decrease in perfusion holds even after correcting for the kidney volume. A decrease in glomerular filtration rate, as reflected by creatinine clearance, was documented in a number of studies in the elderly and is confirmed by the data in this study. This study did not note a variation in gastrointestinal motility with age.

6.2. Conclusions

Based on the data variability tests expressed as the t test statistics, the Mann-Whitney U test statistics, and the corresponding p-values, it can be concluded that:

- The data do not support the null hypothesis #1: *The Reference Man physiological parameters adequately approximate the physiological parameters of adults above the age of 35.* Therefore, the alternative hypothesis #1 must be accepted: *The Reference Man physiological parameters do not adequately approximate the physiological parameters of adults above the age of 35.*

Based on comparison of organ concentration values predicted using the PBPK model to the values predicted using the ICRP default parameters, it can be concluded that:

- For the null hypothesis #2: The urine, kidney, and liver data are consistent with the null hypothesis that *Organ concentrations predicted by biokinetic models built*

using the Reference Man physiological parameters are not significantly different than those built using age-specific biokinetic parameters for men and women aged 51-70, but do not support the data for ages 71-80 or for bone concentrations in women aged 51-80. Therefore, we fail to find support for the null hypothesis and the alternative hypothesis #2 must be accepted: *Organ concentrations predicted by biokinetic models built using the Reference Man physiological parameters are significantly different than those built using age-specific biokinetic parameters.*

Based on measured data comparison to both values predicted using the PBPK model and the values predicted using the ICRP default parameters, it can be concluded that:

- The data do not support the null hypothesis #3: *There are no significant differences between the activity predicted in various organs using Reference Man default parameters and the true measured activity.* Therefore, the alternative hypothesis #3 must be accepted: *There are significant differences between the activity predicted in various organs using the Reference Man default parameters and the true measured activity.*

Changes in body mass, and the associated changes in organ mass and fraction of cardiac output, have the most pronounced influence on the distribution volumes of xenobiotics. This investigation indicates considerable differences in anatomical and physiological parameters due to advancing age. Changes due to age like the lean body fraction of total body mass, the fraction of cardiac output going to various organs, or the respiration rate, in the absence of all other considerations, would be expected to cause a variation in the urine concentration of a substance when compared to values calculated using a reference individual. Changes in body composition, hepatic and renal functions

would be expected to be responsible for an increase in the volume of distribution of materials, and reduced clearance, respectively.

Simulations, however, suggest that there is not a significant change in the organ concentrations or urinary output of a material with age. Closer examination of the physiological data alongside the model sensitivity reveals that there is a possibility for competing influence within the model. While an increase in blood flow to the liver should cause an increase in the urine concentration of a material, an increase in blood flow to the kidneys causes a decrease of the same magnitude.

6.3. Future Work

There is a number of research avenues that can be further explored based on the findings of this study. In particular:

- The pharmacokinetic model used here is relatively simple and does not represent the full range of physiochemical and biophysical parameters at play in determining how substances are absorbed into, distributed within, and excreted from the human body. To use this model with other radionuclides, parameters within the model, such as the partition coefficients, will need to be adjusted based on the chemical form of the isotope of concern.

- This model does not take into account racial and ethnic differences in physiological parameters. The populations considered in this study were strictly United States or Western European populations. The study also does not account for the presence or prevalence of various diseases with age. These factors can reasonably be expected to further alter the pharmacokinetics in a varied population.

- Most biokinetic studies have attempted to modify the transfer rates between biological compartments by optimization of a fit to the available bioassay data (urine and fecal data) and activities in various organs at the time of death. Although a large portion of these studies are case studies, they have contributed largely to a better understanding of the biokinetic behavior of radionuclides. The problem with most human case studies, besides being small in number of individual elements, is that the actual intake is unknown and thus the universal applicability of the new transfer rates is unknown.

  To evaluate parameters of internal radionuclide turnover after ingestion and intravenous injection in humans, it would be beneficial to compare the biokinetic data developed in this study to actual intake and excretion data. In order for such a comparison to be valid, however, the exposures and excretions would need to be controlled in such a way that the exact quantity of radionuclide administered is known, as well as the measured activity in excreta.

REFERENCES

Aaron JE, Makins NB, Segreiya K. The microanatomy of trabecular bone loss in normal aging men and women. Clin Orthop. 215: 260-271; 1987.

Abrahamsson B, Pal A, Sjöberg M, Carlsson M, Laurell E, Brasseur JG. A novel in vitro and numerical analysis of shear-induced drug release from extended release tablets in the fed stomach. Pharmaceutical Research. 22(8): 1215–26; 2005.

Adams WC, Shaffrath JD, Ollison WM. The relation of pulmonary ventilation and heart rate in leg work alone, arm work alone, and in combined arm and leg work. Paper WA-84A.04 presented at the 88th Annual Air & Waste Management Association Conference. 21 June 1995.

Agerbaek MO, Eriksen EF, Kragstrup J, Mosekilde L, Melsen F. A reconstruction of the remodeling cycle in normal human cortical iliac bone. Bone and Mineral. 12: 101-112; 1991.

American Medical Association. Complete Medical Encyclopedia; Random House; 2003.

Andersen ME. Toxicokinetic modeling and its applications in chemical risk assessment. Toxicol Lett, 138(1-2):9-27; 2003.

Avbersek-Luznik I, Gmeiner Stopar T, and Marc J. Activity or mass concentration of bone-specific alkaline phosphatase as a marker of bone formation. Clinical Chemistry and Laboratory Medicine. 45(8), 1014-1018; 2007.

Bacon BR, O'Grady JG, Di Bisceglie AM, Lake JR. Comprehensive Clinical Hepatology. 2nd Ed. Mosby, China; 2006.

Banker GS, Rohodes CT. Modern Pharmaceutics, Informa Health Care,London; 2002.

Barbier O, Jacquillet G, Tauc M, Cougnon M, and Poujeol P. Effect of heavy metals on, and handling by, the kidney. Nephron Physiol. 99(4):105-10; 2005.

Barger-Lux MJ and Recker RR. Bone microstructure in osteoporosis: transilial biopsy and histomorphometry. Top Magn Reson Imaging. 13(5):297-305; 2002.

Baron R. Anatomy and ultrastructure of bone. In: Favus MJ. (Ed.), Primer on the Metabolic Bone Disease and Disorder of Mineral Metabolism, 4th ed. Lippincott-Raven, New York, pp. 356-364; 1999.

Bass S, Delmas PD, Pearce G, Hendrich E, Tabensky A, and Seeman E. The differing tempo of growth in bone size, mass, and density in girls is region specific. J Clin Invest.

104(6): 795-804; 1999.

Baumgartner RN, Heymsfield SB, Lichtman S, Wang J, and Pierson RNJ. Body composition in elderly people: effect of criterion estimates on predictive equations. Am J Clin Nutr. 53:1345-1353; 1991.

Baumgartner RN, Stauber PM, McHugh D, Koehler KM, Garry PJ. Cross-sectional age differences in body composition in persons 60+ years of age. J Gerontol A Biol Sci Med Sci. 50:M307-316; 1995.

Bayless WM, Starling EH. The movements and innervations of the small intestine. J Physiol. 24(2): 99-143; 1899.

Becker C. Pathophysiology and clinical manifestations of osteoporosis. Clin Cornerstone. 8: 19-27; 2006.

Benjamin EJ, Levy D, Anderson KM, Wolf PA, Plehn JF, Evans JC, Comai K, Fuller DL and Sutton MS. Determinants of Doppler indexes of left ventricular diastolic function in normal subjects (the Framingham Heart Study). Am J Cardiol 70: 508-515; 1992.

Bennett WD, Zeman KL, Kim C. Variability of fine particle deposition in healthy adults: Effect of age and gender. Am. J. Respir. Crit. Care Med. 153:1641–1647; 1996.

Berger MJ. Energy deposition in water by photons from point isotropic sources. MIRD Pamphlet No.2. Journal ofNuclear Medicine 9(Supp. 1):15-25; 1968.

Berman M. Kinetic models for absorbed dose calculations. MIRD Pamphlet No. 12. New York: Society of Nuclear Medicine; 1977.

Bernareggi A, Rowland M. Physiologic modeling of cyclosporin kinetics in rat and man. J Pharmacokinet Biopharm 19:21-50; 1991.

Berntsen GK, Fonnebo V, Tollan A, Sogaard AJ, and Magnus JH. Forearm bone mineral density by age in 7,620 men and women: the Tromso study, a population-based study. Am. J. Epidemiol. 153, 465-473; 2001.

Birchall A, Puncher M, Marsh JW, Davis K, Baily MR, Jarvis NS, Peach AD, Dorrian M-D, James AC. IMBA Professional Plus: a flexible approach to internal dosimetry. Radiat Protect Dosim 125:194-197; 2007.

Bischoff KB and Dedrick RL. Thiopental pharmacokinetics. J. Pharm. Sci. 57(8): 1346-1351; 1968.

Bjarnegard N., and Lanne T. Arterial properties along the upper arm in humans: age-related effects and the consequence of anatomical location. J Appl Physiol. 108(1): 34-38; 2010.

Blakey GE, Nestorov IA, Arundel PA, Aarons LJ, Rowland M. Quantitative structure-pharmacokinetics relationships: I. Development of a whole-body physiologically based model to characterize changes in pharmacokinetics across a homologous series of barbiturates in the rat. J Pharmacokinetics and Biopharm. 25: 277-312; 1997.

Blanchardon E, Challeton-de Vathaire, Boisson P, Celier D, Martin JC, Cassot S, Herbelet G, Franck D, Jourdain JR, Biau A. Long term retention and excretion of Tl-201 in a patient after myocardial perfusion imaging. Radiat Protect Dosim. 113(1): 47-53; 2005.

Bode-Boger SM, Muke J, Surdacki A, Brabant G, Boger RH, and Frolich JC. Oral L-arginine improves endothelial function in healthy individuals older than 70 years. Vasc Med. 8: 77-81; 2003.

Bois FY, Zeise L, Tozer TN. Precision and sensitivity of pharmacokinetic models for cancer risk assessment: tetrachloroethylene in mice, rats, and humans. Toxicol Appl Pharmacol 102: 300-315; 1990.

Bolotin HH. The significant effects of bone structure on inherent patient specific DXA in vivo bone mineral density measurement inaccuracies. Med. Phys. 31: 774-788; 2004.

Bonewald LF. Osteocyte biology: its implications for osteoporosis. J Musculoskeletal & Neuronal Interactions. 4: 101-104; 2004.

Bonithon-Kopp C, Touboul PJ, Berr C, Leroux C, Mainard F, Courbon D, and Ducimetiere P. Relation of intima-media thickness to atherosclerotic plaques in carotid arteries. The Vascular Aging (EVA) Study. Arterioscler Thromb Vasc Biol. 16: 310-316; 1996.

Borkan GA, Hults DE, Gerzof SG, Robbins AH, Silbert CK. Age changes in body composition revealed by computed tomography. J Gerontol. 38:673-677; 1983.
Borkan GA, Norris AH. Fat redistribution and the changing body dimensions of the adult male. Hum Biol. 49:495-514; 1977.

Bouchet LG, Bolch WE, Weber DA, Atkins HL, Poston JW Sr. Radionuclide S values in a revised dosimetric model of the adult head and brain. MIRD Pamphlet No. 15. Journal of Nuclear Medicine 40:62S-101S; 1999.

Boyer TD, Wright TL, Manns MP. Zakim and Boyer's Hepatology: A Textbook of Liver Disease. Volume 1, 5th Ed. Saunders, Elsevier Inc. Canada; 2006.

Brain JD, Valberg PA. Deposition of aerosol in the respiratory tract. American Review of Respiratory Disease 120:1325-1373; 1979.

Bressler JP, Olivi L, Cheong JH, Kim Y, Bannona D. Divalent metal transporter 1 in lead and cadmium transport. Ann N Y Acad Sci, 1012: 142-52; 2004.

Bressler JP, Olivi L, Cheong JH, Kim Y, Maerten A, Bannon D. Metal transporters in intestine and brain: their involvement in metal-associated neurotoxicities. Human & Experimental Toxicology, 26(3):221-229; 2007.

Briggs AM, Greig AM and Wark JD. The vertebral fracture cascade in osteoporosis: a review of aetiopathogenesis. Osteoporos Int. 18: 575-584; 2007.

Brochot C, Pery A, Gotti A, Sarigiannis D. A life-time PBPK model for humans describing metabolic interactions between substances. Full-chain and Uncertainty Approaches for Assesshing Health Risks in Future Environmental Scentarios. 03/18/2008. [Web] http://www.2-fun.org/deliverables/d3.1_life%20time%20pbpk%20model.pdf Accessed June 2013.

Brown R, Foran J, Olin S, Robinson D. Physiological Parameter Values for PBPK Models. International Life Sciences Institute and Risk Science Institute, Washington D. C; 1994.

Brown WW. Aging and the kidney. Arch Intern Med. 146:1790-1796; 1986.

Brownell GL, Ellett WH, Reddy R. Absorbed fractions for photon dosimetry. MIRD Pamphlet No.3. Journal of Nuclear Medicine 27(Supp. 1):29-39; 1968.

Brugts JJ, Knetsch AM, Mattace-Raso FUS, Hofman A, Witteman JCM. Renal function and risk of myocardial infarction in an elderly population: The Rotterdam Study. Archives of Internal Medicine. 165(22): 2659-2665; 2005.

Burkhardt H, Hahn T, Gretz N, Gladisch R. Bedside estimation of the glomerular filtration rate in hospitalized elderly patients. Nephron.Clinical Practice. 101(1): c1-8; 2005.

Burlew BS. Diastolic dysfunction in the elderly--the interstitial issue. Am J Geriatr Cardiol 13: 29-38; 2004.

Burr DB. Muscle strength, bone mass, and age-related bone loss. Journal of Bone and Mineral Research. 12: 1547-1551; 1997.

Calabrese EJ. Principles of animal extrapolation. Environmental science and technology. Wiley, New York, 1983. ISBN 0471087629.

Cameron JS, Macias-Nunez JF. Renal function in the elderly; In: Davison AM, Cameron JS, Grünfeld JP, Kerr D, Ritz E, Winearls CQ, Eds. Oxford Textbook of Clinical Oncology.
2nd Ed. Oxford University Press; 1998.

Candow D, Chilibeck P. Differences in size, strength, and power of upper and lower body muscle groups in young and older men. Journals of Gerontology Series A: Biological and Medical Sciences 60(2): 148; 2005.

Cann PA, Read NW, Cammack J, Childs H, Holden S, Kashman R, Longmore J, Nix S, Simms N, Swallow K, Weller J. Psychological stress and the passage of a standard meal through the stomach and small intestine in man. Gut. 24(3): 236-240; 1983.

Carmelli D, McElroy MR, Rosenman RH. Longitudinal changes in fat distribution in the Western Collaborative Group Study: a 23-year follow-up. Int J Obes. 15:67-74; 1991.

Celermajer DS, Sorensen KE, Spiegelhalter DJ, Georgakopoulos D, Robinson J, and Deanfield JE. Aging is associated with endothelial dysfunction in healthy men years before the age-related decline in women. J Am Coll Cardiol. 24: 471-476; 1994.

Chambers TJ: The direct and indirect effects of estrogen on bone formation. Adv in Organ Biol 5B: 627-638; 1998.

Chantler PD, Nussbacher A, Gerstenblith G, Schulman SP, Becker LC, Ferrucci L, Fleg JL, Lakatta EG, and Najjar SS. Abnormalities in arterial-ventricular coupling in older healthy persons are attenuated by sodium nitroprusside. Am J Physiol Heart Circ Physiol. 300: H1914-1922; 2011.

Chapurlat RD, Gamero P, Somay-Rendu E, Arlot ME, Claustrat B, and Delmas PD. Longitudinal study of bone loss in pre- and perimenopausal women: evidence for bone loss in perimenopausal women. Osteoporos. Int. 11, 493-498; 2000.

Chen L, Xin X, Eckhart AD, Yang N, and Faber JE. Regulation of vascular smooth muscle growth by alpha 1-adrenoreceptor subtypes in vitro and in situ. J Biol Chem 270: 30980-30988; 1995.

Chen XM, Zhang Y, Shen XP, Huang Q, Ma H, Huang YL, Zhang WQ, and Wu HJ. Correlation between glucose fluctuations and carotid intima-media thickness in type 2 diabetes. Diabetes Res Clin Pract. 90(1): 95-99; 2010.

Cheng YS. Aerosol deposition in the extrathoracic region. Aerosol Sci Technol. 37(8): 659-671; 2003.

Chien S, Peng MT, Chen KP, Huang TF, Chang C, Fang HS. Longitudinal studies on adipose tissue and its distribution in human subjects. J Appl Physiol. 39:825-830; 1975.

Chiu KM, Ju J, Mayes D, Bacchetti P, Weitz S, Arnaud CD. Changes in bone resorption during the menstrual cycle. J Bone Miner Res 14 (4):609-615; 1999.

Christenson R. Biochemical markers of bone metabolism: An overview. Clinical Biochemistry. 30(8): 573-593; 1997.

Christiansen P. The skeleton in primary hyperparathyroidism: A review focusing on bone remodeling, structure, mass, and fracture. APMIS. 109, 5-52; 2001.

Christou DD, and Seals DR. Decreased maximal heart rate with aging is related to reduced {beta}-adrenergic responsiveness but is largely explained by a reduction in intrinsic heart rate. J Appl Physiol. 105: 24-29; 2008.

Chouker A, Martignoni Andre, Dugas M, Eisenmenger W, Schauer R, Kaufmann I, Schelling G, Lohe F, Jauch KW, Peter K, Thiel M. Estimation of liver size for liver transplantation: the impact of age and gender. Liver Transpl. 10(5): 678-685; 2004.

Chumlea WC, Guo SS, Kuczmarski RJ et al. Body composition estimates from NHANES III bioelectrical impedance data. Int J Obes Relat Metab Disord. 26:1596-1609; 2002.

Clarke B. Normal bone anatomy and physiology. Clin J Am Soc Nephrol. Suppl 3:S131-139; 2008.

Clarke BL, Ebeling PR, Jones JD, Wahner HW, O'Fallon WM, Riggs BL, and Fitzpatrick LA. Changes in quantitative bone histomorphometry in aging healthy men. J. Clin. Endocrinol. Metab. 81, 2264-2270; 1996.

Clewell HJ, Lee TS, Carpenter RL. Sensitivity of physiologically based pharmacokinetic models to variation in model parameters: methylene chloride. Risk Anal 14: 521-531; 1994.

Cockcroft DW, Gault MH. Prediction of creatinine clearance from serum creatinine. Nephron, 16(1): 31-41; 1976.

Coffey JL, Cristy M, Warner GG. Specific absorbed fractions for photon sources uniformly distributed in the heart chambers and heart wall of a heterogeneous phantom. MIRD Pamphlet No. 13. Journal of Nuclear Medicine 22:65-71; 1981.

Cohn SH, Aloia JF, Vaswani AN. Women at risk for developing osteoporosis: determination by total body neutron activation analysis and photon absorptiometry. Calcified Tissue. 38: 9-15; 1986.

Cole EC. Single Compartmental Liver; Benzene and its Effects on Erythropoiesis: Models, Optimal Controls and Analyses; PhD Dissertation; North Carolina State University; 2001.

Collins PJ, Horowitz M, Cook DJ, Harding PE, Shearman DJ. Gastric emptying in normal subjects – a reproducible technique using a single scintillation camera and computer system. Gut. 24(12): 1117-25; 1983.

Cong D, Doherty M, Pang KS. A new physiologically based, segregated-flow model to explain route-dependent intestinal metabolism. Drug Metab Dispos 28:224-235; 2000.

Corley RA, Bartels MJ, Carney EW, Weitz KK, Soelberg JJ, Gies RA, Thrall KD. Development of a physiologically based pharmacokinetic model for ethylene glycol and its metabolite, glycolic acid, in rats and humans. Toxicol Sci. 85(1):476-490; 2005.

Corley RA, Bartels MJ, Carney EW, Weitz KK, Soelberg JJ, Gies RA, Thrall KD. Development of a Physiologically Based Pharmacokinetic Model for Ethylene Glycol and Its Metabolite, Glycolic Acid, in Rats and Humans. Toxicol Sci. 85(1):476-490; 2005.

Crandall D, DiGirolamo M. Hemodynamic and metabolic correlates in adipose tissue: Pathophysiologic considerations. The FASEB Journal. 4(2): 141-147; 1990.

Crandall D, Hausman GJ, Kral JG. A review of the microcirculation of adipose tissue: anatomic, metabolic, and angiogenic perspectives. Microcirculation. 4: 211-232; 1997.

Cristy M. Reference Man Anatomical Model. In: Raabe OG ed. Internal Radiation Dosimetry: Health Physics Society 1994 Summer School. Madison, WI: Medical Physics Publishing; 217-238; 1994.

Culleton BF, Larson MG, Evans JC, Wilson PWF, Barrett BJ, Parfrey PS, Levy D. Prevalence and correlates of elevated serum creatinine levels: the Framingham Heart Study. Arch Intern Med. 159(15):1785-90; 1999.

Davidson IWF, Beliles RP. Consideration of the target organ toxicity of trichloroethylene in terms of metabolite toxicity and pharmacokinetics. Drug Metabolism Reviews. 23: 493-599; 1991.

Dean JR, Ma R. Approaches to Assess the Oral Bioaccessibility of Persistent Organic Pollutants: A Critical Review. Chemosphere. 68(8): 1399-1407; 2007.

DeLorey DS, Babb TG. Progressive mechanical ventilatory constraints with aging. Am J of Respiratory Critical Care Medicine. 160: 169-177; 1999.

Dempster DW, Birchman R, Xu R, Lindsay R and Shen V. Temporal changes in cancellous bone structure of rats immediately after ovariectomy. Bone. 16: 157-161; 1995.

DeSesso JM, Jacobson CF. Anatomical and Physiological Parameters Affecting Gastrointestinal Absorption in Humans and Rats, Food and Chemical Toxicology. 39: 209-228; 2001.

Deurenberg P, Weststrate JA, and van der Kooy K. Is an adaptation of Siri's formula for the calculation of body fat percentage from body density in the elderly necessary? Eur J Clin Nutr. 43:559-568; 1989.

Dillman LT, Von der Lage FC. Radionuclide decay schemes and nuclear parameters for use in radiation-dose estimation. MIRD Pamphlet No. 10. New York: Society of Nuclear Medicine; 1975.

Dillman LT. Radionuclide decay schemes and nuclear parameters for use in radiation dose estimation. MIRD Pamphlet No. 4. Journal of Nuclear Medicine 10(Supp. 2):5-32; 1969.

Dillman LT. Radionuclide decay schemes and nuclear parameters for use in radiation dose estimation, Part 2. MIRD Pamphlet No. 6. Journal of Nuclear Medicine 11(Supp. 4):5-32; 1970.

Dinenno FA, Jones PP, Seals DR, and Tanaka H. Age-associated arterial wall thickening is related to elevations in sympathetic activity in healthy humans. Am J Physiol Heart Circ Physiol. 278: H1205-1210; 2000.

Dixit R, Riviere J, Krishnan K, and Andersen ME. Toxicokinetics and Physiologically Based Toxicokinetics in Toxicology and Risk Assessment. J Toxicol Env Hlth: Part B. 6(1):1; 2003.

Doerfel H, Andrasi A, Bailey M, Berkovski V, Blanchardon E, Castellani CM, Cruz-Suarez R, Etherington G, Hurtgen C, LeGuen B, Malatova I, Marsh J, Stather J. Internal dosimetry: The science and art of internal dose assessment, Refresher course RC 6, IRPA 12 Buenos Aires, Argentina, 19-24 October 2008

Doherty TJ. Invited review: Aging and sarcopenia. J Appl Physiol. 95:1717-1727; 2003

Donato AJ, Gano LB, Eskurza I, Silver AE, Gates PE, Jablonski K, and Seals DR. Vascular endothelial dysfunction with aging: endothelin-1 and endothelial nitric oxide synthase. Am J Physiol Heart Circ Physiol. 297: H425-432; 2009.

Dourson ML, Andersen ME, Erdreich LS, MacGregor JA. Using human data to protect the public's health. Regulatory Toxicol Pharmacol, 33(2):234-256; 2001.

Drusano GL, Muncie HL, Hoopes JM, Damron DJ, Warren JW. Commonly used methods of estimating creatinine clearance are inadequate for elderly debilitated nursing home patients. Journal of the American Geriatrics Society. 36(5): 437-441; 1988.

Dunnill MS, Halley W. Some observations on the quantitative anatomy of the kidney. J Pathol. 110:113-121; 1973.

Easterling MR, Evans MV, Kenyon EM. Comparative analysis of software for physiologically based pharmacokinetic modeling: Simulation, optimization, and sensitivity analysis. Toxicology Methods, 10(3):203-229; 2000.

Ebeling PR, Atley LM, Guthrie JR, Burger HG, Dennerstein L, Hopper JL, and Wark JD. Bone turnover markers and bone density across the menopausal transition. J. Clin. Endocrinol. Metab. 81, 3366-3371; 1996.

Eckerman KF. Dosimetric Methodology of the ICRP. In: Raabe OG ed. Internal Radiation Dosimetry: Health Physics Society 1994 Summer School. Madison, WI: Medical Physics Publishing; 239-354; 1994.

Edginton AN, Schmitt W, Willmann S. Development and evaluation of a generic physiologically based pharmacokinetic model for children. Clinical Pharmacokinetics, 45(10):1013-1034; 2006.

Edwards DAW, Beck ER. Fecal flow, mixing and consistency. Am J Digestive Diseases. 16(8): 706-708; 1971.

Edwards DA, Dunbar C. Bioengineering of therapeutic aerosols. Annual Reviews of Biomedical Engineering. 4: 93-107; 2002.

Edwards KD, Whyte HM. Plasma creatinine level and creatinine clearance as tests of renal function. Australasian Annals of Medicine. 8: 218-224; 1959.

Ehrhardt C, Kim KJ. Drug absorption studies: in situ, in vitro and in silico models. Springer: Arlington, VA, 2008.

Einhorn, TA. The bone organ system: Form and Function. In: Marcus R, Feldman D, Kelsey J. (Eds.), Osteoporosis. Academic Press, San Diego, pp. 3-21; 1996.

Ellett WH, Callahan AB, Brownell GL. Gamma-ray dosimetry of internal emitters: Monte Carlo calculations of absorbed dose from point sources. British Journal of Radiology 38:45-52; 1964.

Ellett WH, Callahan AB, Brownell GL. Gamma-ray dosimetry of internal emitters II: Monte Carlo calculations of absorbed dose from uniform sources. British Journal of Radiology. 38:541-544; 1965.

El-Masri HA and Kenyon EM. Development of a human physiologically based pharmacokinetic (PBPK) model for inorganic arsenic and its mono- and di-methylated metabolites. J Pharmacokinet Pharmacodyn. 35(1):31-68; 2008.

Emamian SA, Nielsen MB, Pedersen JF, Ytte L. Kidney dimensions at sonography: correlation with age, sex, and habitus in 665 adult volunteers. Am J Roentgenol. 160(1):83-6; 1993.

Endo A, Yamaguchi Y, Eckerman, KF. Nuclear decay data for dosimetry calculation, JAERI 1347. 2005. http://jolissrch-inter.tokai-sc.jaea.go.jp/pdfdata/JAERI-1347.pdf

Enzi G, Gasparo M, Biondetti PR, Fiore D, Semisa M, Zurlo F. Subcutaneous and visceral fat distribution according to sex, age, and overweight, evaluated by computed tomography. Am J Clin Nutr. 44:739-746; 1986.

Eriksen EF, Mosekilde L, Melsen F. Trabecular Bone Remodeling and Bone Balance in Hyperthyroidism. Bone. 6: 421-428; 1985.

Eriksen EF, Mosekilde L, Melsen F. Trabecular bone remodeling and balance in primary

hyperparathyroidism. Bone. 7: 213-221; 1986.

Evans MV, Crank WD, Yang HM, Simmons JE. Applications of sensitivity analysis to a physiologically based pharmacokinetic model for carbon tetrachloride in rats. Toxicol Appl Pharmacol 128: 36-44; 1994.

Faas H, Steingoetter A, Feinle C, Lengsfeld H, Boesiger P, Fried M, Schwizer W. Effects of meal consistency and ingested fluid volume on the intragastric distribution of a drug model in humans—a magnetic resonance imaging study. Alimentary Pharmacology and Theraputics. 16(2): 217–24; 2002.

Farrar D, Allen B, Crump K, Shipp A. Evaluation of uncertainty in input parameters to pharmacokinetic models and the resulting uncertainty in output. Toxicol Lett 49: 371-385; 1989.

Fatayerji D. and Eastell R. Age-related changes in bone turnover in men. J. Bone Miner. Res. 14, 1203-1210; 1999.

Faulkner JA, Larkin LM, Claflin DR, Brooks SV. Age-related changes in the structure and function of skeletal muscles. Clin Exp Pharmacol Physiol 34(11): 1091-1096; 2007.

Favus MJ. Primer on the Metabolic Bone Diseases and Disorders of Mineral Metabolism. Washington, DC, American Society for Bone and Mineral Research. 2006.

Fehrman-Ekholm I, Skeppholm L. Renal function in the elderly (>70 years old) measured by means of iohexol clearance, serum creatinine, serum urea and estimated clearance. Scandinavian Journal of Urology and Nephrology. 38(1): 73-77; 2004.

Fernandez-Tresguerres-Hernandez-Gil I, Alobera-Gracia MA, del-Canto-Pingarron M and Blanco-Jerez L. Physiological bases of bone regeneration II. The remodeling process. Med Oral Patol Oral Cir Bucal. 11: E151-7; 2006.

Fink E, Cormier C, Steinmetz P, Kindermans C, Le Bouc Y, and Souberbielle JC. Differences in the capacity of several biochemical bone markers to assess high bone turnover in early menopause and response to alendronate therapy. Osteoporosis International. 11(4): 295-303; 2000.

Fiserova-Bergerova V [Ed]. Introduction to Mathematical Modeling. In: Modeling of Inhalation Exposure to Vapors: Uptake, Distribution and Elimination; Volume 1; Boca Raton, Florida, CRC Press, 1983.

Fiserova-Bergerova V. Inhalation anesthesia using physiologically based pharmacokinetic models. Drug Metabolism Reviews. 24: 531-557; 1992.

Fleg JL, Gerstenblith G, Lakatta EG. Pathophysiology of the aging heart and circulation. In: Messerli, F. H. [Ed.] Cardiovascular Disease in the Elderly, 2nd ed. Boston: Martinus

Nijhoff: 9-35; 1988.

Fleg JL, O'Connor F, Gerstenblith G, Becker LC, Clulow J, Schulman SP, and Lakatta EG. Impact of age on the cardiovascular response to dynamic upright exercise in healthy men and women. J Appl Physiol. 78: 890-900; 1995.

Fleg JL, Schulman S, O'Connor F, Becker LC, Gerstenblith G, Clulow JF, Renlund DG, and Lakatta EG. Effects of acute beta-adrenergic receptor blockade on age-associated changes in cardiovascular performance during dynamic exercise. Circulation. 90: 2333-2341; 1994.

Fliser D, Franek E, Joest M, Block S, Mutschler E, Ritz E. Renal function in the elderly: impact of hypertension and cardiac function. Kidney Int. 51:1196-1204; 1997.

Fontseré N, Bonal J, Navarro M, Riba J, Fraile M, Torres F, Romero R. A comparison of prediction equations for estimating glomerular filtration rate in adult patients with chronic kidney disease stages 4-5. effect of nutritional status and age. Nephron.Clinical Practice. 104(4): c160-8; 2006.

Forbes GB. Longitudinal changes in adult fat-free mass: influence of body weight. Am J Clin Nutr. 70:1025-1031; 1999.

Fox SI. Human Physiology. McGraw Hill, New York NY, 2006.

Friedman JR, Norman DC, Yoshikawa TT. Correlation of estimated renal function parameters versus 24-hour creatinine clearance in ambulatory elderly. Journal of the American Geriatrics Society. 37(2): 145-149; 1989.

Frontera WR, Hughes VA, Fielding RA, Fiatarone RA, Evans EJ, Roubenoff R. Ageing of skeletal muscle: a 12-yr longitudinal study." Journal of Applied Physiology 88(4): 1321-1326; 2000.

Frost HM. *Intermediary Organization of the Skeleton*. CRC Press, Boca Raton, FL; 1986.
Furtaw EJ. An overview of human exposure modeling activities at the USEPA's National Exposure Research Laboraotry. Toxicol. Ind. Health, 17(5-10):302-314; 2001.

Gallagher D, Ruts E, Visser M et al. Weight stability masks sarcopenia in elderly men and women. Am J Physiol Endocrinol Metab. 279:E366-375; 2000.

Ganau A, Saba PS, Roman MJ, de Simone G, Realdi G and Devereux RB. Ageing induces left ventricular concentric remodeling in normotensive subjects. J Hypertens 13: 1818-1822; 1995.

Ganong W. Review of Medical Physiology, U.S.: The McGraw-Hill Companies; 2005.

Gardner JR, Hess CP, Webb AG, Tsika RW, Dawson MJ, Gulani V: Magnetic resonance microscopy of morphological alterations in mouse trabecular bone structure under conditions of simulated microgravity. Magn Reson Med. 45: 1122-1125; 2001.

Garg AX, Blake PG, Clark WF, Clase CM, Haynes RB, Moist LM. Association between renal insufficiency and malnutrition in older adults: Results from the NHANES III. Kidney International. 60(5): 1867-1874; 2001.

Gariepy J, Massonneau M, Levenson J, Heudes D, and Simon A. Evidence for in vivo carotid and femoral wall thickening in human hypertension. Groupe de Prevention Cardio-vasculaire en Medecine du Travail. Hypertension. 22: 111-118; 1993.

Garnero P, Sorney-Rendu E, Chapuy & Delmas PD: Increased bone turnover in late postmenopausal women is a major determinant of osteoporosis. JBMR 11: 337-349; 1996.

Garnett MC. Biodistribution of nanoparticles: insights from drug delivery. In: Nanotoxicology: Characterization, Dosing and Health Effects. Informa Healthcare. USA, Inc., New York NY; 2007.

Garnett MC, Kallinteri P. Nanomedicines and nanotoxicology: some physiological principles. Occupational Medicine, 56: 307-311; 2006.

Garrick MD, Dolan KG, Horbinski C, Ghio AJ, Higgins D, Porubcin M, Moore EG, Hainsworth LN, Umbreit JN, Conrad ME, Feng L, Lis A, Roth JA, Singleton S, Garrick LM. DMT1: a mammalian transporter for multiple metals. Biometals, 16(1):41-54; 2003.

Gass ML, Kagan R, Kohles JD, Martens MG. Bone turnover marker profile in relation to the menstrual cycle of premenopausal healthy women. Menopause. New York, NY 15 (4 Pt 1):667-675; 2008.

Gebhardt R. Metabolic zonation of the liver: Regulation and implications for liver function.
Pharmacology & Therapeutics. 53(3): 275-354; 1992.

Gehr P, Heyder J [Eds]. Particle-lung interactions. M. Dekker: New York; 2000.

Gehron RP, Boskey AL. The biochemistry of bone. In: Marcus R, Feldman D, Kelsey J. (Eds.), Osteoporosis. Academic Press, San Diego, pp. 95-156; 1996.

Gentilcore D, Chaikomin R, Jones KL, Russo A, Feinle-Bisset C, Wishart JM, Rayner CK, Horowitz M. Effects of fat on gastric emptying of and the glycemic, insulin, and incretin responses to a carbohydrate meal in Type 2 diabetes. The Journal of Clinical Endocrinology and Metabolism. 91: 2062–2067; 2006.

Gentilcore D, O'Donovan D, Jones KL, Horowitz M. Nutrition therapy for diabetic gastroparesis. Curr Diab Rep. 3(5): 418-26; 2003.

Gentry PR, Clewell HJ. Use of physiologically based pharmacokinetic modeling to evaluate implications of human variability. In: Lipscomb JC, Ohanian EV, eds. Toxicokinetics and Risk Assessment. New York, NY: Informa Healthcare; 2007: 211-229.

Gerlowski LE, Jain RK. Physiologically based pharmacokinetic modeling: principles and applications. J Pharm Sci, 72(10):1103-1127; 1983.

Gerstenblith G, Frederiksen J, Yin FC, Fortuin NJ, Lakatta EG and Weisfeldt ML. Echocardiographic assessment of a normal adult aging population. Circulation 56: 273-278, 1977.

Giannelli SV, Patel KV, Windham BG, Pizzarelli F, Ferrucci L, Guralnik JM. Magnitude of underascertainment of impaired kidney function in older adults with normal serum creatinine. Journal of the American Geriatrics Society. 55(6): 816-823; 2007.

Gibaldi M. Pharmacokinetic aspects of drug metabolism. Ann N Y Acad Sci. 179:19-31; 1971.

Gibaldi M, Perrier D. Pharmacokinetics. Drugs and the pharmaceutical sciences; v. 1. Decker M. New York, 1975. ISBN 0824762649.

Gibaldi M. In: Prescott LF, Nimmo WS (Eds), Drug Absorption. Lancaster: MTP Press; 1981.

Gilsanz V, Gibbens DT, Carlson M, Boechat MI, Cann CE, Schulz EE. Peak trabecular vertebral density: a comparison of adolescent and adult females. Calcified Tissue Int. 43: 260-262; 1988.

Going SB, Williams DP, and Lohman TG. Aging and body composition: biological changes and methodological issues. In J. Holloszy (Ed.). Exercise and Sport Science Reviews. (Vol 23, pp. 411-458). Baltimore: Williams & Williams; 1995.

Goodpaster BH, Carlson CL,Visser M, Kelley DE, Scherzinger A, Harris TB, Stamm E. Newman AB. Attenuation of skeletal muscle and strength in the elderly: The Health ABC Study. J Appl Physiol 90(6): 2157-2165; 2001.

Gordon T, Kannel WB, Hjortland MC, and McNamara PM. Menopause and coronary heart disease. The Framingham Study. Ann Intern Med. 89: 157-161; 1978.

Gorski JP**.** Is all bone the same? Distinctive distributions and properties of non-collagenous matrix proteins in lamellar vs. woven bone imply the existence of different underlying osteogenic mechanisms. Critical Reviews in Oral Biology and medicine. 9: 201-223; 1998.

Gower S, Hammond D. CSP deposition to the alveolar region of the lung: Implications of

cigarette design. Risk Analysis 27:1519-1533; 2007.

Gral T, Young M. Measured versus estimated creatinine clearance in the elderly as an index of renal function. Journal of the American Geriatrics Society. 28(11): 492-496; 1980.

Granger DN, Richardson PD, Kvietys PR, Mortillaro NA. Intestinal blood flow. Gastroenterology. 78:837-863; 1980.

Guyton AC, Hall JE. Textbook of Medical Physiology, 9th Edition, London: W.B. Saunders; 1996.

Guo SS, Zeller C, Chumlea WC, Siervogel RM. Aging, body composition, and lifestyle: the Fels Longitudinal Study. Am J Clin Nutr. 70:405-411; 1999.

Guthrie JR, Dennerstein L, Taffe JR, Lehert P, and Burger HG. The menopausal transition: a 9-year prospective population-based study. The Melbourne Women's Midlife Health Project. Climacteric. 7: 375-389; 2004.

Haber S, Yitzhak D, Tsuda A. Gravitational deposition in a rhythmically expanding and contracting alveolus. Journal of Applied Physiology. 95:657-671; 2003.

Hadj-Aissa A, Dumarest C, Maire P, Pozet N. Renal function in the elderly. Nephron. 54:364-365; 1990.

Hagberg JM, Allen WK, Seals DR, Hurley BF, Ehsani AA, and Holloszy JO. A hemodynamic comparison of young and older endurance athletes during exercise. J Appl Physiol. 58: 2041-2046; 1985.

Halloran BP, Ferguson VL, Simske SJ, Burghardt A, Venton LL, Majumdar S. Changes in bone structure and mass with advancing age in male C57BL/6J mouse. J Bone Miner Res. 17(6):1044-50; 2002.

Hausman GJ. The comparative anatomy of adipose tissue, In: New Perspectives in Adipose Tissue: Structure, Function and Development. Butterworths, London, 1985.

He Q, Heshka S, Albu J, Boxt L, Krasnow N, Elia M, Gallagher D. Smaller organ mass with age, except for heart. J. Appl. Physiol. 106: 1780-1784; 2009.

Heaney RP, Recker RR, and Saville PD. Menopausal changes in bone remodeling. J. Lab. Clin. Med. 92, 964-970; 1978.

Heaney RP, Weaver CM. Newer perspectives on calcium nutrition and bone quality. J Am Coll Nutr. 24: 574S-581S; 2005.

Heaney RP. Evaluation and interpretation of calcium-kinetic data in man, Clin. Orthop. Relat. Res. 31: 153-183; 1963.

Hees PS, Fleg JL, Lakatta EG, and Shapiro EP. Left ventricular remodeling with age in normal men versus women: novel insights using three-dimensional magnetic resonance imaging. Am J Cardiol. 90: 1231-1236; 2002.

Hemmelgarn BR, Zhang J, Manns BJ, Tonelli M, Larsen E, Ghali WA, Southern DA, McLaughlin K, Mortis G. Culleton BF. Progression of kidney dysfunction in the community-dwelling elderly. Kidney International, 69(12): 2155-2161; 2006.

Hetrick DM, Jarabek AM, Travis CC. Sensitivity analysis for physiologically based pharmacokinetic models. J Pharmacokinet Biopharm 19: 1-20; 1991.

Heyder J, Gebhart J, Scheuch G. Influence of human lung morphology on particle deposition. J. Aerosol Med. 1(2): 81-88; 1988.

Hinderling PH. Red blood cells: a neglected compartment in pharmacokinetics and pharmacodynamics. Pharmacol Rev. 49(3): 279-95; 1997.

Hinds WC. Aerosol technology: Properties, behavior, and measurement of airborne particles, 2nd ed. New York: Wiley & Sons; 1999.

Hinton JM, Lennard-Jones JE, Young AC. A new method for studying gut transit times using radioopaque markers. Gut. 10(10): 842-847; 1969.

Hoellriegl V, Li WB, Greiter M, Oeh U. Plasma clearance and urinary excretion after intravenous injection of stable 84Sr in humans. Rad. Prot. Dosim. 127(1-4)144-147; 2007.

Holzapfel G, Gasser TC, Ogden RW. A New Constitutive Framework for Arterial Wall Mechanics and a Comparative Study of Material Models. J Elasticity. 61: 1–48; 2000.

Horn T, Henriksen JH, Christoffersen P. The sinusoidal lining cells in "normal" human liver. A scanning electron microscopic investigation. Liver 6:98-110; 1986.

Horowitz M, Maddern GJ, Chatterton BE, Collins PJ, Harding PE, Shearman DJC. Changes in gastric emptying rates with age. Clin Sci. 67(2): 231-218; 1984.

Horowitz M, Su YC, Rayner CK, Jones KL. Gastropareiss: prevalence, clinical significance, and treatment. Can J Gastroenterol. 15(12): 805-13; 2001.

Hossack KF, and Bruce RA. Maximal cardiac function in sedentary normal men and women: comparison of age-related changes. J Appl Physiol. 53: 799-804; 1982.

Hotchkiss CE, Brommage R. Changes in bone turnover during the menstrual cycle in cynomolgus monkeys. Calcified Tissue International 66 (3):224-228; 2000.

Howell RW. The MIRD schema: from organ to cellular dimensions. Journal of Nuclear

Medicine 35(3): 531-533; 1994.

Howell RW, Wessels BW, Loevinger R, Watson EE, Bolch WE, Brill AB, Charkes ND, Fisher DR, Hays MT, Robertson JS, Siegel JA, Thomas SR. The MIRD perspective 1999. Journal of Nuclear Medicine 40:3S-10S; 1999.

Hsu CC, Chen PY, Chen CC, Pan LK. Measurement of gastric emptying time of solids in healthy subjects using scintigraphic method: a revised technique. Rad Prot Dosim. 150(4): 405-414; 2012.

Hughes AD, Sinclair AM, Geroulakos G, Mayet J, Mackay J, Shahi M, Thom S, Nicolaides A, and Sever PS. Structural changes in the heart and carotid arteries associated with hypertension in humans. J Hum Hypertens. 7: 395-397; 1993.

Hughes VA, Frontera WR, Roubenoff R, Evans WJ, Singh MA. Longitudinal changes in body composition in older men and women: role of body weight change and physical activity. Am J Clin Nutr. 76:473-481; 2002.

Hughes VA, Roubenoff R, Wood M, Frontera WR, Evans WJ, Fiatarone Singh MA. Anthropometric assessment of 10-y changes in body composition in the elderly. Am J Clin Nutr. 80:475-482; 2004.

Hunt JN, Knox MT, Oginski AJ. The effect of gravity on gastric emptying with various test meals. J Physiol. 178(1): 98-110; 1965.

Hunter E, Fell JT, Sharma H. A comparison of the behavior of tablet and capsule formulations in vivo. J Pharmacy and Pharmacol. 33(1): 617-618; 1981.

Idkaidek NM, Abdel-Jabbar N. A Novel Approach to Increase Oral Drug Absorption, Pharmaceutical Development and Technology. 6: 167-171; 2001.

Igari Y, Sugiyama Y, Awazu S, Hanano M. Comparative physiologically based pharmacokinetics of hexobarbital, phenobarbital and thiopental in the rat. J Pharmacokinet Biopharm 10: 53-75; 1982.

Insel P, Turner E, Ross D. Nutrition, 2nd Edition, Sudbury USA: Jones and Bartlett; 2004.

International Atomic Energy Agency (IAEA). Reference Asian Man: Ingestion and organ content of trace elements of importance in radiological protection. Vienna: IAEA; IAEA-TECDOC-1592; 2008.

International Commission on Radiological Protection (ICRP). Age dependant doses to members of the public from intake of radionuclides: Part 1. Oxford: Pergamon Press; ICRP Publication 56; Ann ICRP 20(2); 1989.

International Commission on Radiological Protection (ICRP). Age dependent doses to

members of the public from intake of radionuclides. Oxford: Pergamon Press; ICRP Publication 67; Ann ICRP 23(3/4); 1993.

International Commission on Radiological Protection (ICRP). Human respiratory tract model for radiological protection. Oxford: Pergamon Press; ICRP Publication 66; Ann ICRP 24(1-3); 1994.

International Commission on Radiological Protection (ICRP). Individual monitoring for internal exposure of workers, replacement of ICRP Publication 54. Oxford: Pergamon Press; ICRP Publication 78; Ann ICRP 27(3/4); 1997.

International Commission on Radiological Protection (ICRP). Limits for intakes of radionuclides by workers. Oxford: Pergamon Press; ICRP Publication 30 Part 1; Ann ICRP 2 (3/4); 1979.

International Commission on Radiological Protection (ICRP). Recommendations of the International Commission on Radiological Protection. Oxford: Pergamon Press; ICRP Publication 60; Ann ICRP 21(1-3); 1991.

International Commission on Radiological Protection (ICRP). Report on committee II on permissible dose for internal radiation. New York: Pergamon; ICRP Publication 2; Adopted July 1959.

International Commission on Radiological Protection. Age-dependent Doses to Members of the Public from Intakes of Radionuclides: Part 3. Ingestion Dose Coefficients. Oxford: Pergamon Press; ICRP Publication 69, Ann ICRP 25(1); 1995a.

International Commission on Radiological Protection. Basic Anatomical and Physiological Data for use in Radiological Protection: The Skeleton. Oxford: Pergamon Press; ICRP Publication 70, Ann ICRP 25(2); 1995b.

International Commission on Radiological Protection. Age-dependent Doses to Members of the Public from Intakes of Radionuclides: Part 4. Inhalation Dose Coefficients. Oxford: Pergamon Press; ICRP Publication 71, Ann ICRP 25(3-4); 1995c.

International Commission on Radiological Protection. Basic Anatomical and Physiological Data for use in Radiological Protection Reference Values. Oxford: Pergamon Press; ICRP Publication 89, Ann ICRP 32(3-4); 2002.

International Commission on Radiological Protection. Doses to the Embryo and Fetus from Intakes of Radionuclides by the Mother. Oxford: Pergamon Press; ICRP Publication 88, Ann ICRP 31(1-3); 2001.

International Commission on Radiological Protection. Human Alimentary Tract Model for Radiological Protection. Oxford: Pergamon Press; ICRP Publication 100, Ann ICRP 36(1-2); 2006.

International Commission on Radiological Protection. Occupational Intakes of Radionuclides: Part 1. Oxford: Pergamon Press; ICRP Draft Report for Consultation, ICRP ref 4828-2081-0510; 2012 February 23. www.icrp.org/docs/Occupational_Intakes_P1_for_consultation.pdf Accessed on Aug. 8, 2012.

International Commission on Radiological Protection. Permissible Dose for Internal Radiation. Oxford: Pergamon Press; ICRP Publication 2; 1960.

International Commission on Radiological Protection. Report on the Task Group on Reference Man. Oxford: Pergamon Press; ICRP Publication 23; 1975.

Isukapalli SS, Roy A. General principles of programming (computer and statistical) (Chapter 2). In: Ene I. Ette and Paul J. Williams, editors, Pharmacometrics: the Science of Quantitative Pharmacology. Wiley, 2007. ISBN 0471677833

JAMA Consensus Conference. NIH Consensus Development Panel on Osteoporosis Prevention, Diagnosis, and Therapy. Osteoporosis prevention, diagnosis, and therapy. JAMA. 285(6): 785-795; 2001.

James AC, Birchall A, Cross FT, Cuddihy RG, Johnson JR. The current approach of the ICRP task group for modeling doses to respiratory tract tissues. Health Phys. 57(S1):271-282; 1989.

Janssen I, Heymsfield SB, Wang ZM, Ross R. Skeletal muscle mass and distribution in 468 men and women aged 18-88 yr. Journal of Applied Physiology 89(1): 81-88; 2000.

Janssens JP. Aging of the respiratory system: impact on pulmonary function tests and adaptation to exertion. Clin Chest Med. 26: 469-484; 2005.

Jee WS. Integrated bone tissue physiology: anatomy and physiology, in: Cowan SC. (Ed.), Bone mechanics handbook. CRC Press, London, pp. 1-68; 2001.

Jelliffe RW. Estimation of creatinine clearance when urine cannot be collected. Lancet. 1(7706): 975-976; 1971.

Jelliffe RW. Letter: Creatinine clearance: Bedside estimate. Annals of Internal Medicine. 79(4): 604-605; 1973.

Jenkins JRF, Hardy JG, Wilson CG. Monitoring antacid preparations in the stomach using gamma scintigraphy. Int J Pharmaceutics. 14(2-3): 143-148; 1983.

Jenkins N, Black M, Paul E, Pasco JA, Kotowicz MA, Schneider HG. Age-related reference intervals for bone turnover markers from an Australian reference population. Bone. 55(2): 271-276; 2013.

Johansson C. Studies of gastrointestinal interactions. VII: Characteristics of the absorption pattern of sugar, fat, and protein from composite meals in man. A quantative study. Scand J Gastroenterol. 10(1): 33-42; 1975.

Jongeneelen F, ten Berge W. IndusChemFate: A multi-chemical PBTK-model in MS-Excel applicable for workers, consumers, and experimental animals. User Manual, version 2.00. November 21, 2011. www.industox.nl. Accessed on June 5, 2013.

Kaku K, Takeuchi M, Otani K, Sugeng L, Nakai H, Haruki N, Yoshitani H, Watanabe N, Yoshida K, Otsuji Y, Mor-Avi V, and Lang RM. Age- and gender-dependency of left ventricular geometry assessed with real-time three-dimensional transthoracic echocardiography. J Am Soc Echocardiogr. 24(5): 541-547; 2011.

Kalyan S, Prior JC. Bone changes and fracture related to menstrual cycles and ovulation. Critical Reviews in Eukaryotic Gene Expression. 20 (3):213-233; 2010

Kanis JA. Maintance of bone mass. In: Kanis JA (Ed.), Textbook of Osteoporosis. Blackwell Science Ltd, Oxford, pp. 1-28; 1996.

Kannel WB, Hjortland MC, McNamara PM, and Gordon T. Menopause and risk of cardiovascular disease: the Framingham study. Ann Intern Med. 85: 447-452; 1976.

Kaplan C, Pasternack B, Shah H, Gallo G. Age related incidence of sclerotic glomeruli in human kidneys. Am J Pathol. 80:227-234; 1975.

Kassem M, Melton LJ, Riggs BL. The Type I/Type II Model for Involutional Osteoporosis. In: Marcus R, Feldman D, Kelsey J. (Eds.), Osteoporosis. Academic Press, San Diego, pp. 691-700; 1996.

Kassis AI. The MIRD approach: remembering the limitations. Journal of Nuclear Medicine 33:781-781; 1992.

Katz NR. Metabolic heterogeneity of hepatocytes across the liver acinus. Journal of Nutrition. 122(3): 843-849; 1992.

Kawai R, Lemaire M, Steimer JL, Bruelisauer A, Niederberger W, Rowland M. Physiologically based pharmacokinetic study on a cyclosporin derivative, SDZ IMM 125. J Pharmacokinet Biopharm 22:327-365; 1994.

Keener J, Sneyd J. Mathematical physiology. Springer-Verlag, New York; 1998.
Kirkendall D and Garrett W. The effects of aging and training on skeletal muscle. Am J of Sports Med. 26(4):598-602; 1998.

Khursheed A, Fell TP, Kendall GM and Phipps AW. Simplified organ retention functions for physiologically based recycling biokinetic models. Health Phys 70(5): 656-664; 1996.

Kim CS, Jaques PA. Analysis of total respiratory deposition of inhaled ultrafine particles in adult subjects at various breathing patterns. Aerosol Science and Technology. 38:525-540; 2004.

Kitzman DW, Sheikh KH, Beere PA, Philips JL, and Higginbotham MB. Age-related alterations of Doppler left ventricular filling indexes in normal subjects are independent of left ventricular mass, heart rate, contractility and loading conditions. J Am Coll Cardiol. 18: 1243-1250; 1991.

Kitzman DW. Diastolic heart failure in the elderly. Heart Fail Rev. 7: 17-27; 2002.

Kitzman DW. Heart failure with normal systolic function. Clin Geriatr Med. 16: 489-512; 2000.

Kleerekoper M, Avioli LV. Evaluation and treatment of postmenopausal osteoporosis. In: Favus MJ (Ed.), Primer on the Metabolic Bone Diseases and Disorders of Mineral Metabolism, Second Ed. Lippincott-Raven, New York, pp. 223-228; 1990.

Knudson RJ, Clark DF, Kennedy TC, Knudson DE. Effect of aging alone on mechanical properties of the normal adult human lung. J Applied Physiology. 43: 1054-1062; 1977.

Kolanjiyil AV. Deposited nanomaterial mass transfer from lung airways to systemic regions. Thesis. North Carolina State University: 2013.

Kong F, Singh RP. Disintegration of solid foods in human stomach. Journal of Food Science. 73(5): 67-80; 2008 a.

Kong F, Singh RP. A model stomach system to investigate disintegration kinetics of solid foods during gastric digestion. Journal of Food Science. 73(5): E202-E210; 2008b.

Krevsky B, Malmud LS, D'Ercole F, Maurer A, Fisher RS. Colonic Transit scintigraphy: a physiologic approach to the quantitative measurement of colonic transit in humans. Gastroenterology. 91(5): 1102-1112; 1986.

Krewski D, Wang Y, Bartlett S, Krishnan K. Uncertainty, variability, and sensitivity analysis in physiological pharmacokinetic models. J Biopharm Stat 5: 245-271; 1995.

Krishnan K, Andersen ME. Physiologically Based Pharmacokinetic Modeling in Toxicology. In: Principles and Methods of Toxicology, 4th edition. Taylor & Francis, Philadelphia PA, pp. 193-241; 2001.

Kuczmarski RJ. Need for body composition information in elderly subjects. Am J Clin Nutr. 50:1150-1157; 1989

Kulkarni TA. A physiologically based toxicokinetic (PBTK) model for inhalation

exposure to benzene and its engineering applications. Doctoral dissertation. Florida State University; 2004.

Kuo LC, Quinones MA, Rokey R, Sartori M, Abinader EG and Zoghbi WA. Quantification of atrial contribution to left ventricular filling by pulsed Doppler echocardiography and the effect of age in normal and diseased hearts. Am J Cardiol 59: 1174-1178; 1987.

Kyle UG, Genton L, Hans D et al. Total body mass, fat mass, fat-free mass, and skeletal muscle in older people: cross-sectional differences in 60-year-old persons. J Am Geriatr Soc. 49:1633-1640; 2001

Lakatta EG. Cardiovascular system. In: Masoro EJ [Ed], Handbook of Physiology, Section 11, Aging. New York: Oxford University Press: 413-474; 1995.

Lakatta EG and Sollott SJ. Perspectives on mammalian cardiovascular aging: humans to molecules. Comp Biochem Physiol A Mol Integr Physiol 132: 699-721; 2002.

Lakatta EG, and Levy D. Arterial and cardiac aging: major shareholders in cardiovascular disease enterprises: Part I: aging arteries: a "set up" for vascular disease. Circulation. 107: 139-146; 2003.

Lakatta EG, and Levy D. Arterial and cardiac aging: major shareholders in cardiovascular disease enterprises: Part II: the aging heart in health: links to heart disease. Circulation. 107: 346-354; 2003.

Lamb EJ, Webb MC, Simpson DE, Coakley AJ, Newman DJ, O'Riordan SE. Estimation of glomerular filtration rate in older patients with chronic renal insufficiency: Is the modification of diet in renal disease formula an improvement? Journal of the American Geriatrics Society. 51(7): 1012; 2003.

Laroche M, Charmes J, Marcheix A, Bouthier F, Merle L. Estimation of glomerular filtration rate in the elderly: Cockcroft-gault formula versus modification of diet in renal disease formula. Pharmacotherapy. 26(7): 1041-1046; 2006.

Later W, Bosy-Westphal A, Kossel E, Gluer CC, Heller M, Mueller MJ. Is the 1975 Reference Man still a suitable reference? Eur. J. Clin. Nutr. 64(10): 1035-1042; 2010.

Lavdaniti M. Invasive and non-invasive methods for cardiac output measurement. Int J Caring Sciences. 1(3): 112-117; 2008.

Layton DW. Metabolically consistent breathing rates for use in dose assessments. Health Phys. 64(1):23−36; 1993.

Le Couteur DG, McLean AJ. The aging liver. Drug clearance and an oxygen diffusion barrier hypothesis. Clinical Pharmacokinetics 34(5): 359-73; 1998.

Lee TD, Lindeman RD, Yiengst MJ, Shock NW. Influence of age on the cardiovascular and renal responses to tilting. J Appl Physiol. 21:55-61; 1966.

Lee WS, Cheung WH, Qin L, Tang N, Leung KS. Age-associated decrease of type IIA/B human skeletal muscle fibers." Clinical orthopaedics and related research 450: 231-237; 2006.

Leggett RW, Eckerman KF, Meck RA. Reliability of current biokinetic and dosimetric models for radionuclides: a pilot study. Oak Ridge National Laboratory. ORNL/TM-2008/131; 2008.

Lerner UH. Bone remodeling in post-menopausal osteoporosis. J Dent Res. 85: 584-595; 2006.

Levey AS, Bosch JP. A more accurate method to estimate glomerular filtration rate from serum creatinine: A new prediction equation. Annals of Internal Medicine. 130(6):461-470; 1999.

Lewis CE, Smith DE, Wallace DD, Williams OD, Bild DE, Jacobs DR, Jr. Seven-year trends in body weight and associations with lifestyle and behavioral characteristics in black and white young adults: the CARDIA study. Am J Public Health. 87:635-642; 1997.

Lian, JB, Stein, GS, Canalis E, Gehron-Robey P, Boskey AL. Bone formation: osteoblast lineage cells, growth factors, matrix proteins and the mineralization process. In Favus, M. (Ed.), Primer on the Metabolic Bone Diseases and Disorders of Mineral Metabolism, 4th ed. Lippincott/Williams & Wilkins, Philadelphia; 1999.

Licata AC, Dekant W, Smith CE, Borghoff SJ. A physiologically based pharmacokinetic model for methyl tert-butyl ether in humans: implementing sensitivity and variability analyses. Toxicol Sci 62: 191-204; 2001.

Lie M, Sejersted OM, and Kiil F. Local regulation of vascular cross section during changes in femoral arterial blood flow in dogs. Circ Res. 27: 727-737; 1970.

Lieber RL. Skeletal Muscle Structure, Function, and Plasticity: The Physiological Basis of Rehabilitation. In: Lupash E (Ed.). Third Edition. Baltimore, MD and Philadelphia, PA: Wolters Kluwer, Lippincott Williams & Wilkins; 2010.

Lin YS, Kupper LL, Rappaport SM. Air samples versus biomarkers for epidemiology. Occup Environ Med 62:750–760; 2005.

Lindeman RD. Renal and urinary tract function. In: Masoro EJ [Ed]. Handbook of Physiology, Section 11, Aging. New York: Oxford University Press: 485-503; 1995.

Lindeman RD, Goldman R. Anatomic and physiologic age changes in the kidney.

Experimental Gerontology. 21(4-5): 379-406; 1986.

Lindeman RD, Tobin J, Shock NW. Longitudinal studies on the rate of decline in renal function with age. Journal of the American Geriatrics Society. 33(4): 278-285; 1985.

Loevinger R. Distributed radionuclide sources. In: Attix FH, Roesch WC, Tochilin E, eds. Radiation Dosimetry. 2nd edition. New York: Academic Press; 1969: 51-90.

Loevinger R. The MIRD perspective. In: Adelstein JS, Kassis AI, Burt R W, eds. Dosimetry of Administered Radionuclides. Washington D.C.: The College; 1990: 29- 43.

Loevinger R, Berman M. A formalism for calculation of absorbed dose from radionuclides. Physics in Medicine and Biology 13:205-217; 1968a.

Loevinger R, Berman M. A schema for absorbed-dose calculations for biologically distributed radionuclides. MIRD Pamphlet No.1. Journal of Nuclear Medicine 9(Supp. 1):7-14; 1968b.

Loevinger R, Budinger T, Watson E. MIRD primer for absorbed dose calculations. Society of Nuclear Medicine, New York, NY. 1988.

Loevinger R, Budinger T, Watson E. MIRD primer for absorbed dose calculations. Revised edition. New York: Society of Nuclear Medicine; 1991.

Loevinger R, Holt JO, Hine OJ. Internally administered radioisotopes. In: Hine GJ, Brownell GL, eds. Radiation dosimetry. New York: Academic Press, Inc.: 801-872; 1956.

Lonnerblad L. Transit time through the small intestine: a roentgenologic study on normal variability. Acta Radiol. 35(S88); 1951.

Lovat LB. Age related changes in gut physiology and nutritional status. Gut. 38:306-309; 1996.

Luciani A, Polig E. Verification and modification of the ICRP-67 model for plutonium dose calculation. Health Phys 78(3): 303-310; 2000.

Luciani A. Plutonium biokinetics in the human body. Dissertation: University of Karlsruhe Fridericiana, Department of Electrical Engineering and Information Technology; 2002.

Ludwig J, Ritman EL, LaRusso NF, Sheedy PF, Zumpe G. Anatomy of the human biliary system studied by quantitative computer-aided three-dimensional imaging techniques. Hepatology. 27(4): 893-899; 1998.

Lynch NA, Metter EJ, Lindle RS, Fozard JL, Tobin JD, Roy TA, Fleg JL, Hurley BF. Muscle quality. I. Age-associated differences between arm and leg muscle groups."

Journal of Applied Physiology. 86(1): 188-194; 1999.

Maaravi Y, Bursztyn M, Hammerman-Rozenberg R, Cohen A, Stessman J. Moderate renal insufficiency at 70 years predicts mortality. QJM: Monthly Journal of the Association of Physicians. 99(2): 97-102; 2006.

MacQueen HA, Waights V, Pond CM. Vascularization in adipose depots surrounding immune-stimulated lymph nodes. Journal of Anatomy. 194: 33-38; 1994.

Madsen JL, Graff J. Effects of ageing on gastrointestinal motor function. Age and Ageing. 33(2): 154-159; 2004.

Mailman D. Effects of vasoactive intestinal polypeptide on intestinal absorption and blood flow. J Physiol. 279:121-132; 1978.

Maina JN, West JB. Thin and strong! The bioengineering dilemma in the structural and functional design of the blood-gas barrier. Physiol Rev. 85: 811-844; 2005.

Majumdar S, Genant HK, Grampp S, Newitt DC, Truong VH, Lin JC, Mathur A. Correlation of trabecular bone structure with age, bone mineral density, and osteoporotic status: in vivo studies in the distal radius using high resolution magnetic resonance imaging. J Bone Miner Res. 12(1):111-8; 1997.

Malagelada JR, Robertson JS, Brown ML, Remindton M, Duenes JA, Thomforde GM, Carryer PW. Intestinal transit of solid and liquid components of a meal in health. Gastroenterology. 87(6): 1255-1263; 1984.

Marciani L, Gowland PA, Spiller RC, Manoj P, Moore RJ, Young P, Al-Sahab S, Bush D, Wright J, Fillery-Travis AJ. Gastric response to increased meal viscosity assessed by echo-planar magnetic resonance imaging in humans. Journal of Nutrition. 130: 122–127; 2000.

Marcus R. Osteoporosis. Amsterdam; Boston, Elsevier Academic Press. 2008.

Marinelli LD. Dosage determinations with radioactive isotopes. American Journal of Roentgenology and Radium Therapy 47:210-216; 1942.

Mathworks. Matlab Simbiology Toolbox, 2012. URL http://www.mathworks.com/products/simbiology/.

Matont A., Hopkins J, McLaughlin WC. Human Biology and Health. Englewood Cliffs, New Jersey, Prentice Hall; 1993.

McCance KL, Huether SE. (Eds.). Pathophysiology : The biologic basis for disease in adults and children (5th ed.). St. Louis, MO: Elsevier Mosby; 2006.

McComas AJ. Skeletal Muscle: Form and Function. Champaign, IL: Human Kinetics; 1996.

McCuskey, R. The hepatic microvascular system in health and its response to toxicants. Anatomical Record. 291(6): 661-671; 2008.

McDonald RK, Solomon DH, Shock NW. Aging as a factor in the renal hemodynamic changes induced by a standardized pyrogen. J Clin Invest. 30:457-462; 1951.

McDonnell P, McHugh PE and O'Mahoney D. Vertebral osteoporosis and trabecular bone quality. Ann Biomed Eng. 35: 170-189; 2007.

McLachlan M. Anatomic structural and vascular changes in the aging kidney. In: Macias-Nunez JF, Cameron JS, eds. Renal function and disease in the elderly. Butterworths, London; 1987.

McLachlan M, Guthrie J, Anderson C, Fulker M. Vascular and glomerular changes in the aging kidney. J Pathol. 121:65-78; 1977.

Mercer RR, Russell ML, Crapo JD. Alveolar septal structure in different species. J Appl Physiol. 77: 1060-6; 1994.

Miller JAA, Schmatz C, Schultz AB. Lumbar disc degeneration: correlation with age, sex, and spine level in 600 autopsy specimens. Spine. 13:173-178; 1988.

Minekus M, Marteau P, Havenaar R, Huisintveld JHJ. A multicompartmental dynamic computer-controlled model simulating the stomach and small-intestine. Atla-Alternatives to Laboratory Animals. 23: 197-209; 1995.

Moore FD. Metabolic Care of the Surgical Patient. Philadelphia, W. B. Saunders; 1959.

Mundy, G.R. Cellular and molecular regulation of bone turnover. Bone. 24: 35-38; 1999.

Munro NB, Eckerman KF. Impacts of physiological changes during pregnancy on maternal biokinetic modeling. Radiat. Prot. Dosim. 79(1-4): 327-333; 1998.

National Center for Environmental Assessment; Office of Research and Development, United States Environmental Protection Agency. Approaches for the application of physiologically based pharmacokinetic (PBPK) models and supporting data in risk assessment. Washington, D.C: EPA/600/R-05/043F; August 2006.

National Council on Radiation Protection and Measurements. Development of a Biokinetic Model for Radionuclide-Contaminated Wounds and Procedures for their Assessment, Dosimetry and Treatment. Bethesda, MD: Report No. 156; 2007.

National Council on Radiation Protection and Measurements. Management of Persons

Contaminated with Radionuclides: Handbook. Bethesda, MD: NCRP Report No. 161; 2008.

National Institutes of Health (NIH). NIH Consensus Development Panel on Osteoporosis Prevention, Diagnosis, and Therapy. Osteoporosis prevention, diagnosis, and therapy. JAMA. 285: 785-795; 2001.

National Kidney Foundation, Inc. K/DOQI. Clinical practice guidelines for chronic kidney disease. Part 5. Evaluation of laboratory measurements for clinical assessment of kidney disease. Guideline 4. Estimation of GFR. Am J Kidney Dis. 39(suppl 1):S76-S92; 2002.

National Nuclear Data Center. Databases: MIRD [online]. Available at: http://www.nndc.bnl.gov/mird/. Accessed on 27 June 2012.

Nestorov IA. Sensitivity analysis of pharmacokinetic and pharmacodynamic systems: I. A structural approach to sensitivity analysis of physiologically based pharmacokinetic models. Journal of Pharmacokinetics and Biopharmaceutics 27: 577-596; 1999.

Nestorov I. Whole body pharmacokinetic models. Clin Pharmacokinet 42: 883-908; 2003.

Nestorov IA, Aarons LJ, Rowland M. Physiologically based pharmacokinetic modeling of a homologous series of barbiturates in the rat: a sensitivity analysis. J Pharmacokinet Biopharm 25: 413-447; 1997.

Newman SP, Pavia D, Moren F, Sheahan NF, Clarke SW. Deposition of pressurized aerosols in the human respiratory tract. Thorax. 36:52-55; 1981.

Ng AV, Callister R, Johnson DG, and Seals DR. Age and gender influence muscle sympathetic nerve activity at rest in healthy humans. Hypertension. 21: 498-503; 1993.

Noppa H, Andersson M, Bengtsson C, Bruce A, Isaakson B. Longitudinal studies of anthropometric data and body composition. The population study of women in Goteborg, Sweeden. Am J Clin Nutr. 33:155-162; 1980.

Nordberg GF. Cadmium and health in the 21st Century - historical remarks and trends for the future. Biometals, 17(5):485-489; 2004.

Nordberg M, Nordberg GF. Toxicological aspects of metallothionein. Cell Mol Biol (Noisy-le-grand), 46(2):451-63; 2000.

Nosske D, Blanchardon E, Bolch WE, Breustedt B, Eckerman KF, Giussani A, Harrison JD, Klein W, Leggett RW, Lopez MA, Luciani A, Zankl M. New developments in internal dosimetry models. Radiation Protection Dosimetry. 144(1-4): 314-320; 2011.

Notivol RR, Carrio II, Cano LL, Estorch MM, Vilardell FF. Gastric emptying of solid and liquid meals in healthy young subjects. Scand J Gastroenterol. 19(8): 1107-13; 1984.

Nussbacher A, Gerstenblith G, O'Connor FC, Becker LC, Kass DA, Schulman SP, Fleg JL, and Lakatta EG. Hemodynamic effects of unloading the old heart. Am J Physiol. 277: H1863-1871; 1999.

Nygaard HA, Naik M, Ruths S, Krüger K. Clinically important renal impairment in various groups of old persons. Scandinavian Journal of Primary Health Care. 22(3): 152-156; 2004a.

Nygaard HA, Naik M, Ruths S, Krüger K. Clinically important renal impairment in various groups of old persons. Scandinavian Journal of Primary Health Care. 22(3): 152-156; 2004b.

Oberdorster G, Oberdorster E, Oberdorster J. Nanotoxicology: an emerging discipline evolving from studies of ultrafine particles. Environ Health Perspect. 113(7): 823-839; 2005.

Oberle RL, Chen TS, Lloys C, Barnett JL, Owyang C, Meyer J, Amidon GL. The Influence of the Interdigestive Migrating Myoelectric Complex on the Gastric-Emptying of Liquids. Gastroenterology. 99(5): 1275-1282; 1990.

Ochs M, Nyengaard JR, Jung A, Knudsen L, Voigt M, Wahlers T, Richter J, Gundersen HJ. The number of alveoli in the human lung. Am J Respir Crit Care Med. 169: 120-4; 2004.

O'Flaherty EJ. Physiologically based models of metal kinetics. Critical Reviews in Toxicology. 28(3):271-317; 1998.

O'Flaherty EJ. Modeling: An Introduction. Pharmacokinetics in Risk Assessment: Drinking Water and Health; National Academy Press; pp. 28-30, 34; 1987.

O'Flaherty EJ. Modeling normal aging bone loss, with consideration of bone loss in osteoporosis. Toxicol Sci. 55(1):171-88; 2000.

Ogawa T, Spina RJ, Martin WH, Kohrt WM, Schechtman KB, Holloszy JO, and Ehsani AA. Effects of aging, sex, and physical training on cardiovascular responses to exercise. Circulation. 86: 494-503 119; 1992.

O'Hare AM, Bertenthal D, Covinsky KE, Landefeld CS, Sen S, Mehta K, Steinman MA, Borzecki A, Walter LC. Mortality risk stratification in chronic kidney disease: One size for all ages? Journal of the American Society of Nephrology: JASN. 17(3): 846-853; 2006.

Olivetti G, Giordano G, Corradi D, Melissari M, Lagrasta C, Gambert SR, and Anversa P. Gender differences and aging: effects on the human heart. J Am Coll Cardiol. 26: 1068-1079; 1995.

O'Mahony D, O'Leary P, and Quigley EMM. Aging and intestinal motility: A review of factors that affect intestinal motility in the aged. Drugs Aging. 19(7): 515-527; 2002.

Pang KS, Rowland M. Hepatic clearance of drugs. I. Theoretical considerations of a "well-stirred" model and a "parallel tube" model. Influence of hepatic blood flow, plasma and blood cell binding, and the hepatocellular enzymatic activity on hepatic drug clearance. J Pharmacokinet Biopharm. 5:625-653; 1977.

Parfitt AM. Osteonal and Hemi-Osteonal Remodeling - the Spatial and Temporal Framework for Signal Traffic in Adult Human Bone. Journal of Cellular Biochemistry. 55: 273-286; 1994.

Parfitt AM. The mechanism of coupling: a role for the vasculature. Bone. 26: 319-323; 2000.

Parfitt AM. The physiologic and clinical significance of bone histomorphometric data, in: Recker RR (Ed.), Bone Histomorphometry: Techniques and Interpretation. CRC Press, Boca Raton, FL; 1983.

Park SH, Shub C, Nobrega TP, Bailey KR, and Seward JB. Two-dimensional echocardiographic calculation of left ventricular mass as recommended by the American Society of Echocardiography: correlation with autopsy and M-mode echocardiography. J Am Soc Echocardiogr. 9: 119-128; 1996.

Parker BA, Ridout SJ, and Proctor DN. Age and flow-mediated dilation: a comparison of dilatory responsiveness in the brachial and popliteal arteries. Am J Physiol Heart Circ Physiol. 291: H3043-3049; 2006.

Patterson DH, Jones GR, Rice CL. Ageing and physical activity: evidence to develop exercise recommendations for older adults." Can J Public Health 98(2): S69-S108; 2007.

Pedone C, Corsonello A, Incalzi RA. Estimating renal function in older people: A comparison of three formulas. Age & Ageing. 35(2): 121-126; 2006.

Pernenkil R, Vinson JM, Shah AS, Beckham V, Wittenberg C, and Rich MW. Course and prognosis in patients > or = 70 years of age with congestive heart failure and normal versus abnormal left ventricular ejection fraction. Am J Cardiol. 79: 216-219; 1997.

Pery ARR, Brochot C, Hoet PHM, Nemmar A, Bois FY. Development of a physiologically based kinetic model for 99m-Technetium-labelled carbon nanoparticles inhaled by humans. Inhalation Toxicology. 21(13): 1099-1107; 2009.

Petersen AM, and Pedersen BK. The anti-inflammatory effect of exercise. J Appl Physiol. 98: 1154-1162; 2005.

Pivonka P, Zimak J, Smith DW, Gardiner BS, Dunstan CR, Sims NA, Martin TJ, Mundy GR. Model structure and control of bone remodeling: A theoretical study. Bone. 43: 249-263; 2008.

Porter MM, Vandervoort AA, Lexell J. Aging of human muscle: structure, function and adaptability. Scand J Med Sci Sports 5(3): 129-142; 1995.

Portier CJ, Kaplan NL. Variability of Safe Dose Estimates When Using Complicated Models of the Carcinogenic Process - a Case-Study - Methylene-Chloride. Fundamental and Applied Toxicology 13: 533-544; 1989.

Potter CA. Internal dosimetry: a review. Health Phys 87(5): 455-468; 2004.

Poulin P, Krishnan K. A biologically-based algorithm for predicting human tissue-blood partition coefficients of organic chemicals. Human & Experimental Toxicology, 14(3):273-280; 1995a.

Poulin P, Krishnan K. A tissue composition-based algorithm for predicting tissue : air partition coefficients of organic chemicals. Toxicol Appl Pharmacol, 136(1):126-130; 1996b.

Poulin P, Krishnan K. An algorithm for predicting tissue-blood partition coefficients of organic chemicals from N-Octanol-water partition coefficient data. Journal of Toxicology and Environmental Health, 46(1):117-129; 1995b.

Poulin P, Krishnan K. Molecular structure-based prediction of the partition coefficients of organic chemicals for physiological pharmacokinetic models. Toxicology Methods, 6(3):117-137; 1996a.

Prasad A, Okazaki K, Arbab-Zadeh A, Dijk E, Fu Q, Thomas JD, and Levine BD. Abnormalities of Doppler measures of diastolic function in the healthy elderly are not related to alterations of left atrial pressure. Circulation. 111: 1499-1503; 2005.

Price PS, Conolly RB, Chaisson CF, Gross EA, Young JS, Mathis ET, Tedder DR. Modeling interindividual variation in physiological factors used in PBPK models of humans. Crit Rev Toxicol. 33(5):469-503; 2003.

Qiu H, Depre C, Ghosh K, Resuello RG, Natividad FF, Rossi F, Peppas A, Shen YT, Vatner DE, and Vatner SF. Mechanism of gender-specific differences in aortic stiffness with aging in nonhuman primates. Circulation. 116: 669-676; 2007.

Quartarolo JM, Thoelke M, Schafers SJ. Reporting of estimated glomerular filtration rate: Effect on physician recognition of chronic kidney disease and prescribing practices for elderly hospitalized patients. J. Hosp Med. 2(2): 74-78; 2007.

Raabe OG. Introduction to internal radiation dosimetry. In: Raabe O, [Ed.] Internal radiation dosimetry: Health Physics Society, 1994 summer school. Madison: Medical Physics Publishing: 1-26; 1994.

Raguso CA, Kyle U, Kossovsky MP et al. A 3-year longitudinal study on body composition changes in the elderly: role of physical exercise. Clin Nutr. 25:573-580; 2006.

Raisz LG. Physiology and pathophysiology of bone remodeling. Clinical Chemistry. 45(8): 1353-1358; 1999.

Ramsey JC, Andersen ME. A physiologically based description of the inhalation pharmacokinetics of styrene in rats and humans. Toxicology and Applied Pharmacology. 73: 159-175; 1984.

Rauch F, Rauch R, Woitge HW, Seibel MJ, and Schonau E. Urinary immunoreactive deoxypyridinoline in children and adolescents: variations with age, sex and growth velocity. Scand J Clin Lab Invest. 56(8): 715-9; 1996.

Rauch F, Schonau E, Woitge H, Remer T, and Seibel M. Urinary excretion of hydroxy-pyridinium cross-links of collagen reflects skeletal growth velocity in normal children. Experimental and Clinical Endocrinology. 102(2): 94-7; 1994.

Reddy AR, Ellett WH, Brownell GL. Gamma-ray dosimetry of internal emitters III: Monte Carlo calculations of absorbed dose for low-energy gamma-rays. British Journal of Radiology 45:512-515; 1967.

Reddy MB, Yang RSH, Clewell HJ, Andersen ME. Physiologically based pharmacokinetic modeling: science and applications. Wiley-Interscience, Hoboken, N.J., 2005. ISBN 0471478148.

Riggs BL, Khosla S, Melton LJ. Sex Steroids and the construction and conservation of the adult skeleton. Endocrine reviews. 23(3): 279-302; 2002.

Riggs BL, Melton LJ. The prevention and treatment of osteoporosis. The New England Journal of Medicine 327: 620-627; 1992.

Riggs, Melton LJ, Robb RA, Camp JJ, Atkinson EJ, Peterson JM, Rouleau PA, McCoulough CH, Bouxein SL, and Khosla S. Population-based study of age and sex differences in bone volumetric density, size, geometry, and structure at different skeletal sites. J. Bone Miner. Res. 19, 1945-1954; 2004.

Ritschel WA. Gerontokinetics: The pharmacokinetics of drugs in the elderly. Caldwell, New Jersey. The Telford Press; 1988.

Ritschel WA, Banerjee PS. Physiological pharmacokinetic models: principles, applications, limitations and outlook. Methods Find Exp Clin Pharmacol 8: 603-614; 1986.

Rivera AM, Pels AE, Sady SP, Sady MA, Cullinane EM, and Thompson PD. Physiological factors associated with the lower maximal oxygen consumption of master runners. J Appl Physiol. 66: 949-954; 1989.

Rodeheffer RJ, Gerstenblith G, Becker LC, Fleg JL, Weisfeldt ML and Lakatta EG. Exercise cardiac output is maintained with advancing age in healthy human subjects: cardiac dilatation and increased stroke volume compensate for a diminished heart rate. Circulation 69: 203-213, 1984.

Roodman GD. Advances in bone biology: the osteoclast. Endocrine reviews. 17: 308-332; 1996.

Rossi A, Ganassini A, Tantucci C, Grassi V. Aging and the respiratory system. Aging Clin. Exp. Res. 8: 143-161; 1996.

Rowe JW, Andres R, Tobin JD, Norris AH, Shock NW. The effect of age on creatinine clearance in men: A cross-sectional and longitudinal study. Journal of Gerontology. 31(2): 155-163; 1976a.

Rowe JW, Andres R, Tobin JD, Norris AH, Shock NW. Age adjusted standards for creatinine clearance. Ann Intern Med. 84:567-569; 1976b.

Rowland M. Protein binding and drug clearance. Clin Pharmacokinet. 9(S 1): 10-17; 1984.

Roy A, Weisel CP, Lioy PJ, Georgopoulos PG. A distributed parameter physiologically-based pharmacokinetic model for dermal and inhalation exposure to volatile organic compounds. Risk Anal, 16(2):147-60; 1996.

Ruiz P, Fowler BA, Osterloh JD, Fisher J, Mumtaz M. Physiologically based pharmacokinetic (PBPK) tool kit foenvironmental pollutants – metals. SAR and QSAR in Environmental Research. 21(7-8): 603-618; 2010.

Russo CR, Lauretani F, Bandinelli S, Bartali B, Di Iorio A, Volpato S, Guralnik JM, Harris T, and Ferrucci L. Aging bone in men and women: beyond changes in bone mineral density. Osteoporos. Int. 14, 531-538; 2003.

Sarangapani R, Teeguarden JG, Cruzan G, Clewell HJ, Andersen ME. Physiologically based pharmacokinetic modeling of styrene and styrene oxide respiratory-tract dosimetry in rodents and humans. Inhalation Toxicology. 14: 789-834; 2002.

Sarangapani R, Gentry PR, Covington TR, Teeguarden JG, Clewell HJ. Evaluation of the potential impact of age- and gender-specific lung morphology and ventilation rate on the dosimetry of vapors. Inhalation Toxicology. 15: 987-1016; 2003.

Schlafke-Stelson AT, Watson EE, Cloutier RJ. A History of internal dosimetry. Health Physics 69:766-782; 1995.

Schlesinger T. Dosimetry of internal emitters - a guide to the MIRD technique. In: Brodsky A, [Ed.] CRC handbook of radiation measurement and protection. West Palm Beach: CRC Press, Inc.; 511-526; 1978.

Schmidt H, Baddon S: High Performance Simulation for the Systems Biology Toolbox for MATLAB. Bioinformatics, 2007.

Schofield WN. Predicting basal metabolic rate, new standards and review of previous work. Hum Nutr Clin Nutr. 39(Suppl.):5−41; 1985.

Schurgers N, de Blaey CJ, Tomlinson E. Non-enhancement of sodium cromoglycate intestinal absorption by quaternary ammonium ions. An effect of salt on ion-pair formation? J Pharm Pharmacol. 36:45; 1984.

Scopacasa F, Wishart JM, Need AG, Horowitz M, Morris HA, and Nordin BE. Bone density and bone-related biochemical variables in normal men: a longitudinal study, J. Gerontol. A 57, M 385-M391; 2002.

Scuteri A, Orru M, Morrell C, Piras MG, Taub D, Schlessinger D, Uda M, and Lakatta EG. Independent and additive effects of cytokine patterns and the metabolic syndrome on arterial aging in the Sardinia Study. Atherosclerosis. 215: 459-464; 2011.

Seeman E, Delmas PD. Bone quality--the material and structural basis of bone strength and fragility. The New England Journal of Medicine 354, 2250-2261; 2006.

Seeman E. Reduced bone formation and increased bone resorption: rational targets for the treatment of osteoporosis. Osteoporosis International. 14: 2-8; 2003.

Seeman E. The structural basis of bone fragility in men. Bone. 25: 143-147; 1999.

Segers P, Rietzschel ER, De Buyzere ML, Vermeersch SJ, De Bacquer D, Van Bortel LM, De Backer G, Gillebert TC, and Verdonck PR. Noninvasive (input) impedance, pulse wave velocity, and wave reflection in healthy middle-aged men and women. Hypertension. 49: 1248-1255; 2007.

Seibel MJ. Biochemical markers of bone remodeling Endocrinology and Metabolism Clinics of North America. 32(1), 83-113; 2003.

Shelley ML, Wagner AJ, Hussain SM, and Bleckmann C. Modeling the in-vivo case with in vitro nanotoxicity data. Int J Toxicol, 27: 259-367; 2008.

Shimokata H, Andres R, Coon PJ, Elahi D, Muller DC, Tobin JD. Studies in the distribution of body fat. II. Longitudinal effects of change in weight. Int J Obes. 13:455-464; 1999.

Shipp AM, Gentry PR, Lawrence G, Van Landingham C, Covington T, Clewell HJ, Gribben K, and Crump K. Determination of a site-specific reference dose for methylmercury for fish-eating populations. Toxicol Ind Health, 16(9-10):335-438; 2000.

Shivakumar K, Dostal DE, Boheler K, Baker KM and Lakatta EG. Differential response of cardiac fibroblasts from young adult and senescent rats to ANG II. Am J Physiol Heart Circ Physiol 284: H1454-H1459, 2003.

Shub C, Klein AL, Zachariah PK, Bailey KR, and Tajik AJ. Determination of left ventricular mass by echocardiography in a normal population: effect of age and sex in addition to body size. Mayo Clin Proc. 69: 205-211; 1994.

Simon LS. Osteoporosis. Rheum Dis Clin North Am. 33: 149-176; 2007.

Sindler AL, Fleenor BS, Calvert JW, Marshall KD, Zigler ML, Lefer DJ, and Seals DR Nitrite supplementation reverses vascular endothelial dysfunction and large elastic artery stiffness with aging. Aging Cell. 10(3), 429-437; 2011.

Sinoway LI, Hendrickson C, Davidson WR Jr, Prophet S, and Zelis R. Characteristics of flow-mediated brachial artery vasodilation in human subjects. Circ Res. 64: 32-42; 1989.

Skelton DA, Greig CA, Davies JM, Young A. Strength, power and related functional ability of healthy people aged 65-89 years. Age and Ageing. 23(5): 371-377; 1994.

Slavin BG. The morphology of adipose tissue, In: New Perspectives in Adipose Tissue: Structure, Function and Development, Butterworths, London, 1985.

Smith EM, Harris CC, Rohrer RH. Calculation of local energy deposition due to electron capture and internal conversion. Journal of Nuclear Medicine 7:23-31; 1965.

Smith EM. Introduction: activities of the Medical Internal Radiation Dose Committee. Journal of Nuclear Medicine. 9(Sl): 5-6; 1968.

Smith EM. General considerations in calculation of the absorbed dose of radiopharmaceuticals used in nuclear medicine. In: Cloutier RJ, Edwards CL, Snyder WS, eds. Medical radionuclides: radiation dose and effects. Proceedings of a symposium held at the Oak Ridge Associated Universities. Oak Ridge: United States Atomic Energy Commission; AEC Symposium Series 20: 17-27; 1970.

Snyder WS, Ford MR, Warner GG, Fisher HL Jr. Estimates of absorbed fractions for monoenergetic photon sources uniformly distributed in various organs of a heterogeneous phantom. MIRD Pamphlet No.5. Journal of Nuclear Medicine 10 (Supp. 3):5-52; 1969.

Sommerfeldt DW, Rubin CT. Biology of bone and how it orchestrates the form and function of the skeleton. European Spine J. 10(S2), 86-95; 2001.

Soong TT, Nicolaides P, Yu CP, Soong SC. A statistical description of the human tracheobronchial tree geometry. Respir. Physiol. 37, 161-172; 1979.

Sotaniemi EA, Arranto AJ, Pelkonen O, Pasanen M. Age and cytochrome P450-linked drug metabolism in humans: an analysis of 226 subjects with equal histopathologic conditions. Clinical Pharmacology & Therapeutics 61(3): 331-9; 1997.

Spear RC, Bois FY, Woodruff T, Auslander D, Parker J, Selvin S. Modeling benzene pharmacokinetics across three sets of animal data: parametric sensitivity and risk implications. Risk Anal. 11: 641-654; 1991.

Stabin MG. A model of the prostate gland for use in internal dosimetry. Journal of Nuclear Medicine 35:516-520; 1994a.

Stabin MG. Internal dosimetry in the use of radiopharmaceuticals in therapy - science at a crossroads? Cancer Biotherapy and Radiopharmaceuticals 14:81-89; 1999.

Stabin MG. Patient dose from diagnostic and therapeutic radiopharmaceuticals. In: Raabe O, ed. Internal radiation dosimetry: Health Physics Society, 1994 summer school. Madison: Medical Physics Publishing: 375-392; 1994b.

Starfield B. Basic concepts in population health and health care. J Epidemiol Community Health. 55(7): 452-454; 2001.

Staub NC. Basic respiratory physiology. Churchill Livingstone: New York, 1991.

Staub NC. The Pulmonary intravascular macrophage. Futura Pub. Co.: Bedford Hills, N.Y., 1989.

Steen B, Isaakson B, Svanborg A. Body composition at 70 and 75 years of age: an longitudinal study. J. Clin Exp Gerontol. 1:185-200; 1979.

Steffes MW, Barbosa J, Bagsen JM, Mata AJ and Mauer MW. Quantitative glomerular morphology of the normal human kidney. Lab Invest. 49:82-86; 1983.

Stepan JJ. Prediction of Bone Loss in Postmenopausal Women. Osteoporos. Int. 11: S45-S54; 2000.

Stepan JJ, Tesarova A, Havranek T, Jodi J, Formankova J, and Pacovsky V. Age and sex dependency of the biochemical indices of bone remodeling, Clin. Chim. Acta 151,273-283; 1985.

Stone KC, Mercer RR, Gehr P, Stockstill B, Crapo JD. Allometric relationships of cell numbers and size in the mammalian lung. Am. Respir. Cell Mol. Biol. 6: 235-243; 1992.

Stoudt HW, Damon A, McFarland RA. Heights and weights of white Americans. Human Biol. 32:331-341; 1960.

Stubbs JB. Results from a new mathematical model of gastrointestinal transit that incorporates age and gender-dependent physiological parameters. Rad. Prot. Dosim. 41(2-4): 63-69; 1992.

Sugawara J, Hayashi K, Yokoi T, and Tanaka H. Age-associated elongation of the ascending aorta in adults. JACC Cardiovasc Imaging. 1: 739-748; 2008.

Sundberg M, Gardsell P, Johnell O, Ornstein E, Karlsson MK, and Sernbo I. Pubertal bone growth in the femoral neck is predominantly characterized by increased bone size and not by increased bone density-a 4-year longitudinal study. Osteoporosis International.14(7): 548-558; 2003.

Taichman RS. Blood and bone: two tissues whose fates are intertwined to create the hematopoietic stem-cell niche. Blood. 105 (7):2631-2639; 2005

Takahashi K, Miura S, Mori-Abe A, Kawagoe J, Takata K, Ohmichi M, and Kurachi H. Impact of menopause on the augmentation of arterial stiffness with aging. Gynecologic and obstetric investigation. 60: 162-166; 2005.

Takasaki S, Hano H. Three dimensional observation of the human hepatic artery (arterial system in the liver). Journal of Hepatology. 34(3): 455-466; 2001.

Tanaka C, Kawai R, Rowland M. Physiologically based pharmacokinetics of cyclosporine A: Reevaluation of dose-nonlinear kinetics in rats. J Pharmacokinetics and Biopharm. 27: 597-623; 1999.

Tanaka H, DeSouza CA, and Seals DR. Absence of age-related increase in central arterial stiffness in physically active women. Arterioscler Thromb Vasc Biol. 18: 127-132; 1998.

Tanaka H, Dinenno FA, and Seals DR. Age-related increase in femoral intima-media thickness in healthy humans. Arterioscler Thromb Vasc Biol. 20: 2172; 2000.

Tanaka H, Monahan KD, and Seals DR. Age-predicted maximal heart rate revisited. J Am Coll Cardiol. 37: 153-156; 2001.

Taren DL, Schler S. The nutritional assessment of the successfully aged. Clin Nutr. 9:7-16; 1990.

Tauchi H, Tsuboi K, Okutomi J. Age changes in the human kidney of the different races. Gerontologia. 17:87-97; 1971.

Theeuwes F. In: Borchardt RT, Repta AJ, Stella VJ (Eds). Directed Drug Delivery; Humana Press, New Jersey; 1985.

Thibodeau GA, Patton KT. Physiology of the Respiratory System. In: Anatomy and Physiology: Fifth Edition; Mosby Elsevier; 2003.

Thomas A. Gut motility, sphincters and reflex control. Anaesthesia and Intensive Care Medicine. 7(2): 57–58; 2006.

Thomas SR, Stabin MG, Chen CT, Samaratunga RC. A dynamic urinary bladder model for radiation dose calculations. MIRD Pamphlet No. 14. Journal of Nuclear Medicine 33:783-802; 1992.

Thomas SR, Stabin MG, Chen CT, Samaratunga RC. A dynamic urinary bladder model for radiation dose calculations. MIRD Pamphlet No. 14, Revised. Journal of Nuclear Medicine 40:102S-123S; 1999.

Thompson CM, Johns DO, Sonawane B, Barton HA, Hattis D, Tardif R, Krishnan K. Database for physiologically based pharmacokinetic (PBPK) modeling: physiological data for healthy and health-impaired elderly. Journal of Toxicology and Environmental Health, Part B. 12: 1-24; 2009.

Thurlbeck WM. The internal surface area of nonemphysematous lungs. Am. Rev. Respir. Dis. 95: 765-770; 1967.

Tippayawong N, Damrongsak D. Prediction of particle deposition in human respiratory system. Thammasat Int. J. Sc. Tech. 8(2): 65-71; 2003.

Tortora GJ, Grabowski SR. The cardiovascular system: The heart, In: Principles of Anatomy and Physiology, 10th ed. John Wiley & Sons, Hoboken, NJ; 2003.

Tronde, A. Pulmonary drug absorption: in vitro and in vivo investigations of drug absorption across the lung barrier and its relation to drug physicochemical properties. Uppsala University, 2002.

Tsuda A, Butler JP, Fredberg JJ. Effects of alveolated duct structure on aerosol kinetics. II. Gravitational sedimentation and inertial impaction. Journal of Applied Physiology 76:2510-2516; 1994.

Ungell AL, Nylander S, Bergstrand S, Sjoberg A, Lenneras H. Membrane transport of drugs in different regions of the intestinal tract of the rat. Journal of Pharmaceutical Sciences. 87(3): 360-366; 1998.

U.S. Congress. Energy Employees Occupational Illness Compensation Program Act of 2000. Public Law 106-398; 42 U.S.C. 7384 et seq. (as amended); 2000.

U.S. Department of Commerce. United States Census Bureau. Population Esimates: National Estimates by age, sex, race – 1900-1979. [Web] http://www.census.gov/popest/data/national/asrh/pre-1980/PE-11.html accessed on 2/17/2014.

U.S. Department of Health and Human Services. National Center for Health Statistics. The third National Health and Nutrition Examination Survey (NHANES III, 1988-1994). Centers for Disease Control and Prevention. Washington, DC; 1996.

U.S. Department of Labor. Bureau of Labor Statistics. The Editor's Desk: Labor force participation of seniors, 1948-2007. [Web] http://www.bls.gov/opub/ted/2008/jul/wk4/art02.htm. Accessed 2/25/2014.

U.S. Environmental Protection Agency (EPA). Metabolically derived human ventilation rates: a revised approach based upon oxygen consumption rates. National Center for Environmental Assessment, Washington, DC; EPA/600/R-06/129F. May 2009.

Vanderschueren D, Gevers G, Raymaekers G, Devos P, Dequeker J. Sex- and age-related changes in bone and serum osteocalcin. Calcified Tissue International, 46, 179-182; 1990.

Vandervoort AA. Aging of the human neuromuscular system. Muscle Nerve 25(1): 17-25; 2002.

Varkonyi P, Bruckner JV, Gallo JM. Effect of parameter variability on physiologically-based pharmacokinetic model predicted drug concentrations. J Pharm Sci 84: 381-384; 1995.

Vestal RE. Aging and pharmacology. Cancer 80(7): 1302-10; 1997.

Villareal DT, Apovian CM, Kushner RF, Klein S. Obesity in older adults: technical review and position statement of the American Society for Nutrition and NAASO, The Obesity Society. Obes Res. 13:1849-1863; 2005.

Virmani R, Avolio AP, Mergner WJ, Robinowitz M, Herderick EE, Cornhill JF, Guo SY, Liu TH, Ou DY, and O'Rourke M. Effect of aging on aortic morphology in populations with high and low prevalence of hypertension and atherosclerosis. Comparison between occidental and Chinese communities. Am J Pathol. 139: 1119-1129; 1991.

Visser M, Pahor M, Tylavsky F et al. One- and two-year change in body composition as measured by DXA in a population-based cohort of older men and women. J Appl Physiol. 94:2368-2374; 2003.

Vogel JA and Friedl KE. Body fat assessment in women: special considerations. Sports Med. 13(4):245-269; 1992.

Wald A, Van Thiel DH, Hoechstetter L, Gavaler JS, Egler KM, Verm R. Scott L, Lester R. Gastrointestinal transit: The effect of the menstrual cycle. Gastroenterology. 80(6): 1497-1500; 1981.

Wang M, Zhang J, Jiang LQ, Spinetti G, Pintus G, Monticone R, Kolodgie FD, Virmani R, and Lakatta EG. Proinflammatory profile within the grossly normal aged human aortic wall. Hypertension. 50: 219-227; 2007.

Wannamethee SG, Shaper AG, Lennon L. Reasons for intentional weight loss, unintentional weight loss, and mortality in older men. Arch Intern Med. 165:1035-1040; 2005.

Warburton DE, Gledhill N, Quinney A. Musculoskeletal fitness and health. Can J Appl Physiol 26(2): 217-237; 2001.

Watson EE, Stabin MG, Davis JL, Eckerman KF. A model of the peritoneal cavity for use in internal dosimetry. Journal of Nuclear Medicine 30:2002-2011; 1989.

Watson EE. The MIRD Internal Dose Methodology. In: Raabe OG ed. Internal Radiation Dosimetry: Health Physics Society 1994 Summer School. Madison, WI: Medical Physics Publishing; 355-374; 1994.

Weber DA, Eckerman KF, Dillman LT, Ryman JC. MIRD: radionuclide data and decay schemes. New York: Society of Nuclear Medicine; 1989.

Weibel E, Cruz-Orive L. Morphometric methods. In: Crystal, West, Weibel, and Barnes, [Eds.], The Lung. 2nd ed. Philadelphia: Lippincott-Raven, 1997.

Weibel ER. Morphometry of the Human Lung. Springer: Heidelberg, 1963.

Wendelhag I, Wiklund O, and Wikstrand J. Arterial wall thickness in familial hypercholesterolemia. Ultrasound measurement of intima-media thickness in the common carotid artery. Arterioscler Thromb. 12: 70-77; 1992.

West DB, Prinz WA, Francendese AA, Greenwood MRC. Adipocyte blood flow is decreased in obese Zucker rats. American Journal of Physiology. 253: R228-R233; 1987.

West JB. Thoughts on the pulmonary blood-gas barrier. Am J Physiol. 285: L501-513; 2003.

Willmann S, Hohn K, Edginton A, Sevestre M, Solodenko J, Weiss W, Lippert J, Schmitt W.
Development of a physiology-based whole-body population model for assessing the influence of individual variability on the pharmacokinetics of drugs. J Pharmacokinet Pharmacodyn. 34(3):401-431; 2007.

Wilder RB, Shen S, DeNardo, GL. Dosimetry for radio immunotherapy: a rapidly evolving

field. Cancer Biotherapy and Radiopharmaceuticals 14:67-70; 1999.

Williams LR. Reference values for total blood volume and cardiac output in humans. ORNL/TN-12814. September 1994.

Willmann S, Schmitt W, Keldenich J, Lippert J, Dressman JB. PK-Sim: a physiologically based pharmacokinetic 'whole-body' model. Biosilico. 1:121-124; 2003.

Witzleb E. Functions of the Vascular System, In: Schmidt RF and Thews G [Eds], Human Physiology, 2nd ed.; 1989.

Wray DW, Uberoi A, Lawrenson L, and Richardson RS. Evidence of preserved endothelial function and vascular plasticity with age. Am J Physiol Heart Circ Physiol. 290: H1271-1277; 2006.

Xin X, Yang N, Eckhart AD, and Faber JE. Alpha1D-adrenergic receptors and mitogen-activated protein kinase mediate increased protein synthesis by arterial smooth muscle. Mol Pharmacol. 51: 764-775; 1997.

Young JF, Luecke RH, Pearce BA, Lee T, Ahn H, Baek S, Moon H, Dye DW, Davis TM, Taylor SJ. Human organ/tissue growth algorithms that include obese individuals and black/white population organ weight similarities from autopsy data. J. Toxicol Env Hlth, Part A. 72: 527-540; 2009.

Yu LX, Amidon GL. A compartmental absorption and transit model for estimating oral drug absorption. Int. J. Pharmaceutics. 186: 119-125; 1999.

Zaidi M. Skeletal remodeling in health and disease. National Medicine. 13: 791-801; 2007.

Zanzonico PB. Internal radionuclide radiation dosimetry: a review of basic concepts and recent developments. J Nucl Med. 41(2):297-308; 2000.

Zaydun G, Tomiyama H, Hashimoto H, Arai T, Koji Y, Yambe M, Motobe K, Hori S, and Yamashina A. Menopause is an independent factor augmenting the age-related increase in arterial stiffness in the early postmenopausal phase. Atherosclerosis. 184: 137-142; 2006.

Yu LX, Amidon GL. A compartmental absorption and transit model for estimating oral drug absorption. International Journal of Pharmaceutics. 186(2): 119-125; 1999.

Yu LX, Crison JR, Amidon GL. Compartmental transit and dispersion model analysis of small intestinal transit flow in humans. International Journal of Pharmaceutics. 140: 111-118; 1996.

Zubal IG, Harrell CR, Smith EO, Rattner Z, Gindi G, Hoffer PB. Computerized three dimensional segmented human anatomy. Medical Physics 21:299-302; 1994.